National Technical University of Athens
School of Mechanical Engineering
Fluids Dept.
Parallel CFD & Optimization Unit

Aeroacoustic Noise Prediction & Continuous Adjoint-based Shape Optimization

Master Thesis
Computational Mechanics
Interdepartmental Program of Postgraduate Studies

Aikaterini I. Karoni

Advisor
Kyriakos C. Giannakoglou, Professor NTUA

Athens, July 2018

National Technical University of Athens
School of Mechanical Engineering
Fluids Sector
Parallel CFD & Optimization Unit

Aeroacoustic Noise Prediction & Continuous Adjoint-based Shape Optimization

Master Thesis

Computational Mechanics

Interdepartmental Program of Postgraduate Studies

Aikaterini I. Karoni

Advisor: Kyriakos C. Giannakoglou , Professor NTUA

Athens, July 2018

Abstract

The present thesis is divided in two parts. The first part deals with the use of the Kirchhoff Integral Method for aeroacoustic noise prediction. Simple noise sources are introduced and the noise perceived by a receiver is computed. The corresponding software was programmed in FORTRAN. The code is validated by comparing the results (i.e. pressure at the receiver) obtained through the Kirchhoff integral to those given by the existing analytical equations for monopoles and dipoles. Optimization of the source (monopole and dipole) position is additionally performed, after setting a desired "target" pressure time-series at the receiver. Having implemented and differentiated the KI, its coupling with CFD for aeroacoustic shape optimization could be the subject of a future work.

The second part of this thesis reflects work carried out at the BMW premises in Munich. Firstly, the flow and continuous adjoint solvers developed by the PCOpt/NTUA and programmed in the OpenFOAM environment are coupled with the BMW optimization software "ShapeModule". The PCOpt/NTUA code is responsible for computing the sensitivities (i.e. the derivatives of the objective function chosen by the designer, with respect to the design variables determining the shape of the geometry being optimized), whereas the surface node displacements are computed by ShapeModule using the node-based optimization method known as Vertex Morphing. After the successful coupling, two geometries are optimized, namely an S-bend duct and an HVAC (Heating, Ventilation and Air Conditioning) duct of a passenger car, using two objective functions. The first one aims at the minimization of the total pressure losses between inlet and outlet, whereas the second one is a surrogate, noise-related objective, which aims at minimizing noise related to turbulence by minimizing the turbulent viscosity.

Εθνικό Μετσόβιο Πολυτεχνείο
Σχολή Μηχανολόγων Μηχανικών
Τομέας Ρευστών
Εργαστήριο Θερμικών Στροβιλομηχανών
Μονάδα Παράλληλης Υπολογιστικής Ρευστοδυναμικής & Βελτιστοποίησης

Αεροακουστική Πρόβλεψη Θορύβου & Βελτιστοποίηση Μορφής με Χρήση της Συνεχούς Συζυγούς Μεθόδου

Περίληψη Μεταπτυχιακής Εργασίας
Δ.Π.Μ.Σ Υπολογιστική Μηχανική

Αικατερίνη Η. Καρώνη

Επιβλέπων
Κυριάκος Χ. Γιαννάκογλου , Καθηγητής ΕΜΠ

Αθήνα, Ιούλιος 2018

Περίληψη

Η παρούσα διπλωματική εργασία αποτελείται από δύο τμήματα. Το πρώτο σχετίζεται με την χρήση της Μεθόδου του Ολοκληρώματος Kirchhoff (Kirchhoff Integral Method) για την πρόβλεψη θορύβου. Συγκεκριμένα, υπολογίζεται σε έναν δέκτη ο θόρυβος που παράγεται από απλές ακουστικές πηγές (μονόπολα, δίπολα). Η μέθοδος προγραμματίστηκε σε FORTRAN. Η ορθότητα του κώδικα ελέγχεται μέσω της σύγκρισης των αποτελεσμάτων (πίεση στον δέκτη) που προέκυψαν μέσω του Kirchhoff ολοκληρώματος, με αυτά που προέκυψαν από τις υπάρχουσες αναλυτικές εξισώσεις για μονόπολο και δίπολο. Στην συνέχεια πραγματοποιείται βελτιστοποίηση της θέσης της πηγής, έχοντας θέσει μια επιθυμητή χρονοσειρά πίεσης-στόχου στην θέση του δέκτη. Έχοντας προγραμματίσει και παραγωγίσει το ολοκλήρωμα Kirchhoff, η σύζευξή του με CFD με στόχο την αεροακουστική βελτιστοποίηση, μπορεί να είναι αντικείμενο μελλοντικής εργασίας.

Το δεύτερο μέρος της εργασίας πραγματοποιήθηκε στις εγκαταστάσεις της BMW στο Μόναχο. Καταρχάς πραγματοποιήθηκε ενσωμάτωση του αναπτυχθέντος στην Μονάδα Παράλληλης Υπολογιστικής Ρευστοδυναμικής & Βελτιστοποίησης (ΜΠΥΡ&Β) επιλύτη της ροής και του συνεχούς adjoint επιλύτη στο λογισμικό βελτιστοποίησης μορφής της BMW, "ShapeModule". Ο κώδικας της ΜΠΥΡ&Β είναι υπεύθυνος για τον υπολογισμό των παραγώγων ευαισθησίας (δηλ. των παραγώγων της επιλεγείσας από τον σχεδιαστή αντικειμενικής συνάρτησης ως προς τις μεταβλητές σχεδιασμού που καθορίζουν το σχήμα της υπό βελτιστοποίηση γεωμετρίας), ενώ οι μετατοπίσεις των επιφανειακών κόμβων του πλέγματος υπολογίζονται από το ShapeModule χρησιμοποιώντας την τεχνική μορφοποίησης πλέγματος, γνωστή ως Vertex Morphing. Μετά την

επιτυχή σύζευξη των δύο κωδίκων, πραγματοποιείται βελτιστοποίηση δύο γεωμετριών, συγκεκριμένα ενός αγωγού σχήματος S-bend και ενός HVAC (Heating, Ventilation and Air Conditioning) αγωγού επιβατικού αυτοκινήτου, χρησιμοποιώντας δύο αντικειμενικές συναρτήσεις. Η πρώτη εξ αυτών στοχεύει στην ελαχιστοποίηση των απωλειών ολικής πίεσης μεταξύ εισόδου και εξόδου, ενώ η δεύτερη σχετίζεται με την παραγωγή θορύβου και στοχεύει στην ελαχιστοποίησή του μέσω της ελαχιστοποίησης του τυρβώδους ιξώδους.

Nationale Technische Universität Athen
Fakultät für Maschinenbau
Fluidsektor
Abteilung für Parallel CFD & Optimierung

Aeroakustische Geräuschvorhersage & Formoptimierung, basiert auf die Kontinuerliche Adjungierte Methodologie

Masterarbeit
Computational Mechanics
Departmentsübergreifender Masterstudiengang

Aikaterini I. Karoni

Akademischer Betreuer: Kyriakos C. Giannakoglou, Professor NTUA

Athen, Juli 2018

Abstract

Die vorliegende Arbeit gliedert sich in zwei Teile. Der erste Teil beschäftigt sich mit der Verwendung der Kirchhoff Integral Methode zur aeroakustischen Geräuschvorhersage. Einfache Lärmquellen werden eingeführt und das an einem Empfänger induzierte Rauschen wird berechnet. Die entsprechende Software wurde in FORTRAN programmiert. Die Ergebnisse der Kirchhoff Integral Methode (Druck am Empfänger) stimmen mit analytischen Rechnungen für Monopol und Dipol überein, damit wurde der Kode validiert. Weiterhin erfolgte die Optimierung der Quellenposition (Monopol und Dipol), nachdem eine gewünschte "Ziel" Druck-Zeitreihe am Empfänger gestellt wurde. Nach der Implementierung und Differenzierung des KI könnte die Kopplung mit CFD zur aeroakustischen Formoptimierung Gegenstand einer zukünftigen Arbeit sein.

Der zweite Teil dieser Arbeit wurde im BMW-Werk in München realisiert. Zuerst werden die von PCOpt/NTUA entwickelten und in Open-FOAM implementierten Strom- und kontinuierlich adjungierten Solver mit der BMW-Optimierungssoftware "ShapeModule" gekoppelt. Der PCOpt/NTUA-Code ist für das Berechnen der Sensitivitäten verantwortlich, während in ShapeModule die Verschiebungen der Oberflächenknoten mit der knotenbasierten Optimierungsmethode Vertex Morphing berechnet werden. Nach der erfolgreichen Kopplung werden mit der Verwendung von zwei Zielfunktionen, zwei Geometrien optimiert, nämlich ein S-Bend Kanal und ein HLK-Kanal eines Personenwagens (HLK steht für Heizung, Lüftung und Klimaanlage). Die erste Zielfunktion zielt auf die Minimierung der Gesamtdruckverluste zwischen Einlass und Auslass, während die zweite Zielfunktion die Minimierung des mit der Turbulenz verbundenen Lärms über die Minimierung der turbulenten Viskosität anstrebt.

Acknowledgements

To all the people who helped me complete this thesis I would like to express my most sincere gratitude.

First and foremost to my professor Kyriakos C. Giannakoglou for his mentoring, for sharing his experience and for trusting me and giving me the opportunity to work on such interesting topics both in NTUA and in the environment of a big international company. This experience I consider invaluable.

I would also like to sincerely thank my BMW supervisors Dr. Majid Hojjat and Dr. Steffen Jahnke for their ample help and guidance and for giving me the opportunity of a six-month internship in the automotive industry, which allowed me to come into contact with real industrial problems and see the workings of an established international company.

Finally, I want to convey my thanks to all the members of the Parallel CFD & Optimization Unit NTUA. In particular I would like to thank Dr. Evangelos Papoutsis-Kiachagias for his guidance and for all the time and effort he put into helping me. I would also like to thank Konstantinos Gkaragkounis for his advice, assistance and support anytime I was in need of it. Last but not least, I want to thank Morteza Monfaredi for all his help and useful insights.

Acronyms

NTUA	National Technical University of Athens
LTT	Laboratory of Thermal Turbomachines
PCOpt	Parallel CFD & Optimization unit
CFD	Computational Fluid Dynamics
PDE	Partial Differential Equation
RHS	Right Hand Side
KIM	Kirchhoff Integral Method
KI	Kirchhoff Integral
FD	Finite Differences
gdPDEs	Grid Displacement PDEs
HVAC	Heating, Ventilation and Air Conditioning

Contents

Part I

Aeroacoustic Noise Prediction based on the Kirchhoff Integral Method

Chapter 1

Mathematical Background and Theory in Aeroacoustics

The first part of this thesis is concerned with noise prediction through the use of the Kirchhoff Integral Method (KIM). The noise studied is produced through simple monopole and dipole sources. What the human ear perceives as sound is the fluctuation in pressure over time. The KIM is a method in aeroacoustics, which allows the computation of pressure perturbation at a receiver location by integrating the pressure and its derivatives on a surface containing the source. The method solves the aeroacoustic wave equation in its PDE form and uses it to propagate information from the near-field of the source to the receiver. Noise computation would also theoretically be possible without the use of aeroacoustics, since pressure perturbation calculation can be performed by solving the Navier-Stokes equations in a domain extending from the source to the receiver. If, however, the receiver is in the source far-field, the cost of performing CFD computations to obtain the pressure value at the receiver is usually prohibitive. Therein lies the advantage of aeroacoustic analogies, which take the information from a CFD domain defined in the near-field of the source and propagate it in the far-field at a much lower computational cost.

1.1 Wave Equation

The wave equation is a second-order hyperbolic linear PDE for the description of waves (e.g. light waves, sound waves, etc.). The aeroacoustic wave equation results from the rearrangement of the Navier-Stokes equations, which govern the flow of a compressible viscous fluid. This was first done by M.J. Lighthill [1], who thereby established a connection between fluid mechanics and acoustics.

The derivation, as can also be found in [2] and [3] starts with the Navier-Stokes equations for mass, momentum and energy of a flowing compressible fluid

$$\frac{\partial \rho}{\partial t} + \boldsymbol{\nabla} \cdot (\rho \boldsymbol{v}) = \dot{m} \tag{1.1}$$

$$\frac{\partial(\rho \boldsymbol{v})}{\partial t} + \boldsymbol{\nabla} \cdot (\rho \boldsymbol{v}\boldsymbol{v}) + \boldsymbol{\nabla} p = \boldsymbol{\nabla} \cdot \boldsymbol{\tau} + \boldsymbol{f} + \dot{m}\boldsymbol{v} \tag{1.2}$$

$$\frac{\partial(\rho e_t)}{\partial t} + \boldsymbol{\nabla} \cdot (\rho e_t \boldsymbol{v}) + \boldsymbol{\nabla} \cdot (p\boldsymbol{v}) = -\boldsymbol{\nabla} \cdot q + \boldsymbol{\nabla} \cdot (\boldsymbol{\tau}\boldsymbol{v}) + \dot{\vartheta} + \boldsymbol{f} \cdot \boldsymbol{v} + \dot{m} e_t \tag{1.3}$$

In the above equations, $e_t = e + \frac{1}{2}\boldsymbol{v}^2$ is the specific (i.e. per unit mass) total energy which equals the sum of the specific internal energy e and the specific kinetic energy $\frac{1}{2}\boldsymbol{v}^2$. The friction-related stress tensor $\boldsymbol{\tau}(\boldsymbol{v}, \mu)$ is a function of the (usually temperature T-dependent) dynamic viscosity $\mu(T)$. For a Newtonian fluid under the Stokes' hypothesis, the stress tensor is given by

$$\boldsymbol{\tau} = \mu \left[\boldsymbol{\nabla}\boldsymbol{v} + (\boldsymbol{\nabla}\boldsymbol{v})^T - \frac{2}{3}\boldsymbol{I}\boldsymbol{\nabla} \cdot \boldsymbol{v} \right] \tag{1.4}$$

The heat flux vector $\boldsymbol{q}(T, k)$ is a function of the temperature-dependent heat conductivity $k(T)$ and is given by the Fourier's law of heat conductivity as

$$q = -k\boldsymbol{\nabla} T \tag{1.5}$$

The symbols $\dot{m}$, $\boldsymbol{f}$ and $\dot{\vartheta}$, correspond to (known) sources of mass, external forces and heat respectively. The mass source term does not only affect the continuity equation, since any mass added to the fluid has to assume its velocity and internal energy and, therefore, contributes to the momentum (the fluid has to exert a force to accelerate the added mass) and energy equations too. In a similar manner, the introduced force source term will affect both the momentum and energy equations. The heat source term affects only the energy equation.

The system of equations 1.1 to 1.5 contains seven unknown quantities i.e. the density ρ, velocity vector $\boldsymbol{v}$ (three components i.e. three unknowns in 3D flows), specific energy e_t, pressure p and temperature T. Two more equations are, therefore, needed in order to close the system. These are the thermal and calorific state equations of the fluid (assuming a fluid in thermodynamic equilibrium i.e. a system with no microscopic flows of matter or energy). In that case, the thermal state equation is

$$\rho = \rho(T, p) \tag{1.6}$$

and the calorific state equation is

$$e = e(T, p) \tag{1.7}$$

Using the definition of the material derivative $\frac{D}{Dt} := \frac{\partial}{\partial t} + \boldsymbol{v} \cdot \boldsymbol{\nabla}$, the mass equation (eq.1.1) can be rewritten as

$$\frac{D\rho}{Dt} = -\rho\boldsymbol{\nabla} \cdot \boldsymbol{v} + \dot{m} \tag{1.8}$$

By multiplying eq. 1.1 with $\boldsymbol{v}$ and subtracting it from eq. 1.2, we obtain

$$\rho\frac{D\boldsymbol{v}}{Dt} = -\boldsymbol{\nabla}p + \boldsymbol{\nabla}\cdot\boldsymbol{\tau} + \boldsymbol{f} \tag{1.9}$$

Next, we take the dot product of eq. 1.2 with $\boldsymbol{v}$ and subtract from eq. 1.3. From the resulting equation, we further subtract eq. 1.1 multiplied by e.

This leads to the following equation

$$\rho\frac{De}{Dt} = -p\boldsymbol{\nabla}\cdot\boldsymbol{v} + \boldsymbol{\tau} : \boldsymbol{\nabla}\boldsymbol{v} - \boldsymbol{\nabla}\cdot\boldsymbol{q} + \dot{\vartheta} \tag{1.10}$$

As will be seen, it is convenient to reformulate the energy balance (eq. 1.10) into the entropy equation. To this end, the fundamental law of thermodynamics for a reversible process,

$$T\delta s = \delta e - (p/\rho^2)\delta\rho = \delta h - (1/\rho)\delta p \tag{1.11}$$

where T is the temperature and h the specific enthalpy is used. In the most general case, change δ involves the material derivative $\frac{D}{Dt}$, i.e. $\delta = dt\cdot\dfrac{D}{Dt}$, which is the change along the pathline of a fluid parcel. Eq. 1.11 then becomes

$$\delta e = T\delta s + (p/\rho^2)\delta\rho$$

or

$$dt\frac{De}{Dt} = Tdt\frac{Ds}{Dt} + (p/\rho^2)dt\frac{D\rho}{Dt}$$

Multiplying this last equation by ρ/dt, we get

$$\rho\frac{De}{Dt} = \rho T\frac{Ds}{Dt} + \frac{p}{\rho}\frac{D\rho}{Dt} \tag{1.12}$$

Using eq. 1.12, eq. 1.10 becomes

$$\rho T\frac{Ds}{Dt} + \frac{p}{\rho}\frac{D\rho}{Dt} = -p\boldsymbol{\nabla}\cdot\boldsymbol{v} + \boldsymbol{\tau} : \boldsymbol{\nabla}\boldsymbol{v} - \boldsymbol{\nabla}\cdot\boldsymbol{q} + \dot{\vartheta} \Rightarrow$$

$$\rho\frac{Ds}{Dt} = \frac{1}{T}\left[\boldsymbol{\tau} : \boldsymbol{\nabla}\boldsymbol{v} - \boldsymbol{\nabla}\cdot\boldsymbol{q} + \dot{\vartheta} - \frac{p}{\rho}\left(\rho\boldsymbol{\nabla}\cdot\boldsymbol{v} + \frac{D\rho}{Dt}\right)\right] \Rightarrow$$

$$\rho\frac{Ds}{Dt} = \frac{1}{T}\left[\boldsymbol{\tau} : \boldsymbol{\nabla}\boldsymbol{v} - \boldsymbol{\nabla}\cdot\boldsymbol{q} + \dot{\vartheta} - \dot{m}\frac{p}{\rho}\right] \tag{1.13}$$

Entropy can now replace the internal energy in eq. 1.7. The calorific equation (eq. 1.7) also contains the internal energy and, therefore, this is to be replaced as

well by a thermodynamic relation between the state variables

$$\rho = \rho(p, s) \Rightarrow \delta\rho = \left(\frac{\partial\rho}{\partial p}\right)_s \delta p + \left(\frac{\partial\rho}{\partial s}\right)_p \delta s$$

We now introduce the following two new quantities:

$$a^2 := \left(\frac{\partial\rho}{\partial p}\right)_s^{-1} \quad \text{and} \quad \sigma := -\frac{1}{\rho}\left(\frac{\partial\rho}{\partial s}\right)_p \tag{1.14}$$

Next we want to use eq. 1.14 to derive an equation for the pressure. Again, the variations δ in the above equation are material derivatives, leading to the following reformulation of eq. 1.14

$$\frac{1}{a^2}\frac{Dp}{Dt} = \frac{D\rho}{Dt} + \sigma\rho\frac{Ds}{Dt} \tag{1.15}$$

The total derivatives of the density and entropy appearing in the RHS of eq. 1.15 are given by eqs. 1.8 and 1.13 respectively. Eq. 1.15, therefore, becomes

$$\frac{1}{a^2}\frac{Dp}{Dt} = -\rho\boldsymbol{\nabla}\cdot\boldsymbol{v} + \frac{\sigma}{T}\left(\boldsymbol{\tau} : \boldsymbol{\nabla}\boldsymbol{v} - \boldsymbol{\nabla}\cdot\boldsymbol{q} + \dot{\vartheta}\right) + \dot{m}\left(1 - \frac{\sigma}{T}\frac{p}{\rho}\right) \tag{1.16}$$

To sum up, the governing equations for density, velocity and pressure are eq. 1.8, 1.9 and 1.16 respectively. The previously defined quantities a^2 and σ are considered to be given fluid properties and, therefore, do not add to the number of unknowns. The internal energy has now been eliminated, so our unknowns are the density, velocity vector, pressure and temperature, i.e. six unknown quantities. This means that along with the five equations, eq. 1.8, 1.9 and 1.16, the thermal equation of state $\rho = \rho(T, p)$ must be included to close the system. Assuming that our fluid is a perfect gas, its thermal and calorical properties are given by the equations

$$\rho = \frac{p}{RT} \quad \text{and} \quad de = c_v dT \tag{1.17}$$

where R is the specific gas constant and c_v the specific heat capacity for constant volume. The specific heat capacity for constant pressure for a perfect gas is given as $c_p = c_v + R$ and the isentropic coefficient is $\gamma = c_p/c_v$.

Going back to eq. 1.14 and given the above formulation for the thermal and caloric properties, a^2 and σ can be expressed in terms of pressure and density as

$$a^2 = \gamma p/\rho \tag{1.18}$$

$$\gamma = 1/c_p \tag{1.19}$$

This closes the system of equations 1.8, 1.9 and 1.16. Furthermore, if viscous friction and heat conduction are neglected, i.e. $\boldsymbol{\tau} = 0$ and $\boldsymbol{q} = 0$, equations 1.8, 1.9 and 1.16 become

$$\frac{D\rho}{Dt} + \rho\boldsymbol{\nabla}\cdot\boldsymbol{v} = \dot{m} \tag{1.20}$$

$$\rho\frac{D\boldsymbol{v}}{Dt} + \boldsymbol{\nabla}p = \boldsymbol{f} \tag{1.21}$$

$$\frac{1}{a^2}\frac{Dp}{Dt} + \rho\boldsymbol{\nabla}\cdot\boldsymbol{v} = \frac{\sigma}{T}\dot{\vartheta} + \dot{m}\left(1 - \frac{\sigma}{T}\frac{p}{\rho}\right) \tag{1.22}$$

Note that for an incompressible fluid, for instance, density ρ is a function of temperature but not of pressure i.e. $\rho = \rho(T)$. Using the definition of a^{-2} in eq. 1.14 we have $a^{-2} = \left(\frac{\partial\rho}{\partial p}\right)_s$ and a^{-2} will therefore be zero for an incompressible fluid, leading to the zeroing of the first term in eq.1.22. Therefore, compressibility or non-compressibility of the fluid plays a significant part in the characterization of sound.

What the human ear perceives as sound, is the temporal deviations p' from the mean ambient pressure p_0. The goal is to formulate an equation for the pressure perturbation using the equations derived so far. To this end, all flow variables are expressed as the sum of a mean value plus a changing small perturbation. Density, for instance, will be expressed as $\rho = \rho_0 + \epsilon\rho'$, where ϵ is a small number $\epsilon << 1$. The same is done for $\boldsymbol{v}, p, \dot{m}, \boldsymbol{f}, a^2, \sigma, T$ and $\dot{\vartheta}$. Substituting the flow quantities with the sum of their mean values plus their perturbations in eq. 1.20, 1.21 and 1.13, differentiating w.r.t. ϵ and letting $\epsilon \to 0$ yields

$$\frac{D^0\rho'}{Dt} + \rho^0\boldsymbol{\nabla}\cdot\boldsymbol{v'} + \boldsymbol{v'}\cdot\boldsymbol{\nabla}\rho^0 + \rho'\boldsymbol{\nabla}\cdot\boldsymbol{v}^0 = \dot{m}' \tag{1.23}$$

$$\rho^0\frac{D^0\boldsymbol{v'}}{Dt} + \boldsymbol{\nabla}p' + \rho^0\boldsymbol{v'}\cdot\boldsymbol{\nabla}\cdot\boldsymbol{v}^0 + \rho'\boldsymbol{v}^0\cdot\boldsymbol{\nabla}\cdot\boldsymbol{v}^0 = \boldsymbol{f'} \tag{1.24}$$

$$\frac{1}{(a^2)^0}\left(\frac{D^0p'}{Dt} + [\boldsymbol{v'} - \boldsymbol{v}^0(a^2)'/(a^2)^0]\cdot\boldsymbol{\nabla}p^0\right) + \rho^0\boldsymbol{\nabla}\cdot\boldsymbol{v'} + \rho'\boldsymbol{\nabla}\cdot\boldsymbol{v}^0 = \frac{\sigma^0}{T^0}\dot{\vartheta}' + \left(1 - \frac{\sigma^0p^0}{\rho^0T^0}\right)\dot{m}' \tag{1.25}$$

where $\dfrac{D^0}{Dt} := \dfrac{\partial}{\partial t} + \boldsymbol{v}^0\cdot\boldsymbol{\nabla}$ is the total derivative along the streamlines of the mean flow.

At this point, we assume that the mean flow satisfies the steady form of eqs. 1.23, 1.24 and 1.25 without any sources i.e. $\dot{m}^0 = \boldsymbol{f}^0 = \dot{\vartheta}^0 = 0$. According to eqs. 1.23, 1.24 and 1.25 this means that

$$\boldsymbol{v}^0\cdot\boldsymbol{\nabla}\rho^0 = -\rho^0\boldsymbol{\nabla}\cdot\boldsymbol{v^0} \tag{1.26}$$

$$\rho^0 \boldsymbol{v}^0 \cdot \boldsymbol{\nabla} \cdot \boldsymbol{v}^0 = -\boldsymbol{\nabla} p^0 \tag{1.27}$$

$$\frac{1}{(a^2)^0} \boldsymbol{v}^0 \cdot \boldsymbol{\nabla} p^0 = -\rho^0 \boldsymbol{\nabla} \cdot \boldsymbol{v}^0 \tag{1.28}$$

Let us also consider the simple case of a non-moving medium i.e. $\boldsymbol{v}^0 = 0$. This means that according to eq. 1.27, $\boldsymbol{\nabla} p^0 = 0$. Now let us rewrite eq. 1.23, 1.24 and 1.25.

$$\frac{\partial \rho'}{\partial t} + \rho^0 \boldsymbol{\nabla} \cdot \boldsymbol{v'} + \boldsymbol{v'} \cdot \boldsymbol{\nabla} \rho^0 = \dot{m}' \tag{1.29}$$

$$\rho^0 \frac{\partial \boldsymbol{v'}}{\partial t} + \boldsymbol{\nabla} p' = \boldsymbol{f'} \tag{1.30}$$

$$\frac{1}{(a^2)^0} \frac{\partial p'}{\partial t} + \rho^0 \boldsymbol{\nabla} \cdot \boldsymbol{v'} = \frac{\sigma^0}{T^0} \dot{\vartheta}' + \left(1 - \frac{\sigma^0 p^0}{\rho^0 T^0}\right) \dot{m}' \tag{1.31}$$

Keeping in mind that the goal is to obtain an equation for the pressure perturbation, next step is to eliminate the velocity perturbation in the above equations. Dividing eq. 1.30 by ρ^0 and taking its divergence gives

$$\frac{\partial \boldsymbol{\nabla} \cdot \boldsymbol{v'}}{\partial t} + \boldsymbol{\nabla} \cdot \left(\frac{1}{\rho^0} \boldsymbol{\nabla} p'\right) = \boldsymbol{\nabla} \cdot \left(\frac{1}{\rho^0} \boldsymbol{f'}\right)$$

Also, taking the time derivative of eq. 1.31 yields

$$\frac{1}{(a^2)^0} \frac{\partial^2 p'}{\partial t^2} + \rho^0 \frac{\partial \boldsymbol{\nabla} \cdot \boldsymbol{v'}}{\partial t} = \frac{\sigma^0}{T^0} \frac{\partial \dot{\vartheta}'}{\partial t} + \left(1 - \frac{\sigma^0 p^0}{\rho^0 T^0}\right) \frac{\partial \dot{m}'}{\partial t}$$

By subtracting the first of the two above equations multiplied by ρ^0 from the second, the following equation is derived

$$\frac{1}{(a^2)^0} \frac{\partial^2 p'}{\partial t^2} - \rho^0 \, \boldsymbol{\nabla} \cdot \left(\frac{1}{\rho^0} \boldsymbol{\nabla} p'\right) = \frac{\sigma^0}{T^0} \frac{\partial \dot{\vartheta}'}{\partial t} + \left(1 - \frac{\sigma^0 p^0}{\rho^0 T^0}\right) \frac{\partial \dot{m}'}{\partial t} - \rho^0 \, \boldsymbol{\nabla} \cdot \left(\frac{1}{\rho^0} \boldsymbol{f'}\right) \tag{1.32}$$

In the case of a constant mean density $\rho^0 = const = \rho_\infty$, eq. 1.32 takes the following form

$$\frac{1}{(a^2)^0} \frac{\partial^2 p'}{\partial t^2} - \boldsymbol{\nabla} \cdot \boldsymbol{\nabla} p' = \frac{\sigma^0}{T^0} \frac{\partial \dot{\vartheta}'}{\partial t} + \left(1 - \frac{\sigma^0 p^0}{\rho^0 T^0}\right) \frac{\partial \dot{m}'}{\partial t} - \boldsymbol{\nabla} \cdot \boldsymbol{f'} \Rightarrow$$

$$\frac{1}{(a^2)^0} \frac{\partial^2 p'}{\partial t^2} - \Delta p' = Q_p \tag{1.33}$$

where

$$Q_p = \frac{\sigma^0}{T^0} \frac{\partial \dot{\vartheta}'}{\partial t} + \left(1 - \frac{\sigma^0 p^0}{\rho^0 T^0}\right) \frac{\partial \dot{m}'}{\partial t} - \boldsymbol{\nabla} \cdot \boldsymbol{f'}$$

Eq. 1.33 is the acoustic wave equation for the pressure perturbation p'. A wave equation can be derived for other flow quantities as well, through appropriate handling of eq. 1.29, 1.30 and 1.31. For instance, eliminating the pressure perturbation instead of $\boldsymbol{v'}$ in the above equations can lead to the wave equation for the velocity perturbation. What differentiates the two wave equations is the resulting source terms on the RHS of the equations.

Looking at the source term Q_p in the pressure perturbation wave equation, it should be noted that although it is the existence of mass, force and heat sources that leads to sound generation, it is not the sources themselves, but rather their change in time or - in the case of the force - space that is actually responsible for sound production.

1.2 Green's Functions

Prior to the derivation of the Kirchhoff integral formula, it is important to introduce a mathematical tool that can assist the solution of linear PDEs, such as the wave equation 1.33 in a simple way. This tool is the so-called Green's functions (for a detailed analysis see [4]).

Let us consider the following linear PDE

$$L[p'] = Q_p(\boldsymbol{x}, t) \tag{1.34}$$

where L is a differential operator. In the case of the wave equation, eq. 1.33, the operator L is $\frac{1}{(a^2)^0}\frac{\partial^2}{\partial t^2} - \Delta$.

First step towards the solution of eq.1.34 using the Green's functions method is to formulate the following equation

$$L[G] = \delta(\boldsymbol{x} - \boldsymbol{\xi})\delta(t - \tau) \tag{1.35}$$

where δ is the Dirac function. The field G obtained by solving eq. 1.35 is the field due to a unit point source at $\boldsymbol{x} = \boldsymbol{\xi}$ firing a needle pulse at $t = \tau$. G is called a Green's function and establishes a physical relation between two points in space ($\boldsymbol{x}$ and $\boldsymbol{\xi}$) and time (t and τ) (see [2]). So, in the case of the wave equation for the pressure perturbation, $G(\boldsymbol{x}, t; \boldsymbol{\xi}, \tau)$ is the pressure perturbation perceived by a receiver at $\boldsymbol{x}$ at time t, caused by a unit point source firing a needle pulse at $\boldsymbol{\xi}$ at time τ. Let us multiply both sides of eq. 1.35 by the RHS of eq. 1.34, i.e. by $Q_p(\boldsymbol{x}, t)$, and integrate the resulting equation over space and time.
By doing so, we obtain

$$\int_{V_\infty}\int_{-\infty}^{t^+} L[G]Q_p(\boldsymbol{\xi}, \tau)d\tau dV(\boldsymbol{\xi}) = \int_{V_\infty}\int_{-\infty}^{t^+} \delta(\boldsymbol{x} - \boldsymbol{\xi})\delta(t - \tau)Q_p(\boldsymbol{\xi}, \tau)d\tau dV(\boldsymbol{\xi}) \tag{1.36}$$

Notice that the above time integration does not represent i.e. $\int_{-\infty}^{\infty} d\tau$, but rather an integral from $-\infty$ till a positive time t^+, where $t^+ = \lim_{\epsilon \to 0} t(1+\epsilon), \epsilon > 0$, i.e. t^+ is slightly bigger than the receiver time t. The reason why the integration does not stretch until positive infinity, but stops slightly after receiver time t, is one of causality (cause and effect). We wish to ensure, that any quantity at the receiver time t depends solely on the past and not on the future. Ideally, we would want a Green's function that satisfies the equality $G(\tau > t^+) = 0$. In such a case, the time integration limits could harmlessly be extended up to positive infinity. However, since this is not a guaranteed property of Green's functions, it is safer to limit the integration up to t^+.

The differential operator L acts on $\boldsymbol{x}$ and t rather than on $\boldsymbol{\xi}$ and τ, which means that it can be taken outside of the integral in eq. 1.36. Also, according to the Delta function properties, the integral on the RHS of eq. 1.36 equals $Q_p(\boldsymbol{x}, t)$. Eq. 1.36 is, therefore, rewritten as

$$L\left[\int_{V_\infty}\int_{-\infty}^{t^+} G(\boldsymbol{x}, t; \boldsymbol{\xi}, \tau) Q_p(\boldsymbol{\xi}, \boldsymbol{\tau}) d\tau dV(\boldsymbol{\xi})\right] = Q_p(\boldsymbol{x}, t) \tag{1.37}$$

By comparing the above equation with eq. 1.34, the following solution for the pressure perturbation is derived

$$p'(\boldsymbol{x}, t) = \int_{V_\infty}\int_{-\infty}^{t^+} G(\boldsymbol{x}, t; \boldsymbol{\xi}, \tau) Q_p(\boldsymbol{\xi}, \boldsymbol{\tau}) d\tau dV(\boldsymbol{\xi}) \tag{1.38}$$

It can be concluded that if the response G to a point source firing a needle pulse is known, the response to any other type of source Q_p can be found as the convolution of G with the source Q_p.

An intuitive way of understanding this would be the following. The response to a point source emitting a needle pulse is known. A more complicated source Q_p can be seen as a "series" of simple sources. Therefore, the response to an arbitrary source Q_p will be something like a "sum" of the responses to each of the simple sources "comprising" Q_p. This logic is only valid in the case when the differential operator L is linear, otherwise the responses to the sources "comprising" Q_p cannot be "superimposed". It is reminded that a linear operator is one for which the following holds: $L(c_1 x_1 + c_2 x_2) = c_1 L(x_1) + c_2 L(x_2)$.

Below follows an example of how the Green's function for the Laplace equation for a 3D domain can be found. (Note that for a specific equation there are different Green's functions depending on whether the cases being dealt with are 1D, 2D or 3D). First, the function G that satisfies the equation

$$\nabla^2 G = \delta(\boldsymbol{x} - \boldsymbol{\xi}) \tag{1.39}$$

must be found, where $\boldsymbol{x}$ is the observation point and $\boldsymbol{\xi}$ the source position. To this

end, eq. 1.39 is integrated over a sphere S centered at $\boldsymbol{\xi}$ with a radius $r = |\boldsymbol{x} - \boldsymbol{\xi}|$, volume V and surface S.

$$\int_V \nabla^2 G dV = \int_V \delta(\boldsymbol{x} - \boldsymbol{\xi}) dV = 1 \tag{1.40}$$

Using the divergence theorem, which states that

$$\int_V \boldsymbol{\nabla} \cdot \boldsymbol{F} dV = \int_S \boldsymbol{F} \cdot \boldsymbol{n} dS \tag{1.41}$$

where $\boldsymbol{n}$ is the outward pointing unit normal vector on each surface element dS of the boundary, eq. 1.40 can be rewritten as

$$\int_V \nabla^2 G dV = \int_S \boldsymbol{\nabla} G \cdot \boldsymbol{n} dS = \int_S \frac{\partial G}{\partial n} dS = \int_S \frac{\partial G}{\partial r} dS = 1 \tag{1.42}$$

where $\frac{\partial G}{\partial n} = \frac{\partial G}{\partial r}$, since the direction of $\boldsymbol{n}$ and $\boldsymbol{r}$ coincide in the sphere case. Furthermore, since $dS = r^2 \sin\phi d\phi d\theta$, eq. 1.42 can be rewritten as

$$\int_S \frac{\partial G}{\partial r} dS = \int_{\phi=0}^{\pi} \int_{\theta=0}^{2\pi} \frac{\partial G}{\partial r} r^2 \sin\phi d\phi d\theta = 2\pi \frac{\partial G}{\partial r} r^2 \int_{\phi=0}^{\pi} \sin\phi d\phi = 4\pi r^2 \frac{\partial G}{\partial r} = 1 \Rightarrow$$

$$\frac{\partial G}{\partial r} = \frac{1}{4\pi r^2} \Rightarrow G = -\frac{1}{4\pi r} \tag{1.43}$$

If the Laplacian (eq. 1.39) is examined in 2D, S is a circle. Thus $dS = r d\theta$. Therefore, in the 2D case, eq. 1.42 is written as

$$\int_S \frac{\partial G}{\partial r} dS = \int_{\theta=0}^{2\pi} \frac{\partial G}{\partial r} r d\theta = 2\pi \frac{\partial G}{\partial r} r = 1 \Rightarrow$$

$$\frac{\partial G}{\partial r} = \frac{1}{2\pi r} \Rightarrow G = \frac{1}{2\pi} \ln r \tag{1.44}$$

Eq. 1.43 is the Green's function for the Laplace equation (eq.1.39) in 3D, whereas eq. 1.44 is the Green's function of eq. 1.39 in 2D. Green's functions for a particular equation are not always so easy to find, but deriving them can greatly facilitate the solution process.

1.3 Kirchhoff Integral

Wave propagation in a free field can be described by the homogeneous wave equation derived in the above section

$$\frac{\partial^2 p'}{\partial t^2} - c^2 \nabla^2 p' = Q_P = 0 \tag{1.45}$$

where the index P in the source term Q_P indicates that this is the source term of the pressure wave equation. Wave equations can also be derived for other acoustic quantities. In that case, the source term Q_P on the RHS of eq. 1.33 changes. The proof of the Kirchhoff integral formula for a non-moving medium that follows, can be found in [2].

A free field, in acoustics, is a situation in which no sound reflections occur i.e. there are no bodies or if there are, they are very sound-absorbing. Also, the flow variables are defined everywhere in space. The free field Green's function for the wave equation is known and it can be used to solve it in free field conditions. In the presence of bodies or sources, the homogeneous wave equation is no longer valid and a source term $Q_p \neq 0$ is introduced. Also, the presence of bodies in the flow means that the flow variables are no longer defined everywhere, but rather only outside the bodies. They are not defined inside the body boundaries. That is an issue that prevents the use of the free field Green's function to solve the wave equation for the flow variables in the presence of bodies. The first step is, therefore, to create new flow variables that are defined over all space. Generalized functions are a useful tool in that direction.

Generalized functions can help us take the presence of obstacles into account. These are functions which are defined by integral properties. They are not necessarily defined at each possible argument [2]. As an example, the Heaviside function $H(x)$ (defined in eq. 1.46) has the value 0 for $x < 0$ and the value 1 for $x > 0$, but is not defined at $x = 0$. The Heaviside and delta functions are two of the most common generalized functions.

A body can be introduced through a level set function $f(\mathbf{x}, t)$ that takes a zero value on its surface, a negative value inside the body and positive values outside it.

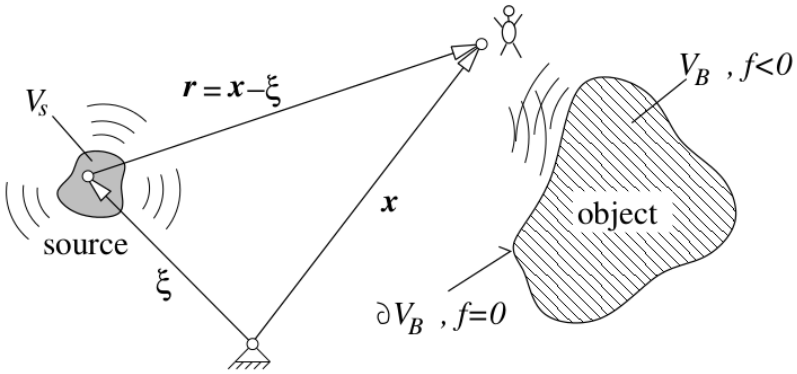

Figure 1.1: *Source, body and receiver. (From [2])*

Since the Heaviside function has the property

$$H(x) = \begin{cases} 0, & \text{if } x < 0 \\ 1, & \text{if } x > 0 \end{cases} \tag{1.46}$$

it follows that

$$H(f(\mathbf{x}, t)) = \begin{cases} 0, & \text{if } f(\mathbf{x}, t) < 0 \\ 1, & \text{if } f(\mathbf{x}, t) > 0 \end{cases} \tag{1.47}$$

This means that the Heaviside function $H(f)$ will have the value of 0 inside the body and 1 everywhere outside it. We can now define a new generalized variable for the pressure

$$\underline{p}' = H(f)p' \tag{1.48}$$

The new generalized pressure variable is - unlike p' - defined over the entire space and will be zero inside the body and equal to p' elsewhere. The fact that $\underline{p}'$ is defined everywhere in space, transforms our boundary value problem to a free field problem, the Green's function of which is already known. Thus, the wave equation can be solved as in a free field problem.

In the following part, a wave equation for the new generalized pressure variable p' is derived, by applying the wave operator on both sides of eq. 1.48. Upon doing that, the gradient and the time derivative of the Heaviside function will appear. Those two terms are calculated below.

The Dirac function can be defined using the Heaviside function as

$$\delta(x) = \frac{dH(f)}{dx}$$

and, also, has the following definition

$$\delta(x) = \begin{cases} +\infty, & \text{if } x = 0 \\ 0, & \text{if } x \neq 0 \end{cases},$$

Since the Heaviside function depends on f we have that

$$\nabla H(f) = \frac{dH(f)}{df}\nabla f = \delta(f)\nabla f \tag{1.49}$$

Also, the time derivative of the Heaviside function can be written as

$$\frac{\partial H(f)}{\partial t} = \frac{dH(f)}{df}\frac{\partial f}{\partial t} = \delta(f)\frac{\partial f}{\partial t} \tag{1.50}$$

Next step, as mentioned, is to apply the wave operator $\frac{1}{c^2}\frac{\partial^2}{\partial t^2} - \nabla^2$ on both sides of eq. 1.48. First, the second-order time derivative of the RHS is

$$\frac{1}{c^2}\frac{\partial^2}{\partial t^2}(H(f)p') = \frac{1}{c^2}\frac{\partial}{\partial t}\left[\frac{\partial}{\partial t}(Hp')\right] = \frac{1}{c^2}\frac{\partial}{\partial t}\left(p'\frac{\partial H}{\partial t}\right) + \frac{1}{c^2}\frac{\partial}{\partial t}\left(H\frac{\partial p'}{\partial t}\right) =$$

$$= \frac{1}{c^2}\left[\frac{\partial}{\partial t}\left(p'\frac{\partial H}{\partial t}\right) + \frac{\partial H}{\partial t}\frac{\partial p'}{\partial t} + H\frac{\partial^2 p'}{\partial t^2}\right]$$

The Laplacian operator applied on the RHS of eq. 1.48 gives

$$\nabla \cdot \nabla(Hp') = \nabla \cdot (p'\nabla H) + \nabla \cdot (H\nabla p') =$$

$$= \nabla \cdot (p'\nabla H) + \nabla H \cdot \nabla p' + H\nabla^2 p'$$

Therefore, the application of the wave operator on both sides of eq. 1.48, yields

$$\frac{1}{c^2}\frac{\partial^2 \underline{p}'}{\partial t^2} - \nabla^2 \underline{p}' = H\frac{1}{c^2}\frac{\partial^2 p'}{\partial t^2} - H\nabla^2 p' + \frac{1}{c^2}\frac{\partial}{\partial t}\left(p'\frac{\partial H}{\partial t}\right) + \frac{1}{c^2}\frac{\partial H}{\partial t}\frac{\partial p'}{\partial t} - \nabla\cdot(p'\nabla H) - \nabla H\cdot\nabla p'$$

Let L be the wave operator, $\frac{1}{c^2}\frac{\partial^2}{\partial t^2} - \nabla^2$; then, the above equation can be written as:

$$L[\underline{p}'] = HL[p'] + \frac{1}{c^2}\frac{\partial}{\partial t}\left(p'\frac{\partial H}{\partial t}\right) + \frac{1}{c^2}\frac{\partial H}{\partial t}\frac{\partial p'}{\partial t} - \nabla \cdot (p'\nabla H) - \nabla H \cdot \nabla p',$$

where $L[p'] = Q_P$. Using eqs. 1.49 and 1.50, we have

$$L[\underline{p}'] = HQ_p + \frac{1}{c^2}\frac{\partial}{\partial t}\left(p'\delta(f)\frac{\partial f}{\partial t}\right) + \frac{1}{c^2}\delta(f)\frac{\partial f}{\partial t}\frac{\partial p'}{\partial t} - \nabla \cdot (p'\delta(f)\nabla f) - \delta(f)\nabla f \cdot \nabla p' \tag{1.51}$$

The last four terms on the RHS of eq. 1.51 exist only on the body surface, since

they all contain the Dirac function $\delta(f)$, which is zero everywhere, except on the body surface.

Next, we evaluate the time derivative of f. The wave equation was derived under the assumption of small pressure perturbations around a mean value p_0. In the case of a deformable body, this means that any deformations of the boundary surface of the body, i.e. any perturbation of f, would have to be very small as well, as large boundary deformations would generate large pressure perturbations. Since perturbations of the surface shape -if any- have to be so small, they can safely be neglected and the body can, in effect, be considered as non-deformable in the analysis that follows. This means, that the second and third term of the RHS of eq. 1.51 also vanish, since they contain the term $\dfrac{\partial f}{\partial t}$, which is equal to zero.

The unit normal vector to the body boundary (pointing from the surface towards the receiver) is

$$\mathbf{n} = (\nabla f/|\nabla f|)_{f=0} \tag{1.52}$$

Given the above, eq. 1.51 takes the form

$$L[\underline{p}'] = H(f)Q_p - \nabla \cdot (p'\delta(f)\nabla f) - \delta(f)\nabla f \cdot \nabla p' \tag{1.53}$$

Eq. 1.53 is the non-homogeneous wave equation, written for the new generalized variable $\underline{p}'$. As stated above, what is important is that the variable $\underline{p}'$ is defined over the entire space, which allows us to solve eq. 1.53 by using the Green's function solution method for free field problems (no sound reflection). We multiply the RHS term by the free field Green's function G and integrate over all (infinite) space V_∞ and time to obtain an expression for the pressure field $\underline{p}'(\mathbf{x}, t)$. Thus, we have

$$\underline{p}'(\mathbf{x}, t) = \int_{-\infty}^{\infty} \int_{V_\infty} \big\{H(f)Q_p - \nabla_\xi \cdot (p'\delta(f)\nabla_\xi f) - \delta(f)\nabla_\xi f \cdot \nabla_\xi p'\big\} G dV(\xi) d\tau$$

or

$$\begin{aligned}\underline{p}'(\mathbf{x}, t) = \int_{-\infty}^{\infty} \int_{V_\infty} \big\{&H(f)Q_p G - [\nabla_\xi \cdot (p'\delta(f)\nabla_\xi f G) - p'\delta(f)\nabla_\xi f \cdot \nabla_\xi G] \\ &- \delta(f)\nabla_\xi f \cdot \nabla_\xi p' G\big\} dV(\xi) d\tau\end{aligned} \tag{1.54}$$

According to eq. 1.52, $\nabla_\xi f = \mathbf{n}|\nabla_\xi f|$. Eq. 1.54 therefore becomes

$$\begin{aligned}\underline{p}'(\mathbf{x}, t) = \int_{-\infty}^{\infty} \int_{V_\infty} \big\{&H(f)Q_p G - \nabla_\xi \cdot [p'\delta(f)\mathbf{n}|\nabla_\xi f|G] \\ &+ \delta(f)|\nabla_\xi f|\big[p'\mathbf{n} \cdot \nabla_\xi G - G\mathbf{n} \cdot \nabla_\xi p'\big]\big\} dV(\xi) d\tau\end{aligned} \tag{1.55}$$

Upon integrating over all space, V_∞, the second term (divergence term) in the above integral is transformed into a surface integral over the bounding surface of V_∞ (which is a surface that contains all bodies). On the bounding surface $\delta(f) = 0$,

therefore this term vanishes.We can also rewrite the terms $\mathbf{n} \cdot \nabla_\xi G$ and $\mathbf{n} \cdot \nabla_\xi p'$ as: $\mathbf{n} \cdot \nabla_\xi G = \frac{\partial G}{\partial n}$ and $\mathbf{n} \cdot \nabla_\xi p' = \frac{\partial p'}{\partial n}$. Eq. 1.55 now becomes:

$$\underline{p}'(\mathbf{x}, t) = \int_{-\infty}^{\infty} \int_{V_\infty} \left\{ H(f) Q_p G + \delta(f) |\nabla_\xi f| \left[p' \frac{\partial G}{\partial n} - G \frac{\partial p'}{\partial n} \right] \right\} dV(\xi) d\tau \Rightarrow$$

$$\underline{p}'(\mathbf{x}, t) = \int_{-\infty}^{\infty} \left\{ \int_{V_\infty} H(f) Q_p G dV(\xi) + \int_{V_\infty} \delta(f) |\nabla_\xi f| \left[p' \frac{\partial G}{\partial n} - G \frac{\partial p'}{\partial n} \right] dV(\xi) \right\} d\tau \tag{1.56}$$

Since the source term Q_p is non-zero only within the source volume V_S, which is of finite extent, it follows that

$$\int_{V_\infty} H(f) Q_p G dV(\xi) = \int_{V_S} H(f) Q_p G dV(\xi)$$

Relation

$$\int_{V_\infty} g(\mathbf{x}) \delta(f(\mathbf{x})) dV = \sum_{S_i(f=0)} \int_{S_i} g(\mathbf{x}_S) \frac{1}{|\nabla f|_{\mathbf{x}_s}} dS \tag{1.57}$$

can be used to transfer a volume integration to the surface S defined by $f = 0$, (i.e. the surface of the body). Thus, the second volume integral can be reduced to a surface one. An explanation about the derivation of eq. 1.57 can be found in [2]. Therefore

$$\int_{V_\infty} \delta(f) |\nabla_\xi f| \left[p' \frac{\partial G}{\partial n} - G \frac{\partial p'}{\partial n} \right] dV(\xi) = \int\limits_{\partial V_B : f=0} \left(p' \frac{\partial G}{\partial n} - G \frac{\partial p'}{\partial n} \right) dS(\xi)$$

Eq. 1.56 now becomes

$$\underline{p}'(\mathbf{x}, t) = \int_{-\infty}^{\infty} \left\{ \int_{V_S} H(f) Q_p G dV(\xi) + \int\limits_{\partial V_B : f=0} \left(p' \frac{\partial G}{\partial n} - G \frac{\partial p'}{\partial n} \right) dS(\xi) \right\} d\tau \tag{1.58}$$

The volume integral in eq. 1.58 contains the source term Q_P multiplied by the Heaviside function. It should be pointed out that, from its definition in eq. 1.47, the Heaviside function is equal to 1 anywhere outside the body. Since the source V_S is outside the body V_B, $H(f)$ will be non-zero inside V_S. Therefore, the volume integral in eq. 1.58 is non-zero. If the Heaviside function was defined on another surface V_H, for instance a surface including both the source and body seen in fig. 1.1, then the volume integral in eq. 1.58 would vanish, since $H(f)$ would be zero anywhere inside V_H, including the source volume V_S.

The second integral in eq. 1.58, is a surface one. The integration surface is the surface on which $f = 0$, i.e. the body surface.

The Green's function for the 3D case is equal to $G_0 = \delta(g)/(4\pi r)$, where $g = t - \tau - r/c$ and $r = |\mathbf{x} - \xi|$ is the distance between source and receiver. By inserting G_0 into eq. 1.58, the following form of the equation can be derived.

Before doing so, let us reformulate some terms:

$$\begin{aligned} p'\frac{\partial G_0}{\partial n} &= p'\frac{\partial G_0}{\partial r}\frac{\partial r}{\partial n} = \frac{p'}{4\pi}\left(\frac{\partial}{\partial r}\left(\frac{\delta(g)}{r}\right)\right)\frac{\partial r}{\partial n} = \frac{p'}{4\pi}\left(\frac{\partial \delta(g)}{\partial r}\frac{1}{r} + \delta(g)\frac{\partial}{\partial r}\left(\frac{1}{r}\right)\right)\frac{\partial r}{\partial n} \\ &= \frac{p'}{4\pi}\left(\frac{d\delta(g)}{dg}\frac{\partial g}{\partial r}\frac{1}{r} - \frac{\delta(g)}{r^2}\right)\frac{\partial r}{\partial n} = \frac{p'}{4\pi}\left(\frac{d\delta(g)}{dg}\frac{\partial}{\partial r}\left(\tau - t + \frac{r}{c}\right)\frac{1}{r} - \frac{\delta(g)}{r^2}\right)\frac{\partial r}{\partial n} \\ &= \frac{p'}{4\pi}\left(\frac{d\delta(g)}{dg}\frac{1}{cr} - \frac{\delta(g)}{r^2}\right)\frac{\partial r}{\partial n} \end{aligned}$$

where $dg = \dfrac{dg}{d\tau}d\tau = \dfrac{d}{d\tau}\left(\tau - t + \dfrac{r}{c}\right)d\tau \Rightarrow dg = 1 \cdot d\tau = d\tau$

Therefore,

$$p'\frac{\partial G_0}{\partial n} = \frac{1}{4\pi}\left(p'\frac{d\delta}{d\tau}\frac{1}{cr} - p'\frac{\delta}{r^2}\right)\frac{\partial r}{\partial n} \tag{1.59}$$

The partial derivative $\frac{\partial r}{\partial n}$ can be written as:

$$\frac{\partial r}{\partial n} = \mathbf{n}\cdot\nabla_\xi r = -\mathbf{n}\cdot\nabla_x r = -\mathbf{n}\cdot\mathbf{e}_r = -\frac{\mathbf{r}\cdot\mathbf{n}}{r} \tag{1.60}$$

Term $p'\dfrac{d\delta}{d\tau}\dfrac{1}{cr}$ which appears on the RHS side of eq. 1.59 can be written as:

$$p'\frac{d\delta}{d\tau}\frac{1}{cr} = \frac{1}{cr}\left(\frac{\partial(p'\delta)}{\partial\tau} - \delta\frac{\partial p'}{\partial\tau}\right)$$

Therefore, eq. 1.59 becomes

$$p'\frac{\partial G_0}{\partial n} = \frac{1}{4\pi}\left(\frac{1}{cr}\frac{\partial(p'\delta)}{\partial\tau} - \frac{1}{cr}\delta\frac{\partial p'}{\partial\tau} - p'\frac{\delta}{r^2}\right)\frac{\partial r}{\partial n} \tag{1.61}$$

Term $\dfrac{1}{cr}\dfrac{\partial(p'\delta)}{\partial\tau}$ appearing on the r.h.s. of eq. 1.61 vanishes upon integration over τ , because a physical signal cannot have existed for all times, i.e $p'(\tau = -\infty) = 0$.

Eq. 1.58 can now be rewritten as:

$$\underline{p}'(\mathbf{x},t) = \int_{V_S} H(f)\frac{Q_p(\tau,\xi)}{4\pi r}dV(\xi) + \int\limits_{\partial V_B: f=0} \left(\frac{1}{4\pi}\left(-\frac{1}{cr}\delta\frac{\partial p'}{\partial \tau} - p'\frac{\delta}{r^2}\right)\frac{\partial r}{\partial n} - \frac{\delta}{4\pi r}\frac{\partial p'}{\partial n}\right)dS(\xi) \Rightarrow$$

$$\underline{p}'(\mathbf{x},t) = \int\limits_{V_S} H(f)\frac{Q_p(\tau,\xi)}{4\pi r}dV(\xi) + \frac{1}{4\pi}\int\limits_{\partial V_B: f=0} \left(-\frac{1}{cr}\delta\frac{\partial p'}{\partial \tau}\frac{\partial r}{\partial n} - p'\frac{\delta}{r^2}\frac{\partial r}{\partial n} - \frac{\delta}{r}\frac{\partial p'}{\partial n}\right)dS(\xi)$$

Using eq. 1.60, the above equation finally takes the form:

$$\underline{p}'(\mathbf{x},t) = \int\limits_{V_S} H(f)\frac{Q_p(\tau,\xi)}{4\pi r}dV(\xi) + \frac{1}{4\pi}\int\limits_{\partial V_B: f=0} \left(\frac{\mathbf{r}\cdot\mathbf{n}}{r^3}p' + \frac{\mathbf{r}\cdot\mathbf{n}}{cr^2}\frac{\partial p'}{\partial \tau} - \frac{1}{r}\frac{\partial p'}{\partial n}\right)dS(\xi) \tag{1.62}$$

There are two terms in eq. 1.62. The first is a volume integral which corresponds to the influence of the source and a surface integral, roughly summing the pressures and their derivatives on the Kirchhoff integration surface. In the above analysis, the integration surface chosen was that of the body. Since that integration surface does not contain the source, the presence of the volume integral in eq. 1.62, is intuitively expected so that the presence of the source can be taken into account.

It is also logical that, if the integration surface was chosen so that the source was included inside it, only the second (surface) integral in eq. 1.62 would remain. That is easy to prove mathematically as was done right after the derivation of eq. 1.62 (the Heaviside function which multiplies the source term will be zero inside V_S), but can also be intuitively understood. If the integration surface is chosen to contain the source, the contribution of the source term is taken into account when summing the pressure and its derivatives on the new integration surface, because these will be influenced by everything contained in it. Therefore, the source contribution does not have to be added as a separate volume integral.

The Kirchhoff integral can be seen as a special case of 1.62, where the integration surface contains not only the bodies V_B but also any sources V_S. The new integration volume, containing both bodies and sources, is symbolized with V_H. Because the source is placed inside V_H, the volume integral in eq. 1.62 vanishes as mentioned above during the evaluation of eq. 1.62 for V_H instead of V_B.

Therefore, eq. 1.62 takes the form:

$$\underline{p}'(\mathbf{x},t) = \frac{1}{4\pi} \int\limits_{\partial V_B : f=0} \left(\frac{\mathbf{r}\cdot\mathbf{n}}{r^3} p' + \frac{\mathbf{r}\cdot\mathbf{n}}{cr^2}\frac{\partial p'}{\partial \tau} - \frac{1}{r}\frac{\partial p'}{\partial n} \right) dS(\xi) \tag{1.63}$$

Eq. 1.63 has been derived for a medium at rest, a stationary receiver and a non-moving integration surface and allows the computation of the pressure at any receiver position outside a closed integration surface containing all bodies and sources, if the pressure perturbation p' and the pressure perturbation derivatives $\frac{\partial p'}{\partial \tau}$ and $\frac{\partial p'}{\partial n}$ on the surface are known.

The Kirchhoff formula for a non-moving Kirchhoff surface and an observer at rest in a medium in uniform flow, can be derived in a similar fashion to eq. 1.63 [2] and is given by the following formula

$$\underline{p}'(\mathbf{x},t) = \frac{1}{4\pi} \int\limits_{\partial V_B : f=0} \left[\frac{1}{cr^*} \left(M_n + \frac{\mathbf{r}\cdot\mathbf{n}}{r^*} \right) \frac{\partial p'}{\partial \tau} + \frac{(1-M^2)\mathbf{r}\cdot\mathbf{n}}{{r^*}^3} p' + \frac{M_n}{r^*} \mathbf{M}\cdot\nabla_\xi p' - \frac{1}{r^*}\frac{\partial p'}{\partial n} \right] dS(\xi) \tag{1.64}$$

where $M_n = \mathbf{n}\cdot\mathbf{M}$ is the surface normal component of the Mach number of the medium and $r^* = \sqrt{(\mathbf{M}\cdot\mathbf{r})^2 + (1-M^2)\mathbf{r}^2}$

1.4 Monopoles

A monopole is a source that radiates sound equally well in all directions. The simplest example of a monopole would be a sphere whose radius alternately contracts and expands sinusoidally, removing and introducing fluid into the surrounding area respectively. A boxed loudspeaker also acts as an omnidirectional monopole source at low frequencies. The equation giving the velocity potential induced by a monopole is derived in the following manner: Let us consider the non-homogeneous wave equation with a source term Q. According to the Green's function method, the solution to the wave equation

$$\frac{\partial^2 \phi}{\partial t^2} - c^2 \nabla^2 \phi = Q$$

is

$$\phi(\mathbf{x},t) = \int\limits_{V_\infty} \int\limits_{-\infty}^{t^+} G(\mathbf{x}-\boldsymbol{\xi}, t-\tau) Q(\boldsymbol{\xi},\tau) dV(\boldsymbol{\xi}) d\tau \tag{1.65}$$

where $\boldsymbol{x}$ is the position vector of the receiver and $\boldsymbol{\xi}$ is that of the source. The distance between source and receiver is symbolized by $r = |\boldsymbol{x} - \boldsymbol{\xi}|$

The 3D Green's function for the wave equation is given by the following equation:

$$G(\mathbf{x}-\boldsymbol{\xi},\tau-t)=\frac{\delta(\tau-t+|\mathbf{x}-\boldsymbol{\xi}|/c)}{4\pi|\mathbf{x}-\boldsymbol{\xi}|}$$

Thus eq. 1.65 becomes:

$$\phi(\mathbf{x},t)=\int_{V_\infty}\int_{-\infty}^{t^+}\frac{\delta(\tau-t+|\mathbf{x}-\boldsymbol{\xi}|/c)}{4\pi|\mathbf{x}-\boldsymbol{\xi}|}Q(\boldsymbol{\xi},\tau)dV(\boldsymbol{\xi})d\tau=\int_{V_\infty}\frac{Q(\boldsymbol{\xi},t-|\mathbf{x}-\boldsymbol{\xi}|/c)}{4\pi|\mathbf{x}-\boldsymbol{\xi}|}dV(\boldsymbol{\xi})$$

If the source $Q(\mathbf{x},t)$ is at the origin, then $Q(\mathbf{x},t)=q(t)\delta(x)$ and, from the above equation, the velocity potential is:

$$\phi(\mathbf{x},t)=\int_{V_\infty}\frac{q(t-|\mathbf{x}-\boldsymbol{\xi}|/c)\delta(x)}{4\pi|\mathbf{x}-\boldsymbol{\xi}|}dV(\boldsymbol{\xi})=\frac{q(t-|\mathbf{x}-\boldsymbol{\xi}|/c)}{4\pi|\mathbf{x}-\boldsymbol{\xi}|}\Rightarrow$$

$$\phi(\mathbf{x},t)=\frac{1}{4\pi r}q(t-r/c) \tag{1.66}$$

Time $t-r/c$ is referred to as the "retarded time". A signal that reaches the receiver at time t has been emitted by the source at time $t-r/c$, where r is the distance between source and receiver and c is the speed of sound. In other words, the signal needs time r/c to travel the distance between source and receiver.

If q is a simple harmonic function of time, then $q(t-r/c)=Ae^{i\omega(t-r/c)}$ and eq. 1.66 can be rewritten as:

$$\phi(\mathbf{x},t)=\frac{A}{4\pi r}e^{i\omega(t-r/c)} \tag{1.67}$$

This is the pressure field generated by a monopole - a single source which is concentrated at one point and whose amplitude changes sinusoidally with time. A monopole is a source that radiates sound equally well in all directions. This can be seen from eq. 1.67, where there is no dependence of the pressure perturbation on the orientation of the vector between monopole and receiver.

1.5 Dipoles

A dipole can be seen as two monopoles with equal but opposite strengths q positioned close together(at a small distance compared to the wavelength of sound). While one source expands the other source contracts and the surrounding fluid is moved back and forth, producing sound. A physical example of a dipole would be an unboxed loudspeaker (while the front is pushing out, the back is sucking inwards). A sphere oscillating back and forth also acts as a dipole.
A dipole does not radiate sound equally well in all directions. A receiver standing

on the dipole oscillation axis, at a distance r from the dipole, will perceive a much more intense sound than any other receiver who is at the same distance from the dipole, but is not standing on the oscillation axis. A receiver standing on an axis perpendicular to the dipole oscillation axis will perceive no sound at all. Therefore, the dipole directivity pattern therefore has the form shown in fig. 1.2.

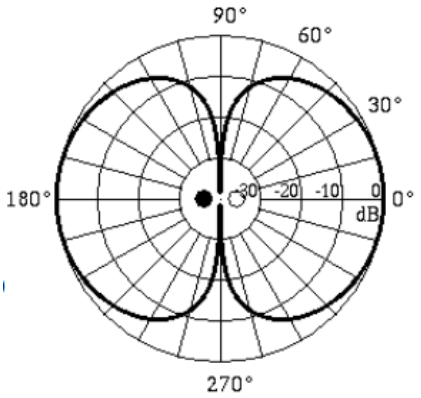

Figure 1.2: *Dipole directivity pattern. (From [2])*

In fig. 1.2 the dipole oscillation axis is horizontal, therefore the maximum sound is perceived on that axis. At 90° and 270° i.e. vertical to the dipole oscillation axis, the radiated sound is minimal - almost zero.

Let us now derive the dipole equation (see [5]). Two monopoles of equal and opposite strengths $q(t)$ and $-q(t)$ are positioned at a small distance from each other. The monopole of strength $-q(t)$ is placed at $\boldsymbol{x}$ and the one with strength $q(t)$ is placed at $(\boldsymbol{x} + \mathbf{d})$. The distance between the receiver and the first monopole is r, whereas the distance between receiver and second monopole is $r + \delta r$. The pressure fluctuations caused by the two monopoles can be superimposed and the pressure fluctuation for the dipole can be written as

$$4\pi\phi = \frac{q(t - (r + \delta r)/c)}{r + \delta r} - \frac{q(t - r/c)}{r} \tag{1.68}$$

Since the distance $|\mathbf{d}|$ between the two monopoles is sufficiently small, one can use FD to express $\frac{\partial}{\partial x_i}\left[\frac{q(t-R/c)}{R}\right]$ as follows :

$$\frac{\partial}{\partial x_i}\left[\frac{q(t - r/c)}{r}\right] = \frac{\dfrac{q(t - (r + \delta r)/c)}{r + \delta r} - \dfrac{q(t - r/c)}{r}}{x_i + d_i - x_i}$$

Therefore:

$$\frac{q(t - (r + \delta r)/c)}{r + \delta r} - \frac{q(t - r/c)}{r} = d_i \frac{\partial}{\partial x_i}\left[\frac{q(t - r/c)}{r}\right]$$

With q being a simple harmonic function of time, i.e. $q(t - r/c) = Ae^{i\omega(t-r/c)}$, eq.1.68 becomes

$$\phi(\mathbf{x}, t) = d_i \frac{\partial}{\partial x_i} \left[\frac{Ae^{i\omega(t-r/c)}}{4\pi r} \right]$$

or using a different notation:

$$\phi(\mathbf{x}, t) = \nabla \left[\frac{A}{4\pi r} e^{i\omega(t-r/c)} \right] \cdot \mathbf{d}$$

Chapter 2

Noise Prediction Results

In the present chapter, the KIM is used to compute the aeroacoustic pressure perturbation caused by a monopole and a dipole source, at a receiver. In the case of monopoles and dipoles, analytical equations giving the pressure perturbation caused by the source at any position, are also available. This allows the comparison of the results obtained through the KIM to those yielded by use of the analytical relations. Using simple acoustic sources with known analytical solution to check the validity of aeroacoustic computation is common practice (see [6], [7] and [8]). Next, optimization of the source position is performed, to find a position which gives a desired "target" pressure perturbation at a receiver position. The optimization algorithm used is the steepest descent method.

Deterministic optimization methods use the derivatives of the objective function F w.r.t. the design variables b_n i.e. $\delta F/\delta b_n$. To find a local minimum of a function F using steepest descent, one takes steps proportional to the negative of the gradient of the function at the current point. The design variables are therefore renewed based on the values of the sensitivity derivatives as follows

$$b_n^{new} = b_n^{old} - \eta \ \delta F/\delta b_n \tag{2.1}$$

The sensitivity derivatives are computed through analytical differentiation of the KI and, also, through FD for the purpose of comparison. The noise propagation is examined for a quiescent fluid in 3D space.

2.1 Pressure Perturbation Generated by a Dipole - Analytical Solution Compared with the KI

2.1.1 Mathematical Formulation

The velocity potential induced by a dipole with directivity vector $\vec{d}$ (i.e. oscillation axis), is given by the following equation (see [8])

$$\phi(x,t) = \nabla\left(\frac{A}{4\pi R^*}e^{\left[i\omega\left(t-\frac{R}{c}\right)\right]}\right)\cdot\vec{d} \tag{2.2}$$

The pressure perturbation at the receiver position $\vec{x}$ and time t can be derived using the linearized Bernoulli equation and is

$$p'(\vec{x},t) = -\rho_0\left[\frac{\partial\phi}{\partial t} + \vec{V}\cdot\nabla\phi\right] \tag{2.3}$$

where $\vec{V} = (V_1, V_2, V_3)$ is the mean flow speed along the x, y, and z axis respectively. Without loss of generality, it can be assumed that the mean flow is along the x direction. Eq. 2.3 then becomes

$$p'(\vec{x},t) = -\rho_0\left[\frac{\partial\phi}{\partial t} + V_x\frac{\partial\phi}{\partial x}\right] \tag{2.4}$$

where:

ρ_0 is the fluid density

A is the dipole oscillation amplitude

ω is the dipole oscillation frequency

M_0 is the Mach number defined as $M_0 = |\vec{V}|/c_0$

$\beta = \sqrt{1 - {M_0}^2}$

Assuming that the dipole is placed at $(0,0,0)$, R and R^* are defined as follows (see [9]):

$$R^* = \sqrt{x^2 + \beta^2(y^2+z^2)} \tag{2.5}$$

$$R = [-M_0 x + R^*]/\beta^2 \tag{2.6}$$

For very low Mach numbers (low flow speed compared to the speed of sound in the medium), β becomes 1 and both R^* and R tend to coincide with the distance between dipole and receiver $d = \sqrt{x^2+y^2+z^2}$.

Eq. 2.2 can be rewritten as:

$$\phi(x,t) = \nabla\psi\cdot\vec{d} = \nabla(\psi_1\psi_2)\cdot\vec{d}$$

where $\psi_1 = \dfrac{A}{4\pi R^*}$ and $\psi_2 = e^{\left[i\omega\left(t-\frac{R}{c_0}\right)\right]}$

The gradient of ψ can be written as: $\nabla\psi = \psi_1\cdot\nabla\psi_2 + \psi_2\cdot\nabla\psi_1$, where

$$\psi_1 = \psi_1(R^*) \ , \ \psi_2 = \psi_2(R)$$

$$\nabla\psi_1 = \frac{\partial\psi_1}{\partial R^*}\nabla R^* \Rightarrow \nabla\psi_1 = -\frac{A}{4\pi{(R^*)}^2}\nabla R^*$$

$$\nabla\psi_2 = \frac{\partial\psi_2}{\partial R}\nabla R \Rightarrow \nabla\psi_2 = -\frac{i\omega}{c_0}e^{\left[i\omega\left(t-\frac{R}{c_0}\right)\right]}\nabla R \Rightarrow \nabla\psi_2 = -\frac{i\omega}{c_0}\psi_2\nabla R$$

where

$$\nabla R = \frac{\partial R}{\partial R^*}\nabla R^* + \left(\frac{-M_0}{\beta^2}, 0, 0\right)$$

The gradient of ψ is:

$$\nabla\psi = -\left[i\psi_1\frac{\omega}{c_0}\frac{\partial R}{\partial R^*} + \frac{A}{4\pi(R^*)^2}\right]\psi_2\nabla R^* + \psi_1\psi_2\frac{i\omega}{c_0}\left(\frac{M_0}{\beta^2}, 0, 0\right)$$

where $\nabla R^* = \frac{1}{R^*}(x, \beta^2 y, \beta^2 z)$ and $\frac{\partial R}{\partial R^*} = \frac{1}{\beta^2}$

Thus, the velocity potential can finally be written as:

$$\phi = -\left[i\psi_1\frac{\omega}{c_0}\frac{1}{\beta^2} + \frac{A}{4\pi(R^*)^2}\right]\psi_2\frac{1}{R^*}(xd_x + \beta^2(yd_y + zd_z)) + \psi_1\psi_2\frac{i\omega}{c_0\beta^2}M_0 d_x \quad (2.7)$$

The time derivative of ϕ can be computed as follows:

$$\phi(x,t) = \nabla\psi\cdot\vec{d} \Rightarrow \frac{\partial\phi}{\partial t} = \frac{\partial}{\partial t}(\nabla\psi\cdot\vec{d}) = \nabla\left(\frac{\partial\psi}{\partial t}\right)\cdot\vec{d}$$

Since only ψ_2 is a function of time,

$$\frac{\partial\psi}{\partial t} = \psi_1\frac{\partial\psi_2}{\partial t} = i\omega\psi_1\psi_2 = i\omega\psi \Rightarrow$$

$$\frac{\partial\phi}{\partial t} = \nabla(i\omega\psi_1\psi_2)\cdot\vec{d} = i\omega\nabla\psi\cdot\vec{d} = i\omega\phi$$

In order to compute the pressure from eq. 2.4,the partial derivative $\frac{\partial\phi}{\partial x}$ should be computed. Eq. 2.7 can be rewritten as:

$$\phi = -\Lambda_1\psi_2\frac{1}{R^*}\Lambda_2 + i\psi_1\psi_2\frac{\omega M_0}{c\beta^2}d_x,$$

where

$$\Lambda_1 = i\psi_1\frac{\omega}{c_0\beta^2} + \frac{A}{4\pi(R^*)^2}$$

and

$$\Lambda_2 = xd_x + \beta^2(yd_y + zd_z)$$

The spatial derivative of ϕ w.r.t x is:

$$\begin{aligned}\frac{\partial\phi}{\partial x} =& -\frac{\partial\Lambda_1}{\partial x}\psi_2\frac{1}{R^*}\Lambda_2 - \Lambda_1\frac{\partial\psi_2}{\partial x}\frac{1}{R^*}\Lambda_2 + \Lambda_1\psi_2\frac{1}{(R^*)^2}\frac{\partial R^*}{\partial x}\Lambda_2 \\ & - \Lambda_1\psi_2\frac{1}{R^*}\frac{\partial\Lambda_2}{\partial x} + i\frac{\partial\psi_1}{\partial x}\psi_2\frac{\omega}{c_0\beta^2}M_0 d_x + i\psi_1\frac{\partial\psi_2}{\partial x}\frac{\omega}{c_0\beta^2}M_0 d_x\end{aligned} \tag{2.8}$$

where

$$\frac{\partial R^*}{\partial x} = \frac{x}{R^*}$$

$$\frac{\partial\Lambda_2}{\partial x} = d_x$$

$$\frac{\partial\psi_1}{\partial x} = \frac{\partial\psi_1}{\partial R^*}\frac{\partial R^*}{\partial x} = -\frac{Ax}{4\pi(R^*)^3}$$

$$\frac{\partial\psi_2}{\partial x} = -\psi_2\frac{i\omega}{c_0}\frac{\partial R}{\partial x} = -\psi_2\frac{i\omega}{c_0}\frac{1}{\beta^2}\left[-M_0 + \frac{\partial R^*}{\partial x}\right]$$

$$\frac{\partial\Lambda_1}{\partial x} = \frac{i\omega}{c_0\beta^2}\frac{\partial\psi_1}{\partial x} - \frac{2A}{4\pi(R^*)^3}\frac{\partial R^*}{\partial x} = -\frac{Ax}{2\pi(R^*)^3}\left[\frac{i\omega}{2c_0\beta^2} + \frac{1}{R^*}\right]$$

The pressure perturbation can analytically be computed from eq. 2.4 at any point $\vec{x}$ and time t. The analytical computations can be compared with the outcome of the KI formula (eq. 1.63). To that end, a Fortran code was written, which performs both analytical and KI-based computation of the pressure at an receiver, and compares the two as follows: The analytical expressions are used to compute the pressure perturbation:

- at an receiver position $\vec{x} = (x, y, z)$
- at the nodes of a spherical surface grid, centered at the dipole location.

The spherical surface acts as our KI surface. By integrating on it, the pressure perturbation at the receiver position $\vec{x} = (x, y, z)$ is computed.

The pressure perturbation at receiver position $\vec{x} = (x, y, z)$ through the use of KI is given by the equation:

$$p'(\vec{x}, t) = \frac{1}{4\pi}\int_S \left[\frac{\vec{r}\cdot\hat{n}}{r}\frac{p'(\vec{x},\tau)}{r^2} + \frac{\vec{r}\cdot\hat{n}}{c_0 r^2}\frac{\partial p'}{\partial t}(\vec{x},\tau) - \frac{1}{r}\frac{\partial p'}{\partial n}(\vec{x},\tau)\right] dS$$

All terms in the integral must be computed at the retarded time τ, which is the emission time of the signal that reaches the receiver at time t. The retarded time is $\tau = t - \frac{r}{c_0}$, where r is the distance between the receiver and each integration surface node. Using the dipole equations, the pressure and pressure derivatives at the receiver time t are obtained. Their values at the retarded time τ are computed through linear interpolation.

Regarding the terms needed for the integration:

- The pressure perturbation $p'(\vec{x},t)$ is computed at all the nodes of the KI surface, by use of the analytical dipole equations as described above. It is easy to interpolate and obtain the pressure perturbation $p'(\vec{x},\tau)$ at retarded time.

- The time derivative of $p'(\vec{x},t)$, $\frac{\partial p'}{\partial t}(\vec{x},\tau)$, is computed through use of FD and linear interpolation in time, in order to obtain its value at the retarded time τ.

- The normal derivative $\frac{\partial p'}{\partial n}(\vec{x},\tau)$ is equal to:

$$\frac{\partial p'}{\partial n} = \nabla p' \cdot \hat{n} \Rightarrow \frac{\partial p'}{\partial n} = \frac{\partial p'}{\partial x} n_x + \frac{\partial p'}{\partial y} n_y + \frac{\partial p'}{\partial z} n_z$$

  where $\hat{n}$ is the unit normal vector of each integration element dS. The gradient $\nabla p'$ is computed through FD and then used to obtain the normal derivative $\frac{\partial p'}{\partial n}$. Again, the gradient at retarded time τ is linearly interpolated.

2.1.2 Results

Directivity pattern and pressure perturbation intensity

The subsequent computations have been made with the use of the analytical formulas that have so far been presented in this section, for a source in quiescent medium with the following characteristics

- dipole oscillation axis orientation (1,0,0) i.e. x-axis
- oscillation frequency $\omega = 2 rad/sec$
- oscillation amplitude $A = 0.05m$
- source position (0,0,0)

The dipole directivity pattern, computed by the code is presented in fig. 2.1

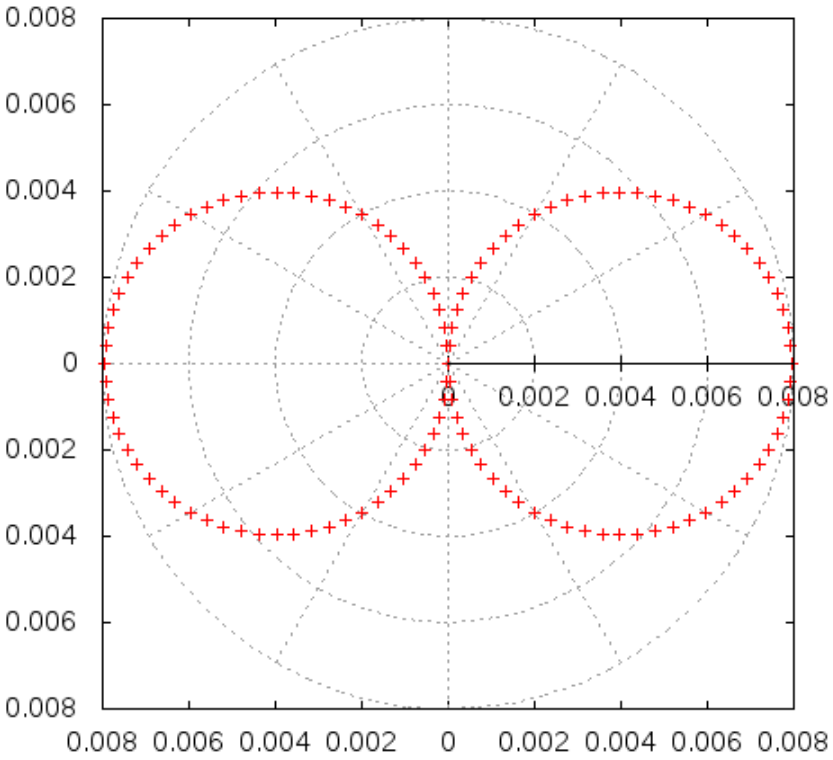

Figure 2.1: *Dipole source. Polar plot of dipole directivity pattern in non-moving medium on the x-y plane. The dipole is placed at (0,0,0) and oscillates along the x-axis (horizontal). For a fixed receiver - source distance, maximum pressure perturbation is perceived on the dipole oscillation axis. Receivers placed on the y-axis (vertical one) receive no pressure perturbation.*

The directivity pattern is produced by keeping the receiver at a constant distance of 1m from the source, but changing the angle θ (using a step $d\theta = 3^o$) that the vector pointing from the source to the receiver forms with the dipole oscillation axis.

As can be seen from the fig. 2.1, if the receiver is not placed on the dipole oscillation axis, it will have to be moved closer to the dipole in order to record the same pressure perturbation magnitude as a receiver placed on the oscillation axis.

In fig. 2.2 the pressure time series at a receiver kept at a constant distance of 7m from the source, but placed at three different angles $\theta = 0^o$, $\theta = 45^o$ and $\theta = 90^o$ is shown. The receiver is displaced on the x-y plane to produce the directivity pattern.

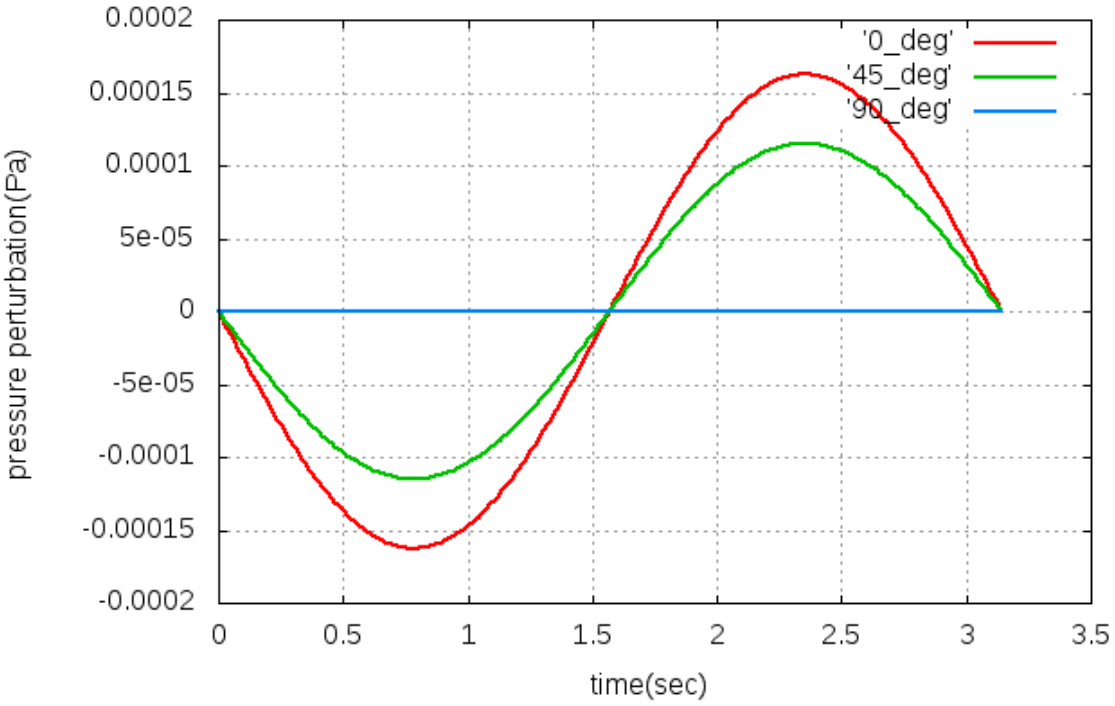

Figure 2.2: *Dipole source. Pressure perturbation time-series at a receiver placed at three different angles $\theta = 0^o$, $\theta = 45^o$ and $\theta = 90^o$ relative to the oscillation axis. The receiver - source distance is kept constant (7m) and the source is placed at (0,0,0). The computations were done using the analytical eqs. 2.2 and 2.3. The maximum pressure perturbation (red curve) occurs on the oscillation axis. The blue curve corresponds to an angle $\theta = 90^o$ where, as expected, no pressure perturbation is perceived.*

Analytical results compared with the KI

As already mentioned in section 1.3, the KIM allows the computation of the pressure perturbation at any receiver position outside a closed integration surface containing all bodies and sources, if the pressure perturbation p' and the pressure perturbation derivatives $\frac{\partial p'}{\partial \tau}$ and $\frac{\partial p'}{\partial n}$ on the surface are known. The KIM is now applied i n order to compare the pressure perturbation time-series at an receiver with the time-series at the receiver obtained by directly using the analytical equations 2.2 to 2.8. It is reminded that the used KI surface is a sphere of radius 1, with the source placed at its center.

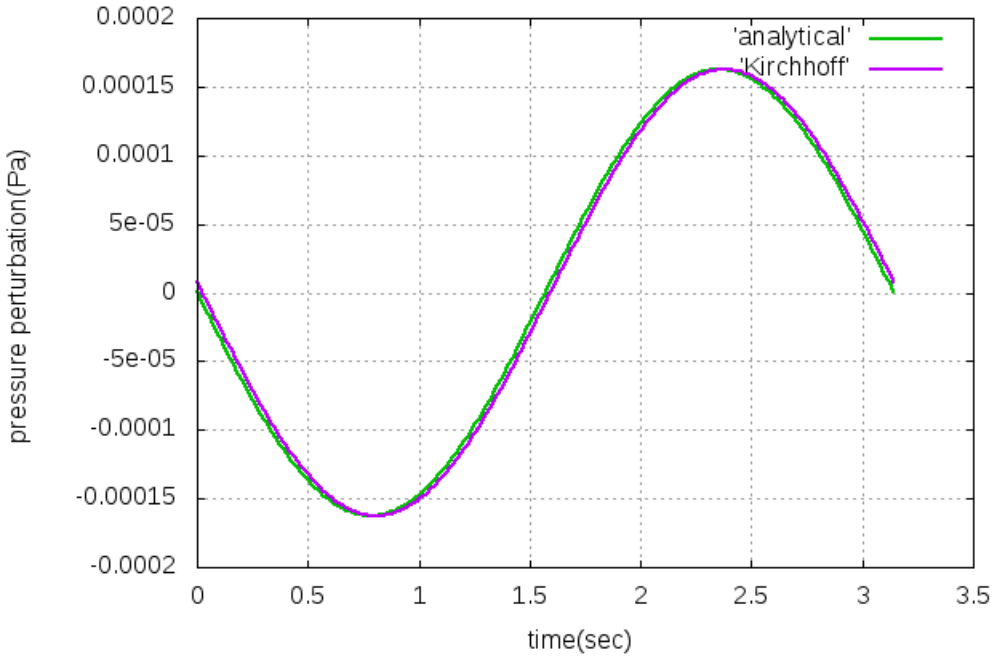

Figure 2.3: *Dipole source. Pressure perturbation time series at a receiver. It can be seen that the time series produced through the use of the KIM (purple curve) almost completely coincides with the results obtained through the use of the analytical relations (green line). The source is placed at (0,0,0) whereas the receiver at (7,0,0).*

As can be seen the KIM and the analytical formula produce almost identical results, which verifies the correctness of the way the KIM was implemented in the created Fortran KI code for the aeroacoustic pressure perturbation computation.

2.2 Computing the Optimal Dipole Position for a User-Defined Target Pressure at the Receiver

Having the tools to compute the pressure perturbation at any desired receiver position, either through the KIM, or the analytical equations 2.2 to 2.8, the next step is to proceed to optimize the source position with the aim of obtaining a desired pressure time series at the receiver. The optimization process can be described as follows:

- The source was initially placed at (0,0,0) and the pressure perturbation time series at the receiver placed at (7,0,0) was computed.

- The computed time-series was stored and set as desired target pressure time-series at the receiver position.

- The source was then placed at a position other that the initial, thus evoking a pressure time-series at the receiver, different than the target time-series set in the previous step.
- The sensitivity derivatives of the pressure perturbation at the receiver w.r.t the source coordinates are computed either with the use of FD or through the direct differentiation of the KI expression (eq.1.63) w.r.t the source coordinates. Those two processes will be described in more detail in the text that follows.
- Having obtained the sensitivity derivatives, the steepest descent method was used to update the design variables (i.e. the source coordinates), in a way that will lead to the minimization of the difference between pressure perceived at the receiver and the target pressure.

To begin with the optimization precess, an objective function to be minimized must be defined. Since the aim is for the pressure time-series at the receiver $p = p(t)$ to coincide with the target time-series, it makes sense to define an objective function dependent on the squared difference of the two time series. Thus, the objective function J is expressed as:

$$J = \frac{1}{T}\int_0^T (p' - p'_t)^2 dt \tag{2.9}$$

Not squaring the difference would allow the objective to take negative values and a zero pressure time series $p'(t)$ does indeed minimize a quantity that can be negative, thus preventing us from ending up with a time series that matches the target one p'_t.

Our design variables $b_n = (b_1, b_2, b_3)$, as already mentioned, are our source coordinates (x_s, y_s, z_s) and are updated using the steepest descent method as

$$b_1^{new} = x_s^{new} = x_s^{old} - \eta\frac{\delta J}{\delta b_1}$$

$$b_2^{new} = y_s^{new} = y_s^{old} - \eta\frac{\delta J}{\delta b_2}$$

$$b_3^{new} = z_s^{new} = z_s^{old} - \eta\frac{\delta J}{\delta b_3}$$

The derivatives $\frac{\delta J}{\delta b_n} = (\frac{\delta J}{\delta b_1}, \frac{\delta J}{\delta b_2}, \frac{\delta J}{\delta b_3})$ are computed from eq. 2.9 in the following manner

$$J = \frac{1}{T}\int_0^T (p' - p'_t)^2 dt \Rightarrow \frac{\delta J}{\delta b_n} = \frac{1}{T}\int_0^T 2(p' - p'_t)\frac{\delta(p' - p'_t)}{\delta b_n} dt \Rightarrow \tag{2.10}$$

$$\frac{\delta J}{\delta b_n} = \frac{1}{T}\int_0^T 2(p' - p'_t)\frac{\delta p'}{\delta b_n}dt \tag{2.11}$$

The computation of $\frac{\delta J}{\delta b_n}$ and the application of steepest descent therefore requires the computation of the derivatives $\frac{\delta p'}{\delta b_n}$. This computation is implemented in two ways in the code: first, through the FD and, then, by directly differentiating the analytical formula of the KI (eq.1.63).

Finite Differences
Applying the FD method is fairly simple. Since the pressure can be computed at any point, either analytically or through the use of the KIM, the sensitivity derivatives i.e the total derivative of the pressure at the receiver position w.r.t the design variable $b_1 = x_s$ for instance can be expressed as

$$\frac{\delta p'}{\delta b_1} = \frac{p'_2 - p'_1}{db_1}$$

where p'_2 is the pressure perturbation at the receiver if the source is displaced by a very small quantity db_1 relative to its initial position, towards the positive of the x-axis. Respectively, p'_2 corresponds to the pressure perturbation at the receiver if the source is displaced by $-db_1$. The FD method is very simple, but has a cost that scales with the number of design variables N, rendering it unsuitable for use in large scale optimization problems.

Before presenting the results of the optimization, one thing should be noted. Since the intensity of the received pressure perturbation depends on both the distance from source and the angle between the source-receiver vector and the dipole oscillation axis, there are many positions in space where the source can be placed and evoke the desired target pressure time-series at the receiver. If the angle increases from $\theta = 0^o$ (receiver placed on the dipole oscillation axis), towards $\theta = 90^o$ the perceived pressure magnitude drops if the source-receiver distance remains unchanged. If, however, the receiver is displaced closer to the source, the same magnitude as that of p_t can still be experienced. To conclude, the fact that the target pressure is computed with the source placed at (0,0,0) does not mean that the optimization process should find that position as the one that gives the desired pressure at the receiver. The optimal source position depends on where the source is initially located.

Fig. 2.4 shows the decreasing objective function value during optimization when the source was initially placed at (-2,-1,-3).

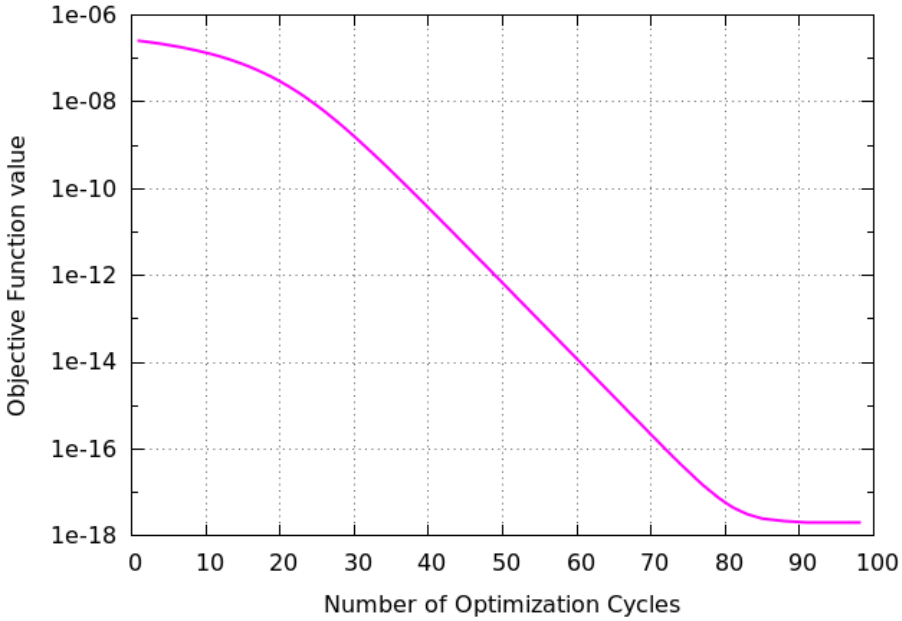

Figure 2.4: *Dipole source. Objective value vs Number of optimization cycles. The source is initially placed at (-2,-1,-3). Observer is, as always, at (7,0,0). The obtained optimal source position is (0.4179, -0.6088, -1.8259)*

For the above run, the source was initially placed at (-2,-1,-3) and the receiver, as always, at (7,0,0). It is reminded that the target pressure has been computed for a source placed at (0,0,0). At the end of the optimization, the dipole is placed at (0.4179, -0.6088, -1.8259). The pressure time-series resulting at the receiver position, compared with the target pressure can be seen in fig.2.5.

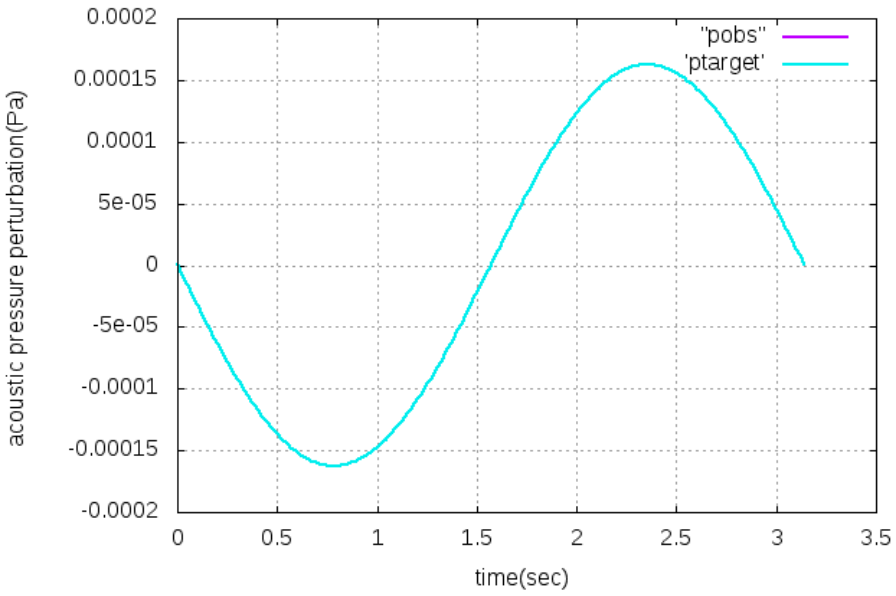

Figure 2.5: *Dipole source. Pressure evoked at the receiver at (7,0,0) by a source placed at (0.4179, -0.6088, -1.8259) (purple line) after optimization, compared with the target pressure (blue). The difference between the two curves is practically invisible.*

Next, the source is initially at (-16, -5, -7). The final source position obtained after optimization is at $(x_s, y_s, z_s) = (-1.854, -0.520, -4.008)$. The course of the objective is presented in fig.2.6

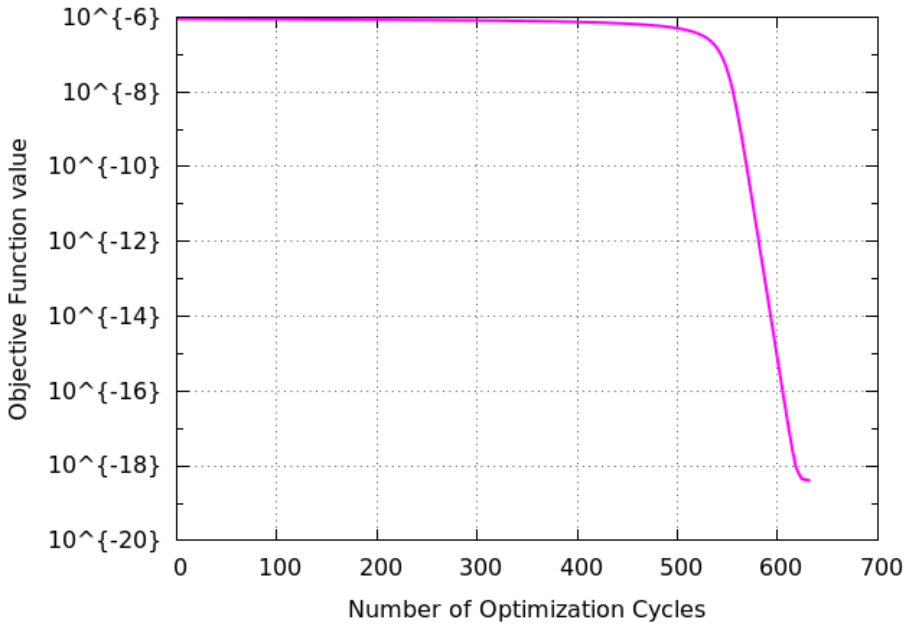

Figure 2.6: *Dipole source. Objective value vs number of optimization cycles. The source is initially placed at (-16,-5,-7). Observer is at (7,0,0).*

The comparison of the obtained pressure at the receiver and the target pressure is seen in fig. 2.7.

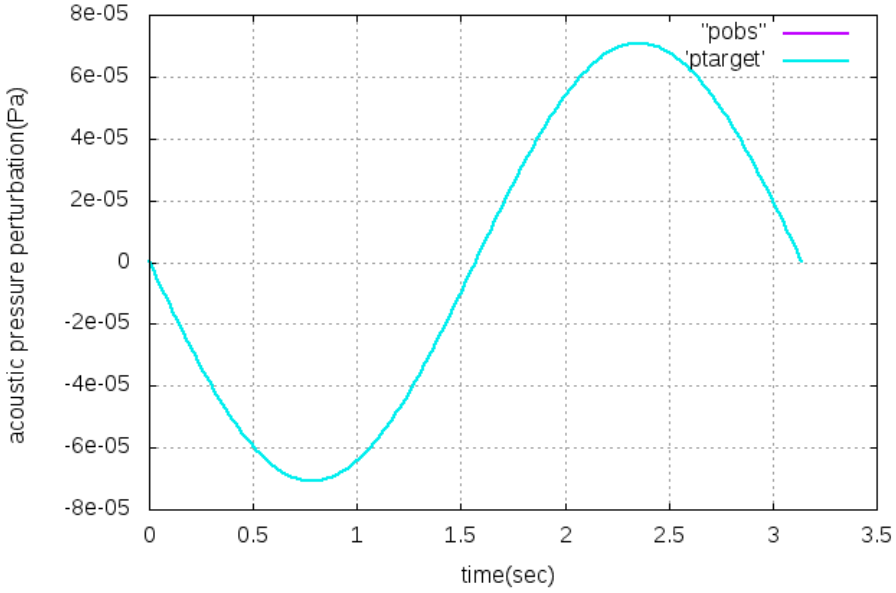

Figure 2.7: *Dipole source. Pressure at the receiver at (7,0,0) caused by a source placed at (-1.854, -0.520 , -4.008) (purple line) after optimization, compared with the target pressure (blue). The two time series coincide completely.*

Below a list of final source positions (x_s, y_s, z_s) obtained after optimization, all of which produce the desired pressure perturbation time-series at the receiver placed at (7,0,0). The final column of the matrix, denoted with d is the distance between source and receiver.

x_s	y_s	z_s	d
0.7991456	1.6818595	−1.9785377	6.7226378
3.4600903	0.0000000	4.3087021	5.5763675
0.6636761	−1.6883515	−1.6883515	6.7712675
1.1719837	−2.3357192	1.9852843	6.5850369
0.3780577	1.8353126	0.0000000	6.8715713
3.2557120	−2.7816742	−3.2441594	5.6817228
0.9800299	−0.5895790	2.7789459	6.6565895
0.7991456	−1.9785377	1.6818595	6.7226378
1.4840865	2.3847840	2.3847840	6.4652680
3.0080183	2.9795164	2.9795164	5.8043910
0.9342282	−0.2511221	−2.7709413	6.6734373
1.0384263	0.2634159	2.9005639	6.6349846

Analytical Differentiation of the KI

Having used FD to find the source position that gives the desired pressure at the receiver, we now proceed to compute the sensitivities by differentiating the KI. Thus, eq. 1.63 is differentiated w.r.t the design variables (b_1, b_2, b_3) which are the source coordinates (x_s, y_s, z_s). It was observed, that the inclusion of the terms arising from the differentiation w.r.t. the normal direction n produces negligible differences in the resulting sensitivities. It is, therefore, excluded from the analysis that follows. After exclusion of the $term \frac{1}{r}\frac{\partial p'}{\partial n}$, eq. 1.63 is written as

$$p' = \frac{1}{4\pi}\int\limits_S \left(\frac{\hat{r}_i\hat{n}_i}{r^2}p + \frac{\hat{r}_i\hat{n}_i}{cr}\frac{\partial p}{\partial t}\right)dS = \frac{1}{4\pi}\int\limits_S G_i dS \tag{2.12}$$

If x_j is the j-th coordinate of a node of the Kirchhoff surface (j=1,2,3) and x_j^{rec} the j-th coordinate of the receiver, then

$$r = |x_j^{rec} - x_j| = \sqrt{(x_j^{rec} - x_j)^2} \tag{2.13}$$

is the distance between Kirchhoff surface node and the receiver

$$r_j = x_j^{rec} - x_j \tag{2.14}$$

is the vector from node to receiver and

$$\hat{r}_j = \frac{r_j}{r} \tag{2.15}$$

is the unit normal vector pointing from node to receiver.
Differentiation of eq. 2.12 yields

$$\frac{\delta p'}{\delta b_n} = \frac{1}{4\pi}\frac{\delta}{\delta b_n}\int\limits_S G_i dS = \frac{1}{4\pi}\int\limits_S \frac{\delta G_i}{\delta b_n}dS + \frac{1}{4\pi}\int\limits_S G_i\frac{\delta(dS)}{\delta b_n} \tag{2.16}$$

Term $\frac{1}{4\pi}\int\limits_S \frac{\delta G_i}{\delta b_n}dS$ in eq. 2.16

The integral $\frac{1}{4\pi}\int\limits_S \frac{\delta G_i}{\delta b_n} dS$ can be written as

$$\begin{aligned}
\frac{1}{4\pi}\int\limits_S \frac{\delta G_i}{\delta b_n} dS &= \frac{1}{4\pi}\int\limits_S \frac{\delta}{\delta b_n}\left(\frac{\hat{r}_i\hat{n}_i}{r^2}p + \frac{\hat{r}_i\hat{n}_i}{cr}\frac{\partial p}{\partial t}\right) dS \\
&= \frac{1}{4\pi}\int\limits_S \left[\frac{\delta}{\delta b_n}\left(\frac{\hat{r}_i\hat{n}_i}{r^2}p\right) + \frac{\delta}{\delta b_n}\left(\frac{\hat{r}_i\hat{n}_i}{cr}\frac{\partial p}{\partial t}\right)\right] dS \\
&= \frac{1}{4\pi}\int\limits_S \left[\frac{\delta}{\delta b_n}\left(\frac{\hat{r}_i\hat{n}_i}{r^2}\right)p + \left(\frac{\hat{r}_i\hat{n}_i}{r^2}\right)\frac{\delta p}{\delta b_n}\right. \\
&\left. + \frac{\delta}{\delta b_n}\left(\frac{\hat{r}_i\hat{n}_i}{cr}\right)\frac{\partial p}{\partial t} + \frac{\hat{r}_i\hat{n}_i}{cr}\frac{\delta}{\delta b_n}\left(\frac{\partial p}{\partial t}\right)\right] dS
\end{aligned}$$

Let $A = \frac{\delta}{\delta b_n}\left(\frac{\hat{r}_i\hat{n}_i}{r^2}\right)p$, $B = \frac{1}{4\pi}\int\limits_S \left(\frac{\hat{r}_i\hat{n}_i}{r^2}\right)\frac{\delta p}{\delta b_n}$, $C = \frac{\delta}{\delta b_n}\left(\frac{\hat{r}_i\hat{n}_i}{cr}\right)\frac{\partial p}{\partial t}dS$, $D = \frac{\hat{r}_i\hat{n}_i}{cr}\frac{\delta}{\delta b_n}\left(\frac{\partial p}{\partial t}\right)$
Each of the terms A, B, C and D is developed separately. First, some terms that are needed for the computation of A, B, C and D are developed.
Differentiation of eq. 2.13 gives

$$\frac{\delta r}{\delta b_n} = \frac{\delta}{\delta b_n}\sqrt{(x_j^{rec} - x_j)^2} = \frac{1}{2\sqrt{(x_j^{rec} - x_j)^2}} 2(x_j^{rec} - x_j)\frac{\delta}{\delta b_n}(x_j^{rec} - x_j)$$

Taking eqs. 2.14 and 2.15 into account and since the receiver maintains the same position during optimization, yields

$$\frac{\delta r}{\delta b_n} = -\hat{r}_j \frac{\delta x_j}{\delta b_n} \tag{2.17}$$

The total derivative of r_i w.r.t. b_n is

$$\frac{\delta r_i}{\delta b_n} = \frac{\delta}{\delta b_n}(x_i^{rec} - x_i) = -\frac{\delta x_i}{\delta b_n} \tag{2.18}$$

The partial derivative of the retarded time τ w.r.t. x_j is

$$\begin{aligned}
\frac{\partial \tau}{\partial x_j} = \frac{\partial}{\partial x_j}\left(t - \frac{r}{c}\right) = -\frac{1}{c}\frac{\partial r}{\partial x_j} = -\frac{1}{c}\frac{1}{2r}(x_j^{rec} - x_j)\frac{\partial}{\partial x_j}(x_j^{rec} - x_j) \Rightarrow \\
\frac{\partial \tau}{\partial x_j} = \frac{\hat{r}_j}{c}
\end{aligned} \tag{2.19}$$

Finally, the total derivative of a function $f = f(x_j, \tau(x_j), b_n)$ can be written as

$$\begin{aligned}
\frac{\delta f}{\delta b_n} &= \frac{\partial f}{\partial b_n}\frac{\delta b_n}{\delta b_n} + \frac{\partial f}{\partial x_j}\frac{\delta x_j}{\delta b_n} + \frac{\partial f}{\partial \tau}\frac{\delta \tau}{\delta b_n} \\
&= \frac{\partial f}{\partial b_n}\frac{\delta b_n}{\delta b_n} + \frac{\partial f}{\partial x_j}\frac{\delta x_j}{\delta b_n} + \frac{\partial f}{\partial \tau}\left(\frac{\partial \tau}{\partial b_n} + \frac{\partial \tau}{\partial x_j}\frac{\delta x_j}{\delta b_n}\right) \\
&= \frac{\partial f}{\partial b_n} + \frac{\partial f}{\partial x_j}\frac{\delta x_j}{\delta b_n} + \frac{\partial f}{\partial \tau}\frac{\partial \tau}{\partial x_j}\frac{\delta x_j}{\delta b_n}
\end{aligned} \tag{2.20}$$

The computation of the terms A to D follows:

$$
\begin{aligned}
A &= \frac{\delta}{\delta b_n}\left(\frac{\hat{r}_i\hat{n}_i}{r^2}\right)p \\
&= \left[\hat{r}_i\hat{n}_i\frac{\delta}{\delta b_n}\left(\frac{1}{r^2}\right) + \frac{1}{r^2}\frac{\delta}{\delta b_n}(\hat{r}_i\hat{n}_i)\right]p \\
&= \left[-\frac{2}{r^3}\hat{r}_i\hat{n}_i\frac{\delta r}{\delta b_n} + \frac{1}{r^2}\hat{n}_i\frac{\delta}{\delta b_n}\left(\frac{r_i}{r}\right) + \frac{1}{r^2}\hat{r}_i\frac{\delta\hat{n}_i}{\delta b_n}\right]p \\
&= \left[\frac{2}{r^3}\hat{r}_i\hat{n}_i\hat{r}_j\frac{\delta x_j}{\delta b_n} + \frac{1}{r^3}\hat{n}_i\frac{\delta r_i}{\delta b_n} + \frac{1}{r^2}\hat{n}_i r_i\left(-\frac{1}{r^2}\frac{\delta r}{\delta b_n}\right) + \frac{1}{r^2}\hat{r}_i\frac{\delta\hat{n}_i}{\delta b_n}\right]p \\
&= \left[\frac{2}{r^3}\hat{r}_i\hat{n}_i\hat{r}_j\frac{\delta x_j}{\delta b_n} - \frac{1}{r^3}\hat{n}_i\frac{\delta x_i}{\delta b_n} + \frac{1}{r^3}\hat{n}_i\hat{r}_i r_j\frac{\delta x_j}{\delta b_n} + \frac{1}{r^2}\hat{r}_i\frac{\delta\hat{n}_i}{\delta b_n}\right]p \\
&= \left[3\hat{r}_i\hat{n}_i\hat{r}_j\frac{1}{r^3}\frac{\delta x_j}{\delta b_n} - \frac{1}{r^3}\hat{n}_j\frac{\delta x_j}{\delta b_n} + \frac{1}{r^2}\hat{r}_i\frac{\delta\hat{n}_i}{\delta b_n}\right]p
\end{aligned}
$$

$$
\begin{aligned}
B &= \frac{\hat{r}_i\hat{n}_i}{r^2}\frac{\delta p}{\delta b_n} \\
&= \frac{\hat{r}_i\hat{n}_i}{r^2}\left[\frac{\partial p}{\partial b_n} + \frac{\partial p}{\partial x_j}\frac{\delta x_j}{\delta b_n} + \frac{\partial p}{\partial \tau}\frac{\partial \tau}{\partial x_j}\frac{\delta x_j}{\delta b_n}\right] \\
&= \frac{\hat{r}_i\hat{n}_i}{r^2}\left[\frac{\partial p}{\partial x_j}\frac{\delta x_j}{\delta b_n} + \frac{\partial p}{\partial t}\frac{\hat{r}_j}{c}\frac{\delta x_j}{\delta b_n} + \frac{\partial p}{\partial b_n}\right]
\end{aligned}
$$

$$
\begin{aligned}
C &= \frac{\delta}{\delta b_n}\left(\frac{\hat{r}_i\hat{n}_i}{cr}\right)\frac{\partial p}{\partial t}dS \\
&= \left[\frac{1}{c}\frac{\delta}{\delta b_n}(\hat{r}_i\hat{n}_i)\frac{1}{r} + \frac{1}{c}\hat{r}_i\hat{n}_i\frac{\delta}{\delta b_n}\left(\frac{1}{r}\right)\right]\frac{\partial p}{\partial t} \\
&= \left[\frac{1}{cr}\hat{n}_i\frac{\delta\hat{r}_i}{\delta b_n} + \frac{1}{cr}\hat{r}_i\frac{\delta\hat{n}_i}{\delta b_n} - \frac{1}{cr^2}\hat{r}_i\hat{n}_i\frac{\delta r}{\delta b_n}\right]\frac{\partial p}{\partial t} \\
&= \left[\frac{1}{cr}\hat{n}_i\left(\frac{1}{r}\frac{\delta r_i}{\delta b_n} + r_i\frac{\delta}{\delta b_n}\left(\frac{1}{r}\right)\right) - \frac{1}{cr^2}\hat{r}_i\hat{n}_i\left(-r_j\frac{\delta x_j}{\delta b_n}\right) + \frac{1}{cr}\hat{r}_i\frac{\delta\hat{n}_i}{\delta b_n}\right]\frac{\partial p}{\partial t} \\
&= \left[-\frac{1}{cr^2}\hat{n}_j\frac{\delta x_j}{\delta b_n} + \frac{1}{cr^2}\hat{n}_i\hat{r}_i\hat{r}_j\frac{\delta x_j}{\delta b_n} + \frac{1}{cr^2}\hat{r}_i\hat{n}_i r_j\frac{\delta x_j}{\delta b_n} + \frac{1}{cr}\hat{r}_i\frac{\delta\hat{n}_i}{\delta b_n}\right]\frac{\partial p}{\partial t} \\
&= \left[(2\hat{r}_i\hat{n}_i\hat{r}_j - \hat{n}_j)\frac{1}{cr^2}\frac{\delta x_j}{\delta b_n} + \frac{\hat{r}_i}{cR}\frac{\delta\hat{n}_i}{\delta b_n}\right]\frac{\partial p}{\partial t}
\end{aligned}
$$

Finally,

$$
\begin{aligned}
D &= \frac{\hat{r}_i \hat{n}_i}{cr} \frac{\delta}{\delta b_n} \left(\frac{\partial p}{\partial t} \right) \\
&= \frac{\hat{r}_i \hat{n}_i}{cr} \left[\frac{\partial^2 p}{\partial t \partial x_j} \frac{\delta x_j}{\delta b_n} + \frac{\partial^2 p}{\partial t^2} \frac{\hat{r}_j}{c} \frac{\delta x_j}{\delta b_n} + \frac{\partial^2 p}{\partial t \partial b_n} \right]
\end{aligned}
$$

Final expression for the derivatives $\frac{\delta p'}{\delta b_n}$

Having computed the terms A,B,C and D, the final expression for the derivatives $\frac{\delta p'}{\delta b_n}$ can be assembled:

$$
\begin{aligned}
\frac{\delta p'}{\delta b_n} =& \frac{1}{4\pi} \int_S (3\hat{r}_i \hat{n}_i \hat{r}_j - \hat{n}_j) \left[\frac{1}{r^3} p + \frac{1}{cr^2} \frac{\partial p}{\partial t} \right] \frac{\delta x_j}{\delta b_n} dS \\
&+ \frac{1}{4\pi} \int_S \left[\frac{\hat{r}_i \hat{n}_i}{r^2} \frac{\partial p}{\partial x_j} + \frac{\hat{r}_i \hat{n}_i}{cr} \left(\frac{\partial^2 p}{\partial t \partial x_j} + \frac{\hat{r}_j}{c} \frac{\partial^2 p}{\partial t^2} \right) \right] \frac{\delta x_j}{\delta b_n} dS \\
&+ \frac{1}{4\pi} \int_S \left[\frac{\hat{r}_i \hat{n}_i}{r^2} \frac{\partial p}{\partial b_n} + \frac{\hat{r}_i \hat{n}_i}{cr} \frac{\partial}{\partial t} \left(\frac{\partial p}{\partial b_n} \right) \right] dS \\
&+ \frac{1}{4\pi} \int_S \left[\frac{\hat{r}_i}{r^2} p + \frac{\hat{r}_i}{cr} \frac{\partial p}{\partial t} \right] \frac{\delta (\hat{n}_i dS)}{\delta b_n}
\end{aligned} \tag{2.21}
$$

where the last integral containing the term $\frac{\delta(\hat{n}_i dS)}{\delta b_n}$ is in our case zero, since the Kirchhoff surface elements do not change in size dS or orientation (i.e their normal vector $\hat{n}_i$ does not change) over the course of optimization, but are translated parallel to themselves, following the movement of the source. (It is reminded that the design variables are the coordinates of the source, while the receiver is kept at a constant position). The terms p, $\frac{\partial p}{\partial t}$, $\frac{\partial p}{\partial x_j}$, $\frac{\partial^2 p}{\partial t \partial x_j}$, $\frac{\partial^2 p}{\partial t^2}$, $\frac{\partial p}{\partial b_n}$, $\frac{\partial}{\partial t}$ and $\frac{\partial p}{\partial b_n}$ appearing in the above integrals need to be computed and, then, interpolated for the retarded time τ in order to perform the integration and compute $\frac{\delta p'}{\delta b_n}$. These terms can be computed in the manner presented in the beginning of the present section, i.e. through the use of FD and linear interpolation to obtain their values at retarded time. To check whether the derivatives computed through eq. 2.21 are correct, they are compared with the ones computed by FD. The two methods, i.e eq. 2.21 and FD, produce very similar results and both methods are successful at performing optimization of the source position, but the slight differences in the computed derivatives mean that even if the starting position of the source is the same both for FD and the analytical formula,

the two methods will not give the same final position for the source. However, as it will be seen, both point to positions that minimize the objective to a very satisfactory degree.

Next, the optimization is run using the analytical formula to compute $\frac{\delta p}{\delta b_n}$. The sensitivity derivatives are subsequently computed and steepest descent is performed. At the same time, in each optimization cycle, $\frac{\delta p}{\delta b_n}$ and the sensitivities based on FD are also computed, without being used anywhere in the code. They are however recorded and compared with the derivatives produced through the analytical formula. The main steps are therefore the following

1. Start with source at arbitrary position,

2. compute $\frac{\delta p}{\delta b_n}$ through FD at current source position,

3. compute $\frac{\delta p}{\delta b_n}$ through eq.2.21 at current source position,

4. compute sensitivities $\frac{\delta J}{\delta b_n}$ based on $\frac{\delta p}{\delta b_n}$ computed through eq. 2.21,

5. compute sensitivities $\frac{\delta J}{\delta b_n}$ based on $\frac{\delta p}{\delta b_n}$ computed through FD,

6. record sensitivities produced by FD and through analytical computation for comparison

7. use the sensitivities computed based on the analytical formula to descend and renew source position and

8. return to step 2.

As a first test, the source was initially placed at (-0.1,0,0) - $(x_s, y_s, z_s) = (0, 0, 0)$ is a position that produces the target time series (since the target pressure time series was computed for a source at (0,0,0)). The comparison of the sensitivities produced through FD and analytical formula can be seen in figs. 2.8, 2.9 and 2.10.

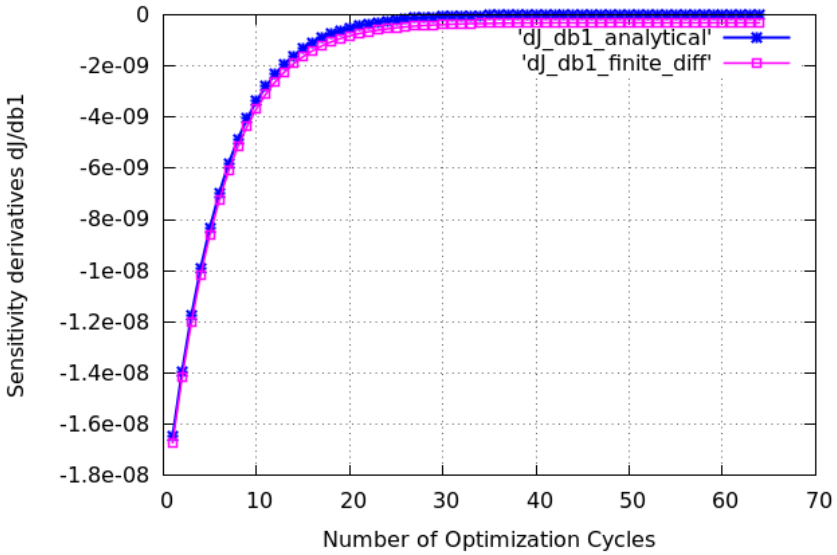

Figure 2.8: *Dipole source. Comparison of the sensitivities $\delta J/\delta b_1 = \delta J/\delta x_s$ produced using the derivatives $\delta p/\delta b_1$ of the analytical formula 2.21 compared with FD. The sensitivities coincide almost completely.*

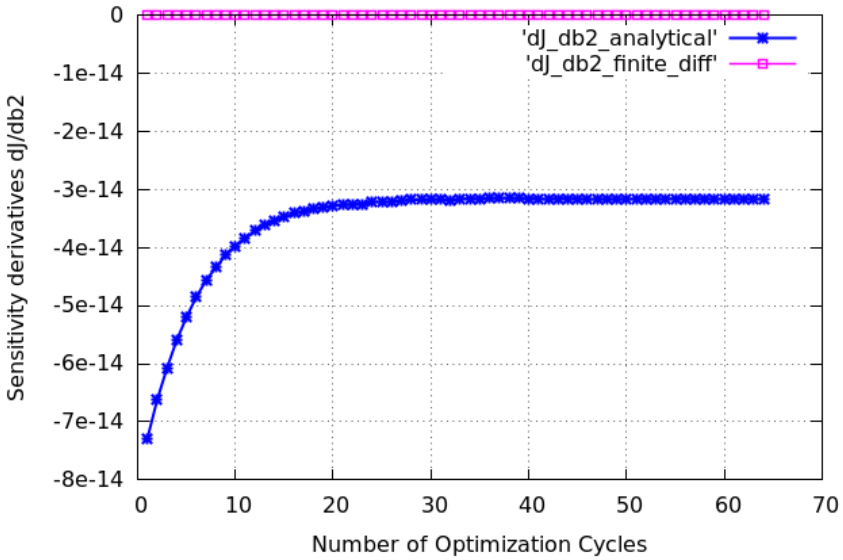

Figure 2.9: *Dipole source. Comparison of the sensitivities $\delta J/db_2 = \delta J/\delta y_s$ produced using the derivatives $\delta p/\delta b_2$ of the analytical formula 2.21 compared with FD. Both methods give very small sensitivities. More specifically, FD give zero sensitivities in the y direction, whereas the analytical formula 2.21 gives sensitivities with of the order of 10^{-14}. Both methods give very similar results.*

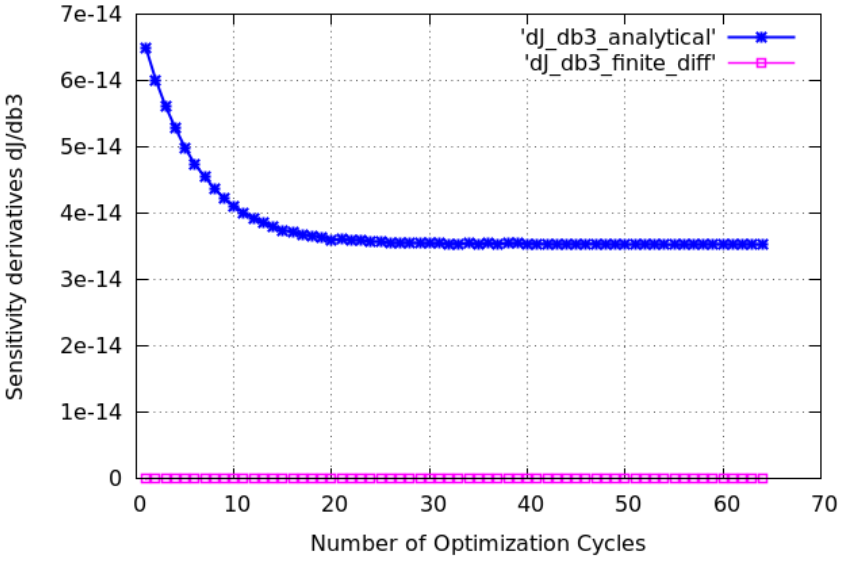

Figure 2.10: *Dipole source. Comparison of the sensitivities* $\delta J/db_3 = \delta J/\delta z_s$ *produced using the derivatives* $\delta p/\delta b_2$ *of the analytical formula 2.21 compared with FD. Both methods yield sensitivities that are very close or equal to zero.*

As mentioned the source was initially placed at (-0.1,0,0). After the end of the optimization it was placed at $(1.94 \cdot 10^{-3}$, $1.17 \cdot 10^{-6}, 0)$. The pressure perturbation induced at the receiver coincides with the target pressure time series as can be seen in fig. 2.11.

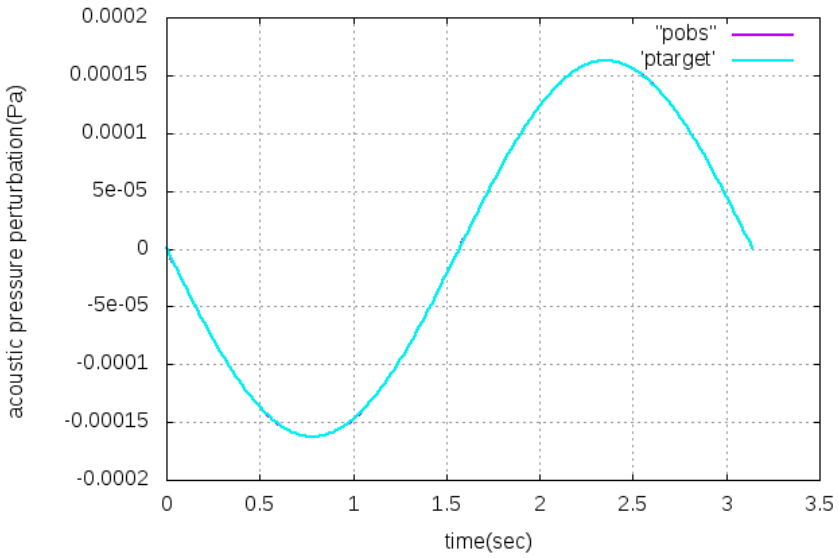

Figure 2.11: *Dipole source. Pressure time series at receiver caused by a dipole placed at the position* $(1.94 \cdot 10^{-3}$, $1.17 \cdot 10^{-6}, 0)$ *after optimization, compared to the target pressure time series.*

2.3 Pressure Perturbation Generated by a Monopole - Analytical Solution Compared with the KI

2.3.1 Mathematical Formulation

For a monopole, the induced velocity potential is given by the equation:

$$\phi(x,t) = \frac{A}{4\pi R^*} e^{\left[i\omega\left(t-\frac{R}{c_0}\right)\right]} \tag{2.22}$$

Again, in order to compute the pressure perturbation from eq. 2.4, the derivatives $\frac{\partial\phi}{\partial t}$ and $\frac{\partial\phi}{\partial x}$ should be computed. For the time derivative, $\frac{\partial\phi}{\partial t} = i\omega\phi$.

The spatial derivative $\frac{\partial\phi}{\partial x}$ is:

$$\frac{\partial\phi}{\partial x} = \frac{\frac{\partial}{\partial x}\left(e^{(i\omega(t-R/c_0))}\right) R^* - e^{(i\omega(t-R/c_0))}\frac{\partial R^*}{\partial x}}{(R^*)^2} =$$

$$= \frac{A}{4\pi(R^*)^2}\left(R^* e^{(i\omega(t-R/c_0))}\frac{\partial}{\partial x}\left(i\omega(t-R/c_0)\right) - e^{(i\omega(t-R/c_0))}\frac{\partial R^*}{\partial x}\right) \Rightarrow$$

$$\frac{\partial \phi}{\partial x} = \frac{Ae^{(i\omega(t-R/c_0))}}{4\pi(R^*)^2}\left(-\frac{i\omega}{c_0}\frac{\partial R}{\partial x}R^* - \frac{\partial R^*}{\partial x}\right) \tag{2.23}$$

Now, $\partial R/\partial x$ and $\partial R^*/\partial x$ should be computed, in order to obtain the final expression for $\partial\phi/\partial x$. According to eq. 2.5:

$$\frac{\partial R^*}{\partial x} = \frac{1}{2R^*}2x = \frac{x}{R^*}$$

and according to eq. 2.6:

$$\frac{\partial R}{\partial x} = \frac{1}{\beta^2}\frac{\partial}{\partial x}(-M_0 x + R^*) = \frac{1}{\beta^2}\left(-M_0 + \frac{\partial R^*}{\partial x}\right) \Rightarrow$$

$$\frac{\partial R}{\partial x} = \frac{1}{\beta^2}\left(-M_0 + \frac{x}{R^*}\right)$$

Finally, eq. 2.23 becomes

$$\frac{\partial \phi}{\partial x} = \frac{Ae^{(i\omega(t-R/c_0))}}{4\pi(R^*)^2}\left(-\frac{i\omega}{c_0}\frac{1}{\beta^2}\left(-M_0 + \frac{x}{R^*}\right)R^* - \frac{x}{R^*}\right)$$

$$= \frac{Ae^{(i\omega(t-R/c_0))}}{4\pi(R^*)^2}\left(-\frac{i\omega}{c_0}\frac{1}{\beta^2}(-M_0R^* + x) - \frac{x}{R^*}\right)$$

$$= \frac{Ae^{(i\omega(t-R/c_0))}}{4\pi(R^*)^2}\left(-\frac{i\omega R^*}{c_0\beta^2 R^*}(-M_0R^* + x) - \frac{c_0\beta^2 x}{c_0\beta^2 R^*}\right)$$

$$= -\frac{Ae^{(i\omega(t-R/c_0))}}{4\pi(R^*)^2}\left(\frac{i\omega R^*(-M_0R^* + x) + c_0\beta^2 x}{c_0\beta^2 R^*}\right)$$

$$= -\frac{Ae^{(i\omega(t-R/c_0))}}{4\pi c_0\beta^2(R^*)^3}\left(i\omega R^*(-M_0R^* + x) + c_0\beta^2 x\right)$$

$$= -\frac{Ae^{(i\omega(t-R/c_0))}}{4\pi c_0\beta^2(R^*)^3}\left(-i\omega M_0(R^*)^2 + i\omega R^* x + c_0\beta^2 x\right) \Rightarrow$$

$$\frac{\partial \phi}{\partial x} = \frac{Ae^{(i\omega(t-R/c_0))}}{4\pi c_0\beta^2(R^*)^3}\left(i\omega M_0(R^*)^2 - (c_0\beta^2 + i\omega R^*)x\right) \tag{2.24}$$

Having computed $\dfrac{\partial \phi}{\partial x}$, the pressure at any point is computed through eq. 2.4 and the analytical calculations are compared with the results of the KI, similarly to the dipole case.

2.3.2 Results

Directivity pattern and pressure perturbation intensity

The following results are derived for a monopole with the characteristics listed below

- oscillation frequency $\omega = 2rad/sec$
- oscillation amplitude $A = 0.05m$
- source position (0,0,0)

The monopole directivity pattern is presented in fig. 2.12.

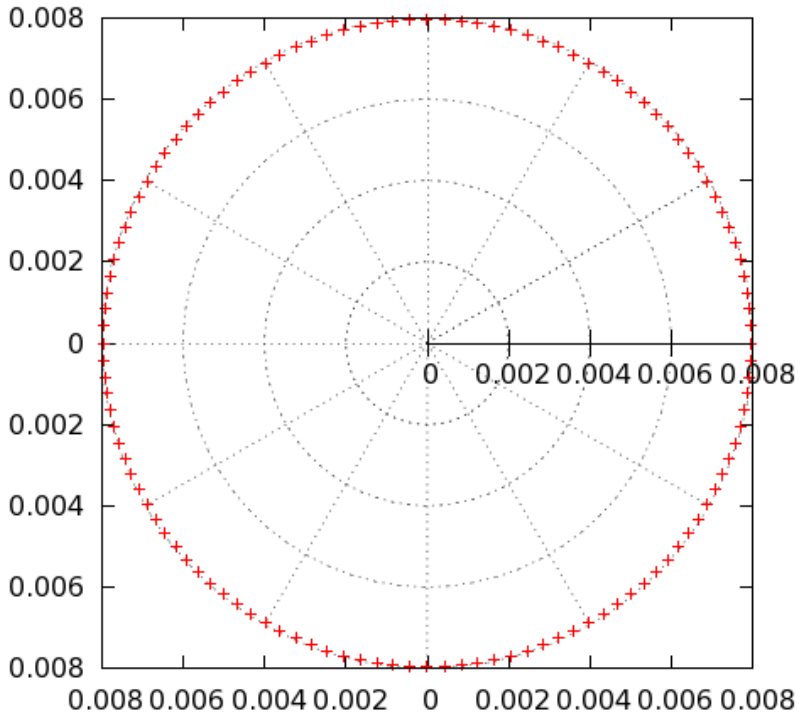

Figure 2.12: *Monopole source. Polar plot of monopole directivity pattern in non-moving medium on the x-y plane. The source is placed at (0,0,0). The monopole emits sound uniformly in all directions, i.e. the perceived pressure perturbation is solely dependent on the distance from the monopole and not on the angular position of the receiver.*

The fact that there is no dependence on the angular position of the receiver is also confirmed by the following graph. Three observers are placed at a constant radius of 7m from the monopole source, but at different angles w.r.t the x-axis, i.e. at $0^o, 45^o$ and 90^o respectively. The pressure signal received by all three observers is, as can be seen in fig. 2.13, exactly the same.

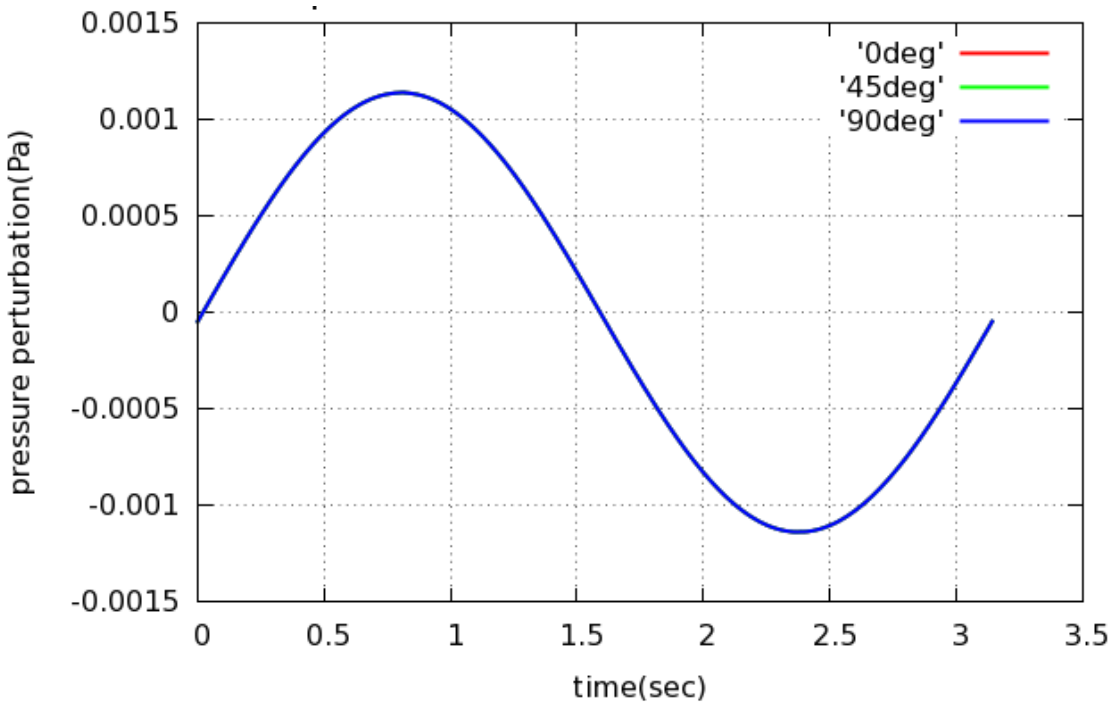

Figure 2.13: *Monopole source. Pressure perturbation time series at a receiver placed at three different angles $\theta = 0^o$, $\theta = 45^o$ and $\theta = 90^o$ relative to the x-axis. The receiver - monopole distance is kept constant at 7m with the monopole placed at (0,0,0). All three receivers record the same acoustic pressure perturbation, as expected.*

Analytical Results Compared with the Results Obtained through the Use of KI

Next, the results obtained through the use of the analytical expressions for monopole are compared to those yielded by the use of KI.

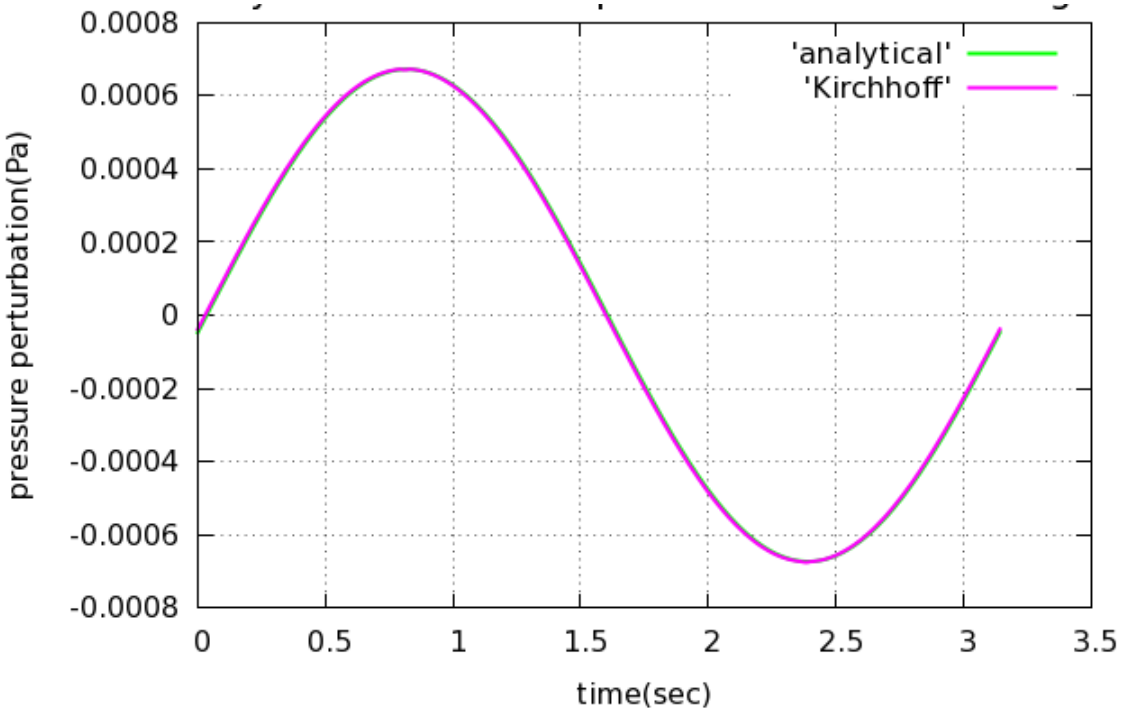

Figure 2.14: *Monopole source. Pressure perturbation time-series at receiver positioned at (-10,2,-6). Source position (0,0,0). The time-series produced through the use of the KIM (purple curve) coincides with the results obtained through the use of the analytical monopole formulas.*

As can be seen the results obtained through the KIM coincide with those produced by the analytical formulas 2.2 to 2.8.

2.3.3 Computing the optimal Monopole Position for a Certain Target Pressure at the Receiver

Next step is to optimize the monopoles' position to achieve a certain target pressure. The steps followed for the optimization process are the same as the ones presented in the previous section for the dipole i.e. the source is initially placed at (0,0,0) and the pressure computed at the receiver (7,0,0) is set as target. Then, the source is placed at an arbitrary position and the optimization starts, by computing the sensitivities through FD or through analytical differentiation of the KI and performing steepest descent until a position that minimizes the objective is reached.

The objective function is the same as in the case of the dipole (see eq. 2.9), therefore the sensitivity derivatives $\frac{\delta J}{\delta b_n}$ are computed from eq. 2.11. $\frac{\delta p}{\delta b_n}$ is, again, computed either through FD or by directly differentiating the analytical formula of the KI (eq.1.63).

It should, once more, be noted that there is no single position that gives us the desired pressure distribution at the receiver. Since the monopole emits wave signals uniformly in all directions, if the distance between source and receiver is kept constant, the pressure signal at the receiver remains unchanged. This means that the locus of the source positions that minimize the objective function is a sphere centered at the receiver.

Finite Differences

Below the results obtained after the computation of $\frac{\delta p}{\delta b_n}$ through FD are presented. Fig. 2.15 shows the decreasing objective function value during optimization, when the initial source position is at (-10,2,-6)

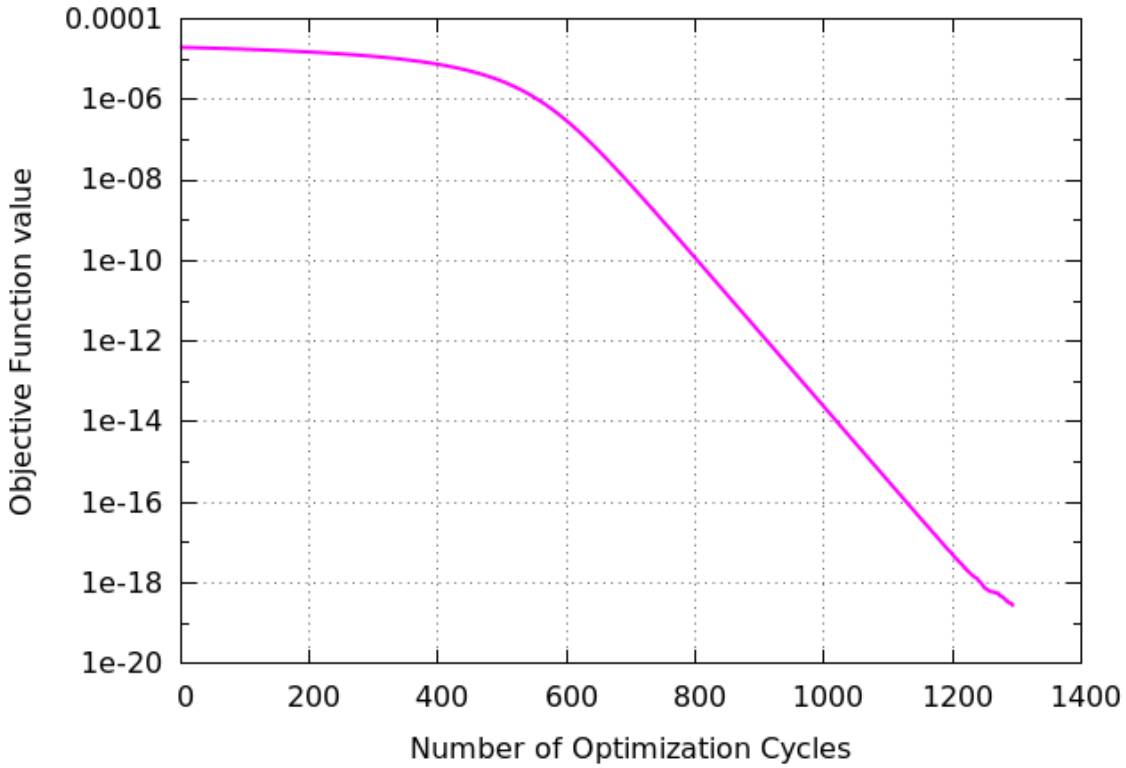

Figure 2.15: *Monopole source. Objective value vs. number of optimization cycles. The source is initially placed at (-10,2,-6). The receiver is, as always, at (7,0,0).*

At the end of the optimization, the monopole is placed at (0.1703 , 1.4964 , -0.3403). At that position the pressure at the receiver completely coincides with the target pressure. Below is a list of final source positions (x_s, y_s, z_s) obtained after optimization, all of which produce the desired pressure perturbation time-series at the receiver placed at (7,0,0). The final column of the matrix denoted with d is the distance between source and receiver, which is invariably very close to 7, as expected.

x_s	y_s	z_s	d
0.1702824	1.49638861	−0.34026859	7.000000296
9.5230317	−6.52943378	0.02863951	7.000001045
1.2471189	−3.95728275	−0.49424404	7.000000342
6.0333524	−6.93293655	−0.00052205	7.000001219
2.7421377	5.55609373	−0.02098918	7.000000661
7.0000000	−7.00000124	0.00021696	7.000001243

Analytical Differentiation of the KI

Here, the sensitivities obtained through the use of FD are compared to those yielded by eq. 2.21. The optimization starts with the source placed at $(5, 3, -2)$, the receiver is placed at a constant position $(7, 0, 0)$ and the target pressure has been computed

(as in all previously examined cases), as the pressure induced at the receiver, when the source is at $(0, 0, 0)$. At the end of the optimization, the source is placed at (3.6045, 5.0932, -3.3954), i.e.at a distance of approximately 7m from the receiver. The pressure time series induced at the receiver by a monopole located there, completely coincides with the target pressure.
The optimization steps were performed using the sensitivities produced by eq. 2.21 but in each cycle, the sensitivities were also computed through FD and the results were stored for the comparison that follows.

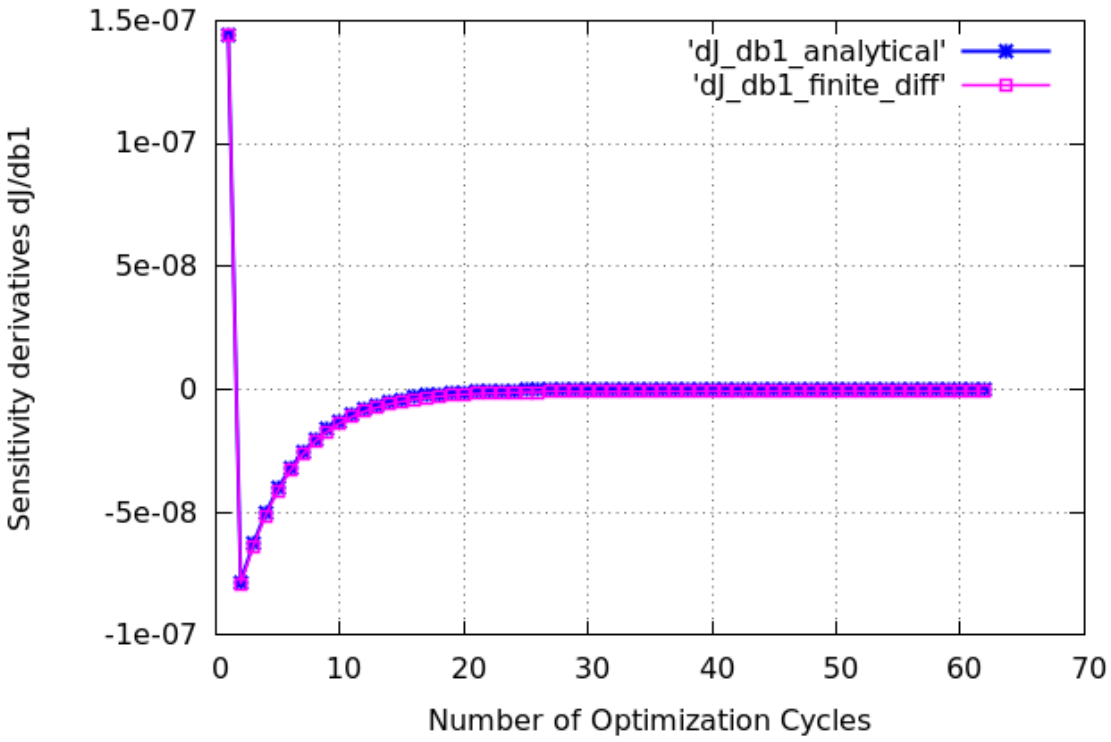

Figure 2.16: *Monopole source. Comparison of the sensitivities $\delta J/\delta b_1 = \delta J/\delta x_s$ obtained using the derivatives $\delta p/\delta b_1$ of the analytical formula 2.21 with those obtained through FD. The sensitivities coincide almost completely.*

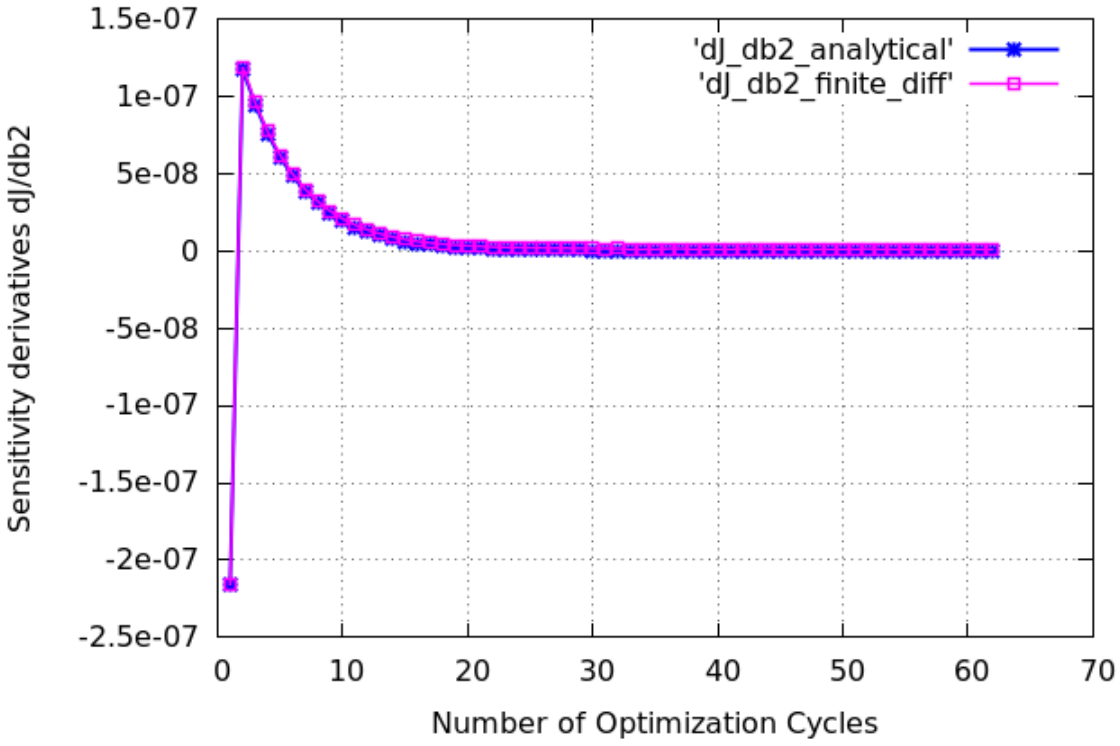

Figure 2.17: *Monopole source. Comparison of the sensitivities* $\delta J/\delta b_2 = \delta J/\delta y_s$ *obtained using the derivatives* $\delta p/\delta b_2$ *of the analytical formula 2.21 with those obtained through FD. The two methods produce almost identical results.*

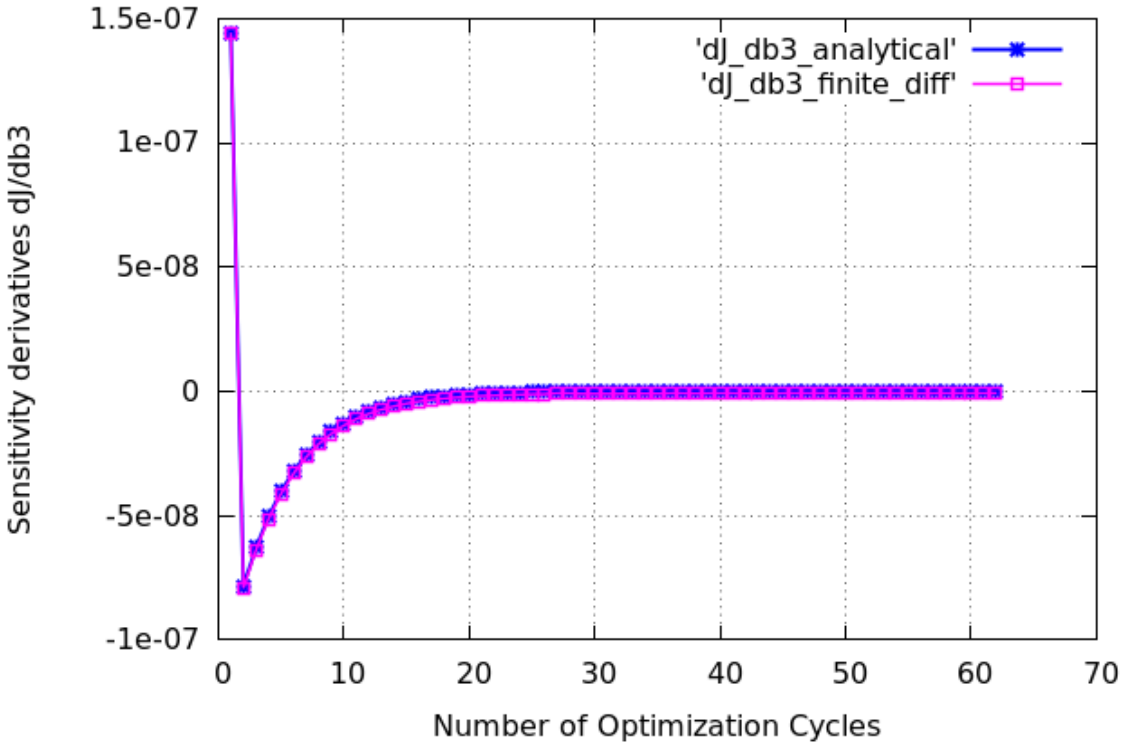

Figure 2.18: *Monopole source. Comparison of the sensitivities* $\delta J/\delta b_3 = \delta J/\delta z_s$ *obtained using the derivatives* $\delta p/\delta b_1$ *of the analytical formula 2.21 with those obtained through FD. The sensitivities resulting from the two methods are almost identical.*

The presentation of the above results concludes the first part of the present thesis. Ultimately, the advantage of the KIM is that it is a tool that enables the computation of noise without the need of costly CFD computations over a domain that extends from the source up to the observer in the source far-field. The method uses only CFD data obtained in the near-field of the source and propagates this information to the far-field where the induced noise is computed. In this thesis the KIM was used to predict the noise generated by sources, for which analytical equations for the induced pressure are available, but that was for demonstration purposes. The value of the KIM can be seen when coupled with a CFD software to perform noise prediction in the far-field of the CFD domain.

Part II

Continuous Adjoint-based Shape Optimization

Chapter 3

Continuous Adjoint Formulation for Incompressible, Steady-State Flow

In the first part of this thesis, the Kirchhoff Integral Method for aeroacoustic noise prediction was tested in the case of simple acoustic sources (monopole, dipole). The second part, carried out at BMW Munich, is also partly related to noise generation, which is always unwanted in industrial applications. In the automotive industry, some common sources of noise and, therefore, of discomfort are the Heating, Ventilation and Air Conditioning (HVAC) units and the exhaust system. Part of the second chapter of this thesis concerns itself with shape optimization for noise reduction. This is done not through the use of acoustic analogies, but rather by choosing a "noise-related" objective function i.e. an objective whose reduction has been shown to also minimize noise levels.

3.1 The PCOpt/NTUA Software

During the last years, a key research activity in PCOpt/NTUA was the development of adjoint-based methods for the computation of first- and higher-order derivatives of objective functions used in aerodynamic optimization. The development was based on in-house flow solvers (for both compressible and incompressible flows, using time-marching techniques for systems of hyperbolic equations and, for incompressible flows in particular, the pseudo-compressibility technique) and OpenFOAM (pressure-based method for incompressible flows). The continuous adjoint methodology utilized is this thesis was developed in the OpenFOAM-2.3.1 environment by the PCOpt/NTUA and its distinguishing features are

1. The full differentiation of turbulence models and
2. The fact that it accounts for the grid sensitivities (for the first time in continuous adjoint).

In contrast to all previous works on continuous adjoint, [10] introduced the continuous adjoint method to both the mean-flow and turbulence (Spalart–Allmaras) equations by overcoming the frequently made assumption of neglecting variations in turbulent viscosity, commonly known as "frozen turbulence asumption". It was demonstrated that the adjoint to the turbulence equations is really needed for the accurate computation of the sensitivity derivatives. Not solving the adjoint to the turbulence model equation(s) results in wrong and, what is worse, wrongly signed sensitivities that may mislead the optimization algorithm. The same work has been extended to variants of the $k-\epsilon$ model.

The second distinctive feature of the software is, as mentioned, the way it accounts for the grid sensitivities i.e. the derivatives of the grid coordinates w.r.t. the design variables, $\frac{\delta x_k}{\delta b_n}$. The basic idea of the adjoint methodology, which is the avoidance of the computation of costly terms such as $\frac{\delta p}{\delta b_n}$ can be extended to the grid sensitivities. The computation of $\frac{\delta x_k}{\delta b_n}$ can, thus, be avoided by differentiating a grid displacement model and deriving an adjoint grid displacement equation[11].

3.1.1 Three Continuous Adjoint Formulations for Shape Optimization (SI - FI - ESI)

The continuous adjoint approach for shape optimization, in flows governed by the Navier-Stokes equations can be formulated in three different ways, each of which produces a different expression for the sensitivity derivatives[11]. All three formulations give rise to the same adjoint mean flow equations and the same adjoint boundary conditions. The first formulation, leads to an expression including only boundary, i.e.surface integrals (SI approach). This means that it has a low computational cost, but can lack accuracy. The second formulation results in a sum of both boundary and field integrals and can be referred to as FI. The FI approach is accurate but costly, because of the need to integrate over the volume of the domain and, also, the need to compute $\frac{\delta x_k}{\delta b_n}$. The Enhanced SI ($E-SI$) approach, eliminates the need to compute $\frac{\delta x_k}{\delta b_n}$, thus reducing the cost, while maintaining an accuracy as high as that of the FI formulation in the computed sensitivities [11].

Next, follows a brief presentation of the three formulations. All formulations start with the definition of the augmented function F_{aug} as

$$F_{aug} = F + \int_{\Omega} \Psi_i R_i d\Omega \tag{3.1}$$

where F is the objective function, $R_i = 0$, i=1,2,..,N (N = number of primal equations) are the state equations, Ψ_i are the adjoint variables and Ω the computational domain. Differentiation of eq. 3.1 w.r.t. the design variables gives

$$\frac{\delta F_{aug}}{\delta b_n} = \frac{\delta F}{\delta b_n} + \frac{\delta}{\delta b_n} \int_{\Omega} \Psi_i R_i d\Omega \tag{3.2}$$

The difference between the FI and both the SI and ESI formulations lies in the way that the differentiation $\frac{\delta}{\delta b_n}\int_\Omega \Psi_i R_i d\Omega$ is performed.

In the FI approach, the term is further developed as follows

$$\frac{\delta}{\delta b_n}\int\limits_\Omega \Psi_i R_i d\Omega = \int\limits_\Omega \Psi_i \frac{\delta R_i}{\delta b_n} d\Omega + \int\limits_\Omega \Psi_i R_i \frac{\delta(d\Omega)}{\delta b_n} \tag{3.3}$$

Using the relations $\frac{\delta(d\Omega)}{\delta b_n} = \frac{\partial}{\partial x_k}(\frac{\delta x_k}{\delta b_n})d\Omega$ and $\frac{\delta}{\delta b_n}\left(\frac{\partial \Phi}{\partial x_j}\right) = \frac{\partial}{\partial x_j}\left(\frac{\delta \Phi}{\delta b_n}\right) - \frac{\partial \Phi}{\partial x_k}\frac{\partial}{\partial x_j}\left(\frac{\delta x_k}{\delta b_n}\right)$ and the Green-Gauss theorem, eq. 3.3 yields a final expression for the sensitivity derivatives, containing field integrals of $\frac{\delta x_k}{\delta b_n}$[11]. This is the basis of the so-called FI adjoint formulation.

The aim of the SI approach is to avoid the appearance of field integrals of the grid sensitivities $\frac{\delta x_k}{\delta b_n}$. To that end, the Leibniz theorem is used, which states that

$$\frac{\delta}{\delta b_n}\int_\Omega \Phi d\Omega = \int_\Omega \frac{\partial \Phi}{\partial b_n} d\Omega + \int_S \Phi n_k \frac{\delta x_k}{\delta b_n} dS \tag{3.4}$$

The term $\frac{\delta}{\delta b_n}\int_\Omega \Psi_i R_i d\Omega$ is, therefore, written as

$$\frac{\delta}{\delta b_n}\int\limits_\Omega \Psi_i R_i d\Omega = \int\limits_\Omega \Psi_i \frac{\partial R_i}{\partial b_n} d\Omega + \int\limits_S \Psi_i R_i n_k \frac{\delta x_k}{\delta b_n} dS \tag{3.5}$$

where S is the boundary of Ω. This results in the following expression for the sensitivity derivatives

$$\frac{\delta F_{aug}}{\delta b_n} = \frac{\delta F}{\delta b_n} + \int\limits_\Omega \Psi_i \frac{\partial R_i}{\partial b_n} d\Omega + \int\limits_S \Psi_i R_i n_k \frac{\delta x_k}{\delta b_n} dS \tag{3.6}$$

Eq. 3.6 is the origin of the SI adjoint formulation. The final expressions for the sensitivity derivatives for the FI and SI formulations for incompressible, steady-state laminar flows can be found in [11]. The last term in eq. 3.6 is called $LBterm$, which stands for Leibniz term. Moving asymptotically from the inside of the computational domain (where the state equations are satisfied) towards the boundary, it can be assumed that the state equations are also satisfied on the boundary, therefore, LBterm is usually ignored. However, the contribution of the $LBterm$ can become very important, depending on the specific case [11]. The FI and SI formulations are mathematically equivalent and should produce the same sensitivities. However, omission of the $LBterm$ leads to disparity between the sensitivity derivatives produced by the two approaches. Computing the $LBterm$ presents substantial numerical difficulties (regarding its discretization on the boundary), rendering its inclusion into the sensitivity derivatives expression impractical. It can be shown that the $LBterm$ is mathematically equivalent to a volume integral containing the

grid sensitivities, which is a more easily computable alternative to the $LBterm$ [11]. However, the cost of computing this volume integral scales linearly with the number of design variables, rendering this approach as costly as the FI formulation. The Enhanced SI ($E-SI$) formulation aims at the complete elimination of the field integrals of $\frac{\delta x_k}{\delta b_n}$ in the sensitivity derivatives expression. The same philosophy of the adjoint methodology, which eliminates the need of computing volume integrals of the variation of the state variables w.r.t. the design variables, can be extended to the grid sensitivities[11]. The grid displacement model used, is mathematically described by the Laplacian gdPDEs and reads

$$R_i^m = \frac{\partial^2 m_i}{\partial x_j^2} = 0 \tag{3.7}$$

where m_i are the Cartesian displacements of the nodes of the grid, whereas x_j are the Cartesian coordinates of the nodes of the grid. When the position of the boundary nodes is renewed during optimization, the computed displacements of the boundary nodes are the boundary conditions used to solve eqs. 3.7 and to compute the new positions of the internal nodes of the geometry. Therefore, following the adjoint methodology, and with the aim of eliminating the need of computing $\frac{\delta x_k}{\delta b_n}$, a new term is added to the augmented function and the following expression for the sensitivities is obtained

$$\frac{\delta F_{aug}}{\delta b_n} = \frac{\delta F}{\delta b_n} + \frac{\delta}{\delta b_n}\int_\Omega u_i R_i^v d\Omega + \frac{\delta}{\delta b_n}\int_\Omega q R^p d\Omega + \frac{\delta}{\delta b_n}\int_\Omega m_i^a R_i^m d\Omega \tag{3.8}$$

where m_i^a is the adjoint to the Cartesian displacements m_i. Further developing eq. 3.8 leads to the derivation of an adjoint equation for the grid displacements m_i and finally to an expression for the sensitivity derivatives that is free of field integrals of the grid sensitivities. In conclusion, the FI approach is, because of the field integrals of the grid sensitivities, computationally costly. However, since no terms are neglected in the FI approach, it is also accurate. The SI approach, is computationally cheap, but, because the $LBterm$ is ignored, less accurate than FI. If the $LBterm$ is not ignored, the two methods are mathematically equivalent. However, inclusion of the $LBterm$ presents numerical difficulties, or, in the case where it is substituted by the mathematically equivalent volume integral mentioned above, the computational cost is increased, so that the cost becomes as high as that of the FI formulation. The $E-SI$ formulation proposed in [11] ,maintains the high accuracy of the FI approach, while the two major advantages of SI are still valid: cost independence from the number of design variables and sensitivity derivatives free of field integrals[11].

The concept of using an adjoint grid displacement model to eliminate the need of grid sensitivities computation, has been proposed in the literature of discrete adjoint methods[12],[13]. The first time, however, that such a formulation was proposed in the continuous adjoint literature was in [11].

Shape optimization in the present thesis was performed using the $E-SI$ formulation, which is presented below.

3.2 State equations

In the present section, the continuous adjoint, [14] [15], [16], [17] approach to steady-state incompressible flows is presented. The Spalart-Allmaras turbulence model [14] has been used. The following analysis can be found in much greater detail in the PhD Thesis of Dr. E.M. Papoutsis, [14] and in [18]. Using the Einstein convention, where repeated indices denote summation, the steady-state Navier-Stokes equations for an incompressible flow and the Spalart-Allmaras turbulence model are written as [14], [19], [20]

$$R^p = -\frac{\partial v_j}{\partial x_j} = 0 \tag{3.9a}$$

$$R_i^v = v_j \frac{\partial v_i}{\partial x_j} - \frac{\partial}{\partial x_j}\left[(\nu+\nu_t)\left(\frac{\partial v_i}{\partial x_j}+\frac{\partial v_j}{\partial x_i}\right)\right] + \frac{\partial p}{\partial x_i} = 0\ , \qquad i=1,2(,3) \tag{3.9b}$$

$$R^{\tilde{\nu}} = v_j \frac{\partial \tilde{\nu}}{\partial x_j} - \frac{\partial}{\partial x_j}\left[\left(\nu+\frac{\tilde{\nu}}{\sigma}\right)\frac{\partial \tilde{\nu}}{\partial x_j}\right] - \frac{c_{b2}}{\sigma}\left(\frac{\partial \tilde{\nu}}{\partial x_j}\right)^2 - \tilde{\nu}P(\tilde{\nu}) + \tilde{\nu}D(\tilde{\nu}) = 0 \tag{3.9c}$$

where v_i are the velocity components, ν is the bulk viscosity, ν_t the turbulent viscosity and p is the static pressure divided by the constant density (its units are therefore m^2/s^2).The turbulence state variable is $\tilde{\nu}$ and the eddy viscosity coefficient can be written as

$$\nu_t = \tilde{\nu} f_{v1}$$

$P(\tilde{\nu})$ and $D(\tilde{\nu})$ are the production and dissipation terms [14]. The production and dissipation terms depend, among other quantities, on the distance Δ from the wall.

Furthermore, since the $E-SI$ formulation is being used, eqs. 3.7 are to be included in the state equations. Eqs. 3.9 and 3.7 along with their boundary conditions, are the primal / state equations of the optimization problem. The boundary conditions required to close the problem are:

- At the inlet and walls: Dirichlet condition for velocity v_i and for the turbulence model variables and zero Neumann conditions for the pressure.

- At the outlet: A Dirichlet condition for p (usually zero) and Neumann conditions for v_i and the turbulence variables (internal aerodynamics).

3.3 Introduction of the Adjoint Variables

The aim of an optimization problem is the minimization of an objective function F in the design space defined by a vector of design variables $\boldsymbol{b}$. The objective function may depend directly on the design variables $\boldsymbol{b}$ but there is also an indirect dependence, since F is a function of the flow variables $\boldsymbol{U}$, which in turn depend on the design variables $\boldsymbol{b}$ (if the design variables i.e. the geometry changes the flow field will change in turn). The vector of primal variables $\boldsymbol{U}$ contains v_i, p and the turbulence model variable. The objective function F can therefore be written as $F = F(\mathbf{U}(\mathbf{b}), \mathbf{b})$.

There are various methods to compute $\delta F/\delta b_n$. There is the FD method which as already mentioned has a cost that scales with the number of design variables N. Another method is that of direct differentiation, where the state equations are differentiated w.r.t. the design variables in order to obtain the values $\delta \boldsymbol{U}/\delta b_n$. N systems of equations must be solved in order to find the derivatives $\delta \boldsymbol{U}/\delta b_n$, meaning this method also scales with the number of the design variables. The adjoint methodology has the advantage that its cost is independent of N.

Application of the continuous adjoint methodology starts with the introduction of an augmented objective function. Here, the aforementioned $E - SI$ formulation is used.

$$F_{aug} = F + \int_\Omega u_i R_i^v d\Omega + \int_\Omega q R^p d\Omega + \int_\Omega \tilde{\nu}_a R^{\tilde{\nu}} d\Omega + \int_\Omega m_i^a R_i^m d\Omega \tag{3.10}$$

where Ω is the computational domain, u_i is the adjoint velocity and q the adjoint pressure and m_i^a the adjoint grid displacements. Note that from eq. 3.9 R_i^v, R^p, $R^{\tilde{\nu}}$ and R_i^m are zero for every solution to the primal state equations and the value of F is therefore the same as that of F_{aug}.

As mentioned above, the goal is to compute the derivatives of F w.r.t. the design variables, or equivalently $\delta F_{aug}/\delta b_n$.

By differentiating eq.3.10 and through the use of the Leibniz (eq.3.4) and Green-Gauss theorem, we obtain

$$\begin{aligned}
\frac{\delta F_{aug}}{\delta b_n} &= \frac{\delta F}{\delta b_n} + \frac{\delta}{\delta b_n}\int_\Omega u_i R_i^v d\Omega + \frac{\delta}{\delta b_n}\int_\Omega q R^p d\Omega + \frac{\delta}{\delta b_n}\int_\Omega \tilde{\nu}_a R^{\tilde{\nu}} d\Omega \\
&= \frac{\delta F}{\delta b_n} + \int_\Omega u_i \frac{\partial R_i^v}{\partial b_n} d\Omega + \int_\Omega q \frac{\partial R^p}{\partial b_n} d\Omega + \int_\Omega \tilde{\nu}_a \frac{\partial R^{\tilde{\nu}}}{\partial b_n} d\Omega + \int_S m_i^a n_j \frac{\partial}{\partial x_j}\left(\frac{\delta x_i}{\delta b_n}\right) dS \\
&- \int_{S_W} \frac{\partial m_i^a}{\partial x_j} n_j \frac{\delta x_i}{\delta b_n} dS + \int_\Omega \frac{\partial^2 m_i^a}{\partial x_j^2}\frac{\delta x_i}{\delta b_n} d\Omega + \int_S (u_i R_i^v + q R^p + \tilde{\nu}_a R^{\tilde{\nu}} + m_i^a R_i^m) n_k \frac{\delta x_k}{\delta b_n} dS
\end{aligned} \tag{3.11}$$

The boundary of the computational domain S consists of the inlet S_I and outlet S_O, the fixed walls S_W and the controlled walls S_{Wp}. The components of the unit

vector normal to the surface are denoted by n_k, and x_k are the grid nodes positions. For the non-controlled boundaries $\dfrac{\delta x_k}{\delta b_n} = 0$.

The total derivative of a quantity Φ can be written as

$$\frac{\delta \Phi}{\delta b_n} = \frac{\partial \Phi}{\partial b_n} + \frac{\partial \Phi}{\partial x_k}\frac{\delta x_k}{\delta b_n} \tag{3.12}$$

The above definition of the total derivative can be seen in analogy with the definition of the material derivative in fluid dynamics i.e. $\frac{\delta \Phi}{\delta t} = \frac{\partial \Phi}{\partial t} + \frac{\partial \Phi}{\partial x}\frac{\delta x}{\delta t}$.

For an arbitrary quantity Φ computed on a surface (such as the pressure on the surface of an airfoil), eq. 3.12 takes a slightly different form. Since any sufficiently small surface deformation can be seen as a normal perturbation, only the normal part of the surface deformation velocity $\delta x_k/\delta b_n$ causes a change in Φ, hence

$$\frac{\delta_s \Phi}{\delta b_n} = \frac{\partial \Phi}{\partial b_n} + \frac{\partial \Phi}{\partial x_k} n_k \frac{\delta x_m}{\delta b_n} n_m \tag{3.13}$$

3.4 Differentiation of the Objective Function

The computation of the sensitivity derivatives $\delta F_{aug}/\delta b_n$ through eq.3.11 requires an expression for $\delta F/\delta b_n$. In the general case, an objective function will consist both of volume and surface integrals. The normal vector to the surface appears in the definition of most surface objective functions and, therefore, a general objective can be written as

$$F = \int_S F_{S_i} n_i dS + \int_\Omega F_\Omega d\Omega \tag{3.14}$$

Differentiation of eq. 3.14 w.r.t. b_n yields

$$\frac{\delta F}{\delta b_n} = \frac{\delta}{\delta b_n}\int_S F_{S_i} n_i dS + \frac{\delta}{\delta b_n}\int_\Omega F_\Omega d\Omega \tag{3.15}$$

The detailed derivation of the expressions for the surface and volume integral on the RHS of eq. 3.14 can be found in [14]. The surface integral is written as

$$\begin{aligned}\frac{\delta}{\delta b_n}\int_S F_{S_i} n_i dS = &\int_S \frac{\partial F_{S_i}}{\partial v_k} n_i \frac{\partial v_k}{\partial b_n} dS + \int_S \frac{\partial F_{S_i}}{\partial p} n_i \frac{\partial p}{\partial b_n} dS + \int_S \frac{\partial F_{S_i}}{\partial \tau_{kj}} n_i \frac{\partial \tau_{kj}}{\partial b_n} dS + \int_S \frac{\partial F_{S_i}}{\partial \tilde{\nu}} n_i \frac{\partial \tilde{\nu}}{\partial b_n} dS \\ &+ \int_S n_i \frac{\partial F_{S_i}}{\partial x_m} n_m \frac{\delta x_k}{\delta b_n} n_k dS - \int_S F_{S_i} \frac{\partial_t}{\partial x_i}\left(\frac{\delta x_k}{\delta b_n} n_k\right) dS - \int_S F_{S_i} n_i \kappa \frac{\delta x_k}{\delta b_n} n_k dS\end{aligned} \tag{3.16}$$

whereas the volume integral can be written as

$$\frac{\delta}{\delta b_n}\int_\Omega F_\Omega d\Omega = \int_\Omega \acute{F}^v_{\Omega,i}\frac{\partial v_i}{\partial b_n}d\Omega + \int_\Omega \acute{F}^p_\Omega \frac{\partial p}{\partial b_n}d\Omega + \int_\Omega \acute{F}^{\tilde{\nu}}_\Omega \frac{\partial \tilde{\nu}}{\partial b_n}d\Omega + \int_S \acute{F}^v_{S,i}\frac{\partial v_i}{\partial b_n}dS + \int_S \acute{F}^p_S \frac{\partial p}{\partial b_n}dS + \int_S \acute{F}^{\tilde{\nu}}_S \frac{\partial \tilde{\nu}}{\partial b_n}dS + \int_S F_\Omega n_k \frac{\delta x_k}{\delta b_n}dS \tag{3.17}$$

The expression 3.17 results from applying the Leibniz theorem on $\frac{\delta}{\delta b_n}\int_\Omega F_\Omega d\Omega$ and the Green-Gauss theorem, if necessary, i.e. if any differential operators of v_i, p or $\tilde{\nu}$ are included in the expression of F_Ω. The quantity $\acute{F}^\Phi_\Omega$ includes the partial derivatives $\frac{\partial F_\Omega}{\partial \Phi}$, plus any term that might result from the use of the Green-Gauss theorem for integrals of the form $\int_\Omega \frac{\partial}{\partial b_n}\left(\frac{\partial \Phi}{\partial x_j}\right)d\Omega$.

Given the above, the final expression for $\delta F \backslash \delta b_n$ is

$$\begin{aligned}\frac{\delta F}{\delta b_n} = &\int_\Omega \acute{F}^v_{\Omega,i}\frac{\partial v_i}{\partial b_n}d\Omega + \int_\Omega \acute{F}^p_\Omega \frac{\partial p}{\partial b_n}d\Omega + \int_\Omega \acute{F}^{\tilde{\nu}}_\Omega \frac{\partial \tilde{\nu}}{\partial b_n}d\Omega + \int_S \left(\acute{F}^v_{S,i} + \frac{\partial F_{S_k}}{\partial v_i}n_k\right)\frac{\partial v_i}{\partial b_n}dS \\ &+ \int_S \left(\frac{\partial F_{S_i}}{\partial p}n_i + \acute{F}^p_S\right)\frac{\partial p}{\partial b_n}dS + \int_S \left(\frac{\partial F_{S_i}}{\partial \tilde{\nu}}n_i + \acute{F}^{\tilde{\nu}}_S\right)\frac{\partial \tilde{\nu}}{\partial b_n}dS + \int_S \frac{\partial F_{S_k}}{\partial \tau_{ij}}n_k\frac{\partial \tau_{ij}}{\partial b_n}dS \\ &+ \int_{S_{W_p}} F_\Omega n_k \frac{\delta x_k}{\delta b_n}dS + \int_{S_{W_p}} n_i \frac{\partial F_{S_i}}{\partial x_m}n_m \frac{\delta x_k}{\delta b_n}n_k dS + \int_{S_{W_p}} F_{S_i}\frac{\delta n_i}{\delta b_n}dS + \int_{S_{W_p}} F_{S_i}n_i\frac{\delta(dS)}{\delta b_n}\end{aligned} \tag{3.18}$$

The above equation includes the partial derivatives of the flow variables w.r.t. the design variables. The aim of the adjoint methodology is to avoid the computation of those terms, which for N design variables would require the solution of N systems of equations similar to the Navier-Stokes.

3.5 Derivation of the Adjoint Equations

Now, having an expression for $\frac{\delta F}{\delta b_n}$, a final expression for $\frac{\delta F_{aug}}{\delta b_n}$ can be obtained. Going back to eq. 3.11, one sees that an expression also has to be derived for the partial derivatives $\frac{\partial R^v_i}{\partial b_n}$, $\frac{\partial R^p}{\partial b_n}$ and $\frac{\partial R^{\tilde{\nu}}}{\partial b_n}$.

Differentiation of eqs. 3.9 yields

$$\frac{\partial R^p}{\partial b_n} = -\frac{\partial}{\partial x_j}\left(\frac{\partial v_j}{\partial b_n}\right) \tag{3.19}$$

and

$$\begin{aligned}\frac{\partial R^v_i}{\partial b_n} = &\frac{\partial v_j}{\partial b_n}\frac{\partial v_i}{\partial x_j} + v_j\frac{\partial}{\partial x_j}\left(\frac{\partial v_i}{\partial b_n}\right) + \frac{\partial}{\partial x_i}\left(\frac{\partial p}{\partial b_n}\right) - \frac{\partial}{\partial x_j}\left[(\nu+\nu_t)\frac{\partial}{\partial x_j}\left(\frac{\partial v_i}{\partial b_n}\right) + \frac{\partial}{\partial x_i}\left(\frac{\partial v_j}{\partial b_n}\right)\right] \\ &- \frac{\partial}{\partial x_j}\left[\frac{\partial \nu_t}{\partial b_n}\left(\frac{\partial v_i}{\partial x_j} + \frac{\partial v_j}{\partial x_i}\right)\right]\end{aligned} \tag{3.20}$$

The differentiation of the turbulence model equation, eq.3.9c yields

$$\begin{aligned}\frac{\partial R^{\tilde{\nu}}}{\partial b_n} =& \frac{\partial \tilde{\nu}}{\partial x_j}\frac{\partial v_j}{\partial b_n} + v_j\frac{\partial}{\partial x_j}\left(\frac{\partial \tilde{\nu}}{\partial b_n}\right) - \frac{\partial}{\partial x_j}\left[\left(\nu+\frac{\tilde{\nu}}{\sigma}\right)\frac{\partial}{\partial x_j}\left(\frac{\partial \tilde{\nu}}{\partial b_n}\right)\right] - \frac{1}{\sigma}\frac{\partial}{\partial x_j}\left(\frac{\partial \tilde{\nu}}{\partial b_n}\frac{\partial \tilde{\nu}}{\partial x_j}\right) \\ & - 2\frac{c_{b2}}{\sigma}\frac{\partial \tilde{\nu}}{\partial x_j}\frac{\partial}{\partial x_j}\left(\frac{\partial \tilde{\nu}}{\partial b_n}\right) + \tilde{\nu}\left(-\frac{\partial P}{\partial b_n}+\frac{\partial D}{\partial b_n}\right) + (-P+D)\frac{\partial \tilde{\nu}}{\partial b_n} \end{aligned} \tag{3.21}$$

where the fact that the partial derivatives w.r.t. b_n and x_j are interchangeable has been used. The continuous adjoint to the Spalart-Allmaras model can be found in great detail in [14].

Finally, differentiation of eq. 3.7 produces

$$\frac{\partial R_i^m}{\partial b_n} = \frac{\partial}{\partial b_n}\left(\frac{\partial^2 m_i}{\partial x_j^2}\right) = \frac{\partial^2}{\partial x_j^2}\left(\frac{\partial m_i}{\partial b_n}\right) = 0 \tag{3.22}$$

The integrals $\int_\Omega u_i \frac{\partial R_i^v}{\partial b_n} d\Omega$, $\int_\Omega q\frac{\partial R^p}{\partial b_n} d\Omega$ and $\int_\Omega \tilde{\nu}_a \frac{\partial R^{\tilde{\nu}}}{\partial b_n} d\Omega$ appearing in eq. 3.11 can now be expressed using eqs. 3.19, 3.20, 3.21 and the Green-Gauss theorem. Regarding the volume integral $\int_\Omega q\frac{\partial R^p}{\partial b_n} d\Omega$, the use of eq. 3.19 and the Green-Gauss theorem yields

$$\int_\Omega -q\frac{\partial}{\partial x_j}\left(\frac{\partial v_j}{\partial b_n}\right) d\Omega = -\int_S q\frac{\partial v_j}{\partial b_n} n_j dS + \int_\Omega \frac{\partial q}{\partial x_j}\frac{\partial v_j}{\partial b_n} d\Omega \tag{3.23}$$

The integrals $\int_\Omega u_i \frac{\partial R_i^v}{\partial b_n} d\Omega$ and $\int_\Omega \tilde{\nu}_a \frac{\partial R^{\tilde{\nu}}}{\partial b_n} d\Omega$ are analyzed in the same manner. After this step the final expression for the sensitivity derivatives of the objective function F can be derived

$$\begin{aligned}\frac{\delta F_{aug}}{\delta b_n} =& \int_S \left[u_i v_j n_j + (\nu+\nu_t)\left(\frac{\partial u_i}{\partial x_j}+\frac{\partial u_j}{\partial x_i}\right)n_j - q n_i + \tilde{\nu}_a\tilde{\nu}\frac{C_Y}{Y}e_{mjk}\frac{\partial v_k}{\partial x_j}e_{mli}n_l + \frac{\partial F_{S_k}}{\partial v_i}n_k + \acute{F}^v_{S,i}\right]\frac{\partial v_i}{\partial b_n}dS \\ & + \int_S (u_j n_j + \frac{\partial F_{S_i}}{\partial p}n_i + \acute{F}^p_S)\frac{\partial p}{\partial b_n}dS \\ & + \int_S \left[\tilde{\nu}_a v_j n_j + \left(\nu+\frac{\tilde{\nu}}{\sigma}\right)\frac{\partial \tilde{\nu}_a}{\partial x_j}n_j - \frac{\tilde{\nu}_a}{\sigma}(1+2c_{b_2})\frac{\partial \tilde{\nu}}{\partial x_j}n_j + \frac{\partial F_{S_k}}{\partial \tilde{\nu}}n_k + \acute{F}^{\tilde{\nu}}_S\right]\frac{\partial \tilde{\nu}}{\partial b_n}dS \\ & + \int_S (-u_i n_j + \frac{\partial F_{S_k}}{\partial \tau_{ij}}n_k)\frac{\partial \tau_{ij}}{\partial b_n}dS - \int_S \tilde{\nu}_a\left(\nu+\frac{\tilde{\nu}}{\sigma}\right)\frac{\partial}{\partial b_n}\left(\frac{\partial \tilde{\nu}}{\partial x_j}\right)n_j dS \\ & + \int_\Omega R_i^u\frac{\partial v_i}{\partial b_n}d\Omega + \int_\Omega R^q\frac{\partial p}{\partial b_n}d\Omega + \int_\Omega R^{\tilde{\nu}_a}\frac{\partial \tilde{\nu}}{\partial b_n}d\Omega + \int_\Omega R_k^{m^a}\frac{\delta x_k}{\delta b_n}d\Omega \\ & + \int_{S_{W_p}} n_i\frac{\partial F_{S_{W_{p,i}}}}{\partial x_m}n_m\frac{\delta x_k}{\delta b_n}n_k dS + \int_{S_{W_p}} F_{S_{W_{p,i}}}\frac{\delta n_i}{\delta b_n}dS + \int_{S_{W_p}} F_{S_{W_{p,i}}}n_i\frac{\delta(dS)}{\delta b_n} \\ & + \int_{S_W}\frac{\partial m_i^a}{\partial x_j}n_j\frac{\delta x_i}{\delta b_n}dS + \int_\Omega \tilde{\nu}\tilde{\nu}_a C_\Delta\frac{\partial \Delta}{\partial b_n}d\Omega \end{aligned} \tag{3.24}$$

where R_i^u, R^q, $R^{\tilde{\nu}_a}$ and $R_k^{m_a}$ are given by eqs. 3.25, 3.26 3.27 and 3.28 respectively.

Four volume integrals containing the terms whose computation is to be avoided, namely $\frac{\partial v_i}{\partial b_n}$, $\frac{\partial p}{\partial b_n}$, $\frac{\partial \tilde{\nu}}{\partial b_n}$ and $\frac{\partial x_k}{\partial b_n}$ can be seen in the above expression. The multipliers of those terms in the volume integrals are set to zero. Thus, the adjoint set of equations is obtained. To sum up, the process of deriving the adjoint equations started with the Navier-Stokes, turbulence model and gdPDEs. To compute $\frac{\partial v_i}{\partial b_n}$, $\frac{\partial p}{\partial b_n}$, $\frac{\partial \tilde{\nu}}{\partial b_n}$ and $\frac{\delta x_k}{\delta b_n}$ with Direct Differentiation one would have to solve the primal equations and compute the objective function. Then, the primal equations would be differentiated w.r.t. each design variable b_n in order to compute $\frac{\partial v_i}{\partial b_n}$, $\frac{\partial p}{\partial b_n}$ $\frac{\partial \tilde{\nu}}{\partial b_n}$ and $\frac{\delta x_k}{\delta b_n}$. This would be done N times i.e. N such systems of equations would have to be solved. This is where the adjoint comes in. An augmented objective function F_{aug} was defined, which is the same as the objective function F, with the addition of some zero integrals. The integrals are as many as the primal state variables, so that during their differentiation, the derivatives of each primal state variable w.r.t. b_n will emerge. When differentiating the objective function F w.r.t. b_n, the "unwanted" terms $\frac{\partial v_i}{\partial b_n}$, $\frac{\partial p}{\partial b_n}$, $\frac{\partial \tilde{\nu}}{\partial b_n}$ and $\frac{\partial x_k}{\partial b_n}$ appear. However, the introduction of the zero integrals in the expression of F_{aug} has also led to the appearance of $\frac{\partial v_i}{\partial b_n}$, $\frac{\partial p}{\partial b_n}$, $\frac{\partial \tilde{\nu}}{\partial b_n}$ and $\frac{\partial x_k}{\partial b_n}$, multiplied with expressions containing the adjoint variables. This allows us to group together all terms containing $\frac{\partial v_i}{\partial b_n}$, $\frac{\partial p}{\partial b_n}$, $\frac{\partial \tilde{\nu}}{\partial b_n}$ and $\frac{\partial x_k}{\partial b_n}$ respectively, and demand that their multipliers be zero. This can be done, since the adjoint fields are artificial, introduced to facilitate the process of computing the sensitivity derivatives.

The derived adjoint equations therefore read

$$R^q = -\frac{\partial u_j}{\partial x_j} + \acute{F}^p_\Omega = 0 \tag{3.25}$$

$$\begin{aligned} R^u_i =& u_j\frac{\partial v_j}{\partial x_i} - \frac{\partial (v_j u_i)}{\partial x_j} - \frac{\partial}{\partial x_j}\left[(\nu+\nu_t)\left(\frac{\partial u_i}{\partial x_j}+\frac{\partial u_j}{\partial x_i}\right)\right] + \frac{\partial q}{\partial x_i} + \acute{F}^v_{\Omega,i} \\ &+\tilde{\nu}_a\frac{\partial \tilde{\nu}}{\partial x_i} - \frac{\partial}{\partial x_l}\left(\tilde{\nu}_a\tilde{\nu}\frac{C_Y}{Y}e_{mjk}\frac{\partial v_k}{\partial x_j}e_{mli}\right) = 0 \ , \ i = 1,2(,3) \end{aligned} \tag{3.26}$$

$$\begin{aligned} R^{\tilde{\nu}_a} =& -\frac{\partial (v_j\tilde{\nu}_a)}{\partial x_j} - \frac{\partial}{\partial x_j}\left[\left(\nu+\frac{\tilde{\nu}}{\sigma}\right)\frac{\partial \tilde{\nu}_a}{\partial x_j}\right] + \frac{1}{\sigma}\frac{\partial \tilde{\nu}_a}{\partial x_j}\frac{\partial \tilde{\nu}}{\partial x_j} + 2\frac{c_{b2}}{\sigma}\frac{\partial}{\partial x_j}\left(\tilde{\nu}_a\frac{\partial \tilde{\nu}}{\partial x_j}\right) \\ &+\tilde{\nu}_a\tilde{\nu}C_{\tilde{\nu}} + \frac{\partial \nu_t}{\partial \tilde{\nu}}\frac{\partial u_i}{\partial x_j}\left(\frac{\partial u_i}{\partial x_j}+\frac{\partial u_j}{\partial x_i}\right) + (-P+D)\tilde{\nu}_a + \acute{F}^{\tilde{\nu}}_\Omega = 0 \end{aligned} \tag{3.27}$$

$$R^{m^a}_k = \frac{\partial^2 m^a_k}{\partial x_j^2} + \frac{\partial}{\partial x_j}\left\{u_i v_j\frac{\partial v_i}{\partial x_k} + u_j\frac{\partial p}{\partial x_k} + \tau^a_{ij}\frac{\partial v_i}{\partial x_k} - u_i\frac{\partial \tau_{ij}}{\partial x_k} - q\frac{\partial v_j}{\partial x_k}\right\} = 0 \tag{3.28}$$

and the expression for the sensitivity derivatives after the elimination of the volume

integrals containing the adjoint equations is

$$\begin{aligned}
\frac{\delta F_{aug}}{\delta b_n} = &\int_S \Bigg[u_i v_j n_j + (\nu + \nu_t)\left(\frac{\partial u_i}{\partial x_j} + \frac{\partial u_j}{\partial x_i}\right) n_j - q n_i + \tilde{\nu}_a \tilde{\nu} \frac{C_Y}{Y} e_{mjk} \frac{\partial v_k}{\partial x_j} e_{mli} n_l + \frac{\partial F_{S_k}}{\partial v_i} n_k + \acute{F}^v_{S,i} \Bigg] \frac{\partial v_i}{\partial b_n} dS \\
&+ \int_S (u_j n_j + \frac{\partial F_{S_i}}{\partial p} n_i + \acute{F}^p_S) \frac{\partial p}{\partial b_n} dS \\
&+ \int_S \left[\tilde{\nu}_a v_j n_j + \left(\nu + \frac{\tilde{\nu}}{\sigma}\right) \frac{\partial \tilde{\nu}_a}{\partial x_j} n_j - \frac{\tilde{\nu}_a}{\sigma}(1 + 2c_{b_2}) \frac{\partial \tilde{\nu}}{\partial x_j} n_j + \frac{\partial F_{S_k}}{\partial \tilde{\nu}} n_k + \acute{F}^{\tilde{\nu}}_S \right] \frac{\partial \tilde{\nu}}{\partial b_n} dS \\
&+ \int_S (-u_i n_j + \frac{\partial F_{S_k}}{\partial \tau_{ij}} n_k) \frac{\partial \tau_{ij}}{\partial b_n} dS - \int_S \tilde{\nu}_a \left(\nu + \frac{\tilde{\nu}}{\sigma}\right) \frac{\partial}{\partial b_n} \left(\frac{\partial \tilde{\nu}}{\partial x_j}\right) n_j dS \\
&+ \int_{S_{W_p}} n_i \frac{\partial F_{S_{W_{p,i}}}}{\partial x_m} n_m \frac{\delta x_k}{\delta b_n} n_k dS + \int_{S_{W_p}} F_{S_{W_{p,i}}} \frac{\delta n_i}{\delta b_n} dS + \int_{S_{W_p}} F_{S_{W_{p,i}}} n_i \frac{\delta (dS)}{\delta b_n} \\
&+ \int_{S_W} \frac{\partial m^a_i}{\partial x_j} n_j \frac{\delta x_i}{\delta b_n} dS + \int_\Omega \tilde{\nu} \tilde{\nu}_a C_\Delta \frac{\partial \Delta}{\partial b_n} d\Omega
\end{aligned} \tag{3.29}$$

Had the SI formulation been used instead, the derived expression of the sensitivity derivatives would have been the same, but

1. The $LBterm$, i.e. $\int_{S_{W_p}} (u_i R^v_i + q R^p + \tilde{\nu}_a R^{\tilde{\nu}} + F_\Omega) \frac{\delta x_k}{\delta b_n} n_k dS$ would be present in the SI sensitivity derivatives.
2. The term $\int_{S_W} \frac{\partial m^a_i}{\partial x_j} n_j \frac{\delta x_i}{\delta b_n} dS$ would not be present

3.6 Adjoint Boundary Conditions

Just as the adjoint field equations were derived to eliminate the volume integrals containing the partial derivatives of the primal state variables w.r.t. the design variables, the adjoint boundary conditions are in turn derived so that the surface integrals containing these derivatives are eliminated. For the sake of brevity, let I_1, I_2, I_3 be the first, second and third and fourth integral respectively in eq. 3.29 i.e.

$$I_1 = \int_S \left[u_i v_j n_j + (\nu + \nu_t)\left(\frac{\partial u_i}{\partial x_j} + \frac{\partial u_j}{\partial x_i}\right) n_j - q n_i + \tilde{\nu}_a \tilde{\nu} \frac{C_Y}{Y} e_{mjk} \frac{\partial v_k}{\partial x_j} e_{mli} n_l + \frac{\partial F_{S_k}}{\partial v_i} n_k + \acute{F}^v_{S,i} \right] \frac{\partial v_i}{\partial b_n} dS$$

$$I_2 = \int_S (u_j n_j + \frac{\partial F_{S_i}}{\partial p} n_i + \acute{F}^p_S) \frac{\partial p}{\partial b_n} dS$$

$$I_3 = \int_S \left[\tilde{\nu}_a v_j n_j + \left(\nu + \frac{\tilde{\nu}}{\sigma}\right) \frac{\partial \tilde{\nu}_a}{\partial x_j} n_j - \frac{\tilde{\nu}_a}{\sigma}(1 + 2c_{b_2}) \frac{\partial \tilde{\nu}}{\partial x_j} n_j + \frac{\partial F_{S_k}}{\partial \tilde{\nu}} n_k + \acute{F}^{\tilde{\nu}}_S \right] \frac{\partial \tilde{\nu}}{\partial b_n} dS$$

$$I_4 = \int_S (-u_i n_j + \frac{\partial F_{S_k}}{\partial \tau_{ij}} n_k) \frac{\partial \tau_{ij}}{\partial b_n} dS$$

$$I_5 = \int_S \tilde{\nu}_a \left(\nu + \frac{\tilde{\nu}}{\sigma}\right) \frac{\partial}{\partial b_n} \left(\frac{\partial \tilde{\nu}}{\partial x_j}\right) n_j dS$$

The derivation of the adjoint boundary conditions can be found in [14] in great detail.

Inlet S_I

The primal boundary conditions applied at inlet boundaries are
• Dirichlet boundary conditions for the velocity. Since velocity is fixed at the inlet, $\delta v_i / \delta b_n = 0$. Since the inlet is a non-controlled boundary i.e. $\delta x_k / \delta b_n = 0$ and taking eq.3.12 for the material derivative into account, it follows that $\delta v_i / \delta b_n = \partial v_i / \partial b_n = 0$. This means that the the first integral in eq.3.29 is zero i.e. $\boldsymbol{I_1 = 0}$. The same applies to the third integral I_3, since a Dirichlet boundary condition is imposed on $\tilde{\nu}$ at the inlet as well. Thus, $\boldsymbol{I_3 = 0}$ at the inlet.

• Zero Neumann condition for the pressure.

The integrals $\boldsymbol{I_2}$ and $\boldsymbol{I_4}$ can be eliminated by demanding

$$u_j n_j = u_{\langle n \rangle} = -\frac{\partial F_{S_{I,i}}}{\partial p} n_i - \acute{F}^p_{S_I} \tag{3.30a}$$

$$u^I_{\langle t \rangle} = \frac{\partial F_{S_{I,k}}}{\partial \tau_{ij}} n_k t^I_i n_j + \frac{\partial F_{S_{I,k}}}{\partial \tau_{ij}} n_k t^I_j n_i \tag{3.30b}$$

$$u^{II}_{\langle t \rangle} = \frac{\partial F_{S_{I,k}}}{\partial \tau_{ij}} n_k t^{II}_i n_j + \frac{\partial F_{S_{I,k}}}{\partial \tau_{ij}} n_k t^{II}_j n_i \tag{3.30c}$$

where t_i^I, t_i^{II} are the components of the tangent to the surface unit vectors. One of them e.g. t_i^I can be an arbitrary unit vector parallel to the surface, whereas the other, t_i^{II}, forms an orthogonal system with n and t_i^I.

Eq.3.30a gives the normal component of the adjoint velocity, whereas eq.3.30b and 3.30c its two tangential components. Since the above three velocity components at the inlet are, as can be seen, functions of the objective function F, they are zero in the case that F is not defined on the inlet.

The three integrals I_1, I_2, I_3, I_4 have been eliminated, giving the boundary conditions for the three components of the adjoint velocity, but no boundary condition has been derived for the adjoint pressure q. For that reason, a zero Neumann boundary condition for q is applied. Finally, a zero Dirichlet boundary condition is imposed on $\tilde{\nu}_a$, rendering eq. 3.29 independent of $\frac{\partial}{\partial b_n}\left(\frac{\partial \tilde{\nu}}{\partial b_n}\right)n_j$, i.e $\boldsymbol{I_5 = 0}$.

Outlet S_O

At the outlet the following boundary conditions for the primal state variables apply

• A Dirichlet boundary condition for the pressure, which means that $\delta p/\delta b_n = 0$. Again taking into account that the outlet is - like the inlet - a fixed boundary, it follows that $\delta p/\delta b_n = \partial p/\partial b_n = 0$. Therefore $\boldsymbol{I_2 = 0}$.

• zero Neumann conditions for the velocity components v_i and for $\tilde{\nu}$. This means that $\frac{\partial v_i}{\partial x_j}n_j = \frac{\partial v_i}{\partial n} = 0$ and $\frac{\partial \tilde{\nu}}{\partial x_j}n_j = \frac{\partial \tilde{\nu}}{\partial n} = 0$, thus $\boldsymbol{I_5 = 0}$

Since the outlet is at a distance from the controlled boundaries, an almost uniform velocity profile can be assumed along S_O and thus negligible shear stresses (since the stress tensor is defined as $\tau_{ij} = (\nu + \nu_t)\left(\frac{\partial v_i}{x_j} + \frac{\partial v_j}{x_i}\right)$). This means the integral $\boldsymbol{I_4}$ can be neglected.

In order to eliminate $\boldsymbol{I_1}$, it is set equal to zero, i.e.

$$u_i v_j n_j + (\nu+\nu_t)\left(\frac{\partial u_i}{\partial x_j} + \frac{\partial u_j}{\partial x_i}\right)n_j - q n_i + \tilde{\nu}_a \tilde{\nu}\frac{C_Y}{Y}e_{mjk}\frac{\partial v_k}{\partial x_j}e_{mli}n_l + \frac{\partial F_{S_k}}{\partial v_i}n_k + \acute{F}^v_{S,i} = 0 \quad (3.31)$$

That gives rise to three equations (for i=1,2,3) with four unknown quantities i.e. the adjoint pressure q and the three components of the adjoint velocity u_i. After a zero Neumann boundary condition is imposed on the normal component of the adjoint velocity $u_{<n>}$, the boundary conditions for the adjoint pressure and tangential components of the velocity can be derived by decomposing eqs. 3.31 into their normal and tangential components. The expression for the adjoint pressure q is thus derived by multiplying eq. 3.31 with the normal to the surface vector, n_i. Therefore

$$q = u_{\langle n\rangle}v_{\langle n\rangle} + 2(\nu+\nu_t)\frac{\partial u_{\langle n\rangle}}{\partial n} + \frac{\partial F_{S_{O,k}}}{\partial v_i}n_k n_i + \acute{F}^v_{S_{O,i}}n_i + \tilde{\nu}_a\tilde{\nu}\frac{C_Y}{Y}e_{mjk}\frac{\partial v_k}{\partial x_j}e_{mli}n_l n_i = 0 \quad (3.32)$$

An expression for the tangential adjoint velocity components is derived by mul-

tiplying *eq.* 3.31 with the tangent to the surface vectors, $t_i^l, l=1,2$

$$v_n u^l_{\langle t\rangle}+(\nu+\nu_t)\left(\frac{\partial u^l_{\langle t\rangle}}{\partial n}+\frac{\partial u_{\langle n\rangle}}{\partial t^l}\right)+\frac{\partial F_{S_{O,k}}}{\partial v_i}n_k t_i^l+\acute{F}^v_{S_{O,i}}t_i^l-\tilde{\nu}_a\tilde{\nu}\frac{C_Y}{Y}e_{mjk}\frac{\partial v_k}{\partial x_j}e_{mzi}n_z t_i^l=0 \tag{3.33}$$

Finally, a Robin-type boundary condition for $\tilde{\nu}_a$ can be obtained by setting $\boldsymbol{I_3}=\mathbf{0}$, taking into account that $\frac{\partial\tilde{\nu}}{\partial x_j}=0$. Therefore:

$$\tilde{\nu}_a v_j n_j+\left(\nu+\frac{\tilde{\nu}}{\sigma}\right)\frac{\partial\tilde{\nu}_a}{\partial x_j}n_j+\frac{\partial F_{S_{O,k}}}{\partial\tilde{\nu}}n_k+\acute{F}^{\tilde{\nu}}_{S_O}=0 \tag{3.34}$$

Non-controlled / Fixed Wall Boundaries S_W

The primal boundary conditions applied on the fixed wall boundaries are: a zero Dirichlet condition for $\tilde{\nu}$ ($\Rightarrow \boldsymbol{I_3}=\mathbf{0}$), a no penetration condition for the velocity, a zero Neumann condition for the pressure and the law of the wall for the normal component of the stress tensor along S_W. A zero Dirichlet boundary condition imposed on $\tilde{\nu}_a$, leads to the elimination of the fifth integral in eq. 3.29, i.e. $\boldsymbol{I_5}=\mathbf{0}$. The elimination of the integral $\boldsymbol{I_2}$ yields

$$u_{\langle n\rangle}=-\frac{\partial F_{S_{W,i}}}{\partial p}n_i-\acute{F}^p_{S_W} \tag{3.35}$$

Further development of $\boldsymbol{I_1}$ and $\boldsymbol{I_4}$ gives the following

$$u^{II}_{\langle t\rangle}=\frac{\partial F_{S_{W,k}}}{\partial\tau_{ij}}n_k t_i^{II}n_j+\frac{\partial F_{S_{W,k}}}{\partial\tau_{ij}}n_k t_j^{II}n_i \tag{3.36}$$

and

$$u_\tau^2=(\nu+\nu_t)\left(\frac{\partial u_i}{\partial x_j}+\frac{\partial u_j}{\partial x_i}\right)n_j t_i^I \tag{3.37}$$

where u_τ is the adjoint friction velocity. Finally, a zero Neumann condition is imposed on the adjoint pressure q.

Controlled Wall Boundaries, S_{W_p}

The boundary conditions for the primal state variables on paramaterized wall boundaries, are the same as the ones imposed on non-controlled walls. Contrary however to the case of fixed walls, $\delta x_k/\delta b_n$ is not zero, since for controlled boundaries the position of the boundary nodes x_k changes during optimization. Thus, the total and partial derivatives of flow quantities do not coincide. In addition, the total variation of the normal and tangent to the surface vectors are not zero, leading to the appearance of some extra terms during the formulation of the adjoint boundary conditions [14].

3.6.1 Final Expression for the Sensitivity Derivatives

Having produced the adjoint field equations and derived their boundary conditions, the remaining terms in eq. 3.29 will form the final expression for the sensitivity derivatives, which is as follows

$$\begin{aligned}
\frac{\delta F_{aug}}{\delta b_n} =& T_{SD}^{WF} - \int_{S_{W_p}} SD_1 \frac{\partial \tau_{ij}}{\partial x_m} n_j t_i^I n_m n_k \frac{\delta x_k}{\delta b_n} dS - \int_{S_{W_p}} SD_1 \tau_{ij} \frac{\delta (n_j t_i^I)}{\delta b_n} \frac{\delta x_k}{\delta b_n} dS \\
&+ \int_{S_{W_p}} SD_{2,i} v_{\langle t \rangle}^I \frac{\delta t_i^I}{\delta b_n} dS - \int_{S_{W_p}} SD_{2,i} \frac{\partial v_i}{\partial x_m} n_m n_k \frac{\delta x_k}{\delta b_n} dS \\
&- \int_{S_{W_p}} \left[\left(\nu + \frac{\tilde{\nu}}{\sigma} \right) \frac{\partial \tilde{\nu}_a}{\partial x_j} n_j + \frac{\partial F_{S_z}}{\partial \tilde{\nu}} n_z + \acute{F}_S^{\tilde{\nu}} \right] \frac{\partial \tilde{\nu}}{\partial x_m} n_m n_k \frac{\delta x_k}{\delta b_n} dS \\
&- \int_{S_{W_p}} (-u_{\langle n \rangle} + \phi_{\langle n \rangle \langle n \rangle}) \left(\tau_{ij} \frac{\delta (n_i n_j)}{\delta b_n} + \frac{\partial \tau_{ij}}{\partial x_m} n_m \frac{\delta x_k}{\delta b_n} n_k n_i n_j \right) dS \\
&- \int_{S_{W_p}} \phi_{\langle t^I \rangle \langle t^I \rangle} \left(\tau_{ij} \frac{\delta (t_i^I t_j^I)}{\delta b_n} + \frac{\partial \tau_{ij}}{\partial x_m} n_m \frac{\delta x_k}{\delta b_n} n_k t_i^I t_j^I \right) dS \\
&- \int_{S_{W_p}} (\phi_{\langle t^{II} \rangle \langle t^I \rangle} + \phi_{\langle t^I \rangle \langle t^{II} \rangle}) \left(\tau_{ij} \frac{\delta (t_i^{II} t_j^I)}{\delta b_n} + \frac{\partial \tau_{ij}}{\partial x_m} n_m \frac{\delta x_k}{\delta b_n} n_k t_i^{II} t_j^I \right) dS \\
&- \int_{S_{W_p}} \phi_{\langle t^{II} \rangle \langle t^{II} \rangle} \left(\tau_{ij} \frac{\delta (t_i^{II} t_j^{II})}{\delta b_n} + \frac{\partial \tau_{ij}}{\partial x_m} n_m \frac{\delta x_k}{\delta b_n} n_k t_i^{II} t_j^{II} \right) dS \\
&- \int_{S_{W_p}} n_i \frac{\partial F_{S_{W_{p,i}}}}{\partial x_m} n_m \frac{\delta x_k}{\delta b_n} n_k dS + \int_{S_{W_p}} F_{S_{W_{p,i}}} \frac{\delta n_i}{\delta b_n} dS + \int_{S_{W_p}} F_{S_{W_{p,i}}} n_i \frac{\delta (dS)}{\delta b_n} \\
&+ \int_{S_{W_p}} A_\Delta^{WF} \frac{\partial \Delta^P}{\partial b_n} dS + \int_{S_W} A_\Delta^{WF} \frac{\partial \Delta^P}{\partial b_n} dS + \int_\Omega \tilde{\nu} \tilde{\nu}_a C_\Delta \frac{\partial \Delta}{\partial b_n} d\Omega - \int_{S_W} \frac{\partial m_i^a}{\partial x_j} n_j \frac{\delta x_i}{\delta b_n} dS
\end{aligned} \tag{3.38}$$

where

$$SD_1 = -u_{\langle t \rangle}^I + \phi_{\langle t^I \rangle \langle n \rangle} + \phi_{\langle n \rangle \langle t^I \rangle} \tag{3.39}$$

$$SD_{2,i} = (\nu + \nu_t) \left(\frac{\partial u_i}{\partial x_j} + \frac{\partial u_j}{\partial x_i} \right) n_j - q n_i + \frac{\partial F_{S_{W_{p,k}}}}{\partial v_i} n_k + \acute{F}_{S_{W_{p,i}}}^v \tag{3.40}$$

$$\phi_{ij} = \frac{\partial F_{S_{W_{p,k}}}}{\partial \tau_{ij}} n_k \tag{3.41}$$

This is a general expression that can be used with any objective function comprising surface and volume integrals. As can be seen, eq. 3.38 contains only one field integral and, therefore, all but the last term in it can be computed at a cost practically negligible compared to that of solving the primal and adjoint equations. The computation of the last term in eq. 3.38 can be done through use of finite differences, which would however increase the cost, making it scale with the number

of design variables N and would perhaps also be less accurate. As an alternative way of dealing with the differentiation of the distance Δ from the wall, the adjoint methodology can be applied to avoid the computation of $\frac{\partial \Delta}{\partial b_n}$. The Hamilton-Jacobi equation ($R_\Delta = \frac{\partial (c_j \Delta)}{\partial x_j} - \Delta \frac{\partial^2 \Delta}{\partial x_j^2} - 1 = 0$, where $c_j = \frac{\partial \Delta}{\partial x_j}$), which gives a very good approximation of the Euclidean distance field[14], can be used as the PDE governing Δ [21]. The same procedure is then used to eliminate the field integral of $\frac{\partial \Delta}{\partial b_n}$, as was used to eliminate all other "unwanted" volume integrals so far, namely, one more integral comprising the product of the adjoint distance variable Δ^a with the Hamilton-Jacobi equation is added to the expression of the augmented function. The term containing $\frac{\partial \Delta}{\partial b_n}$ is then eliminated by setting its multiplier equal to zero, thus giving rise to the adjoint equation for the distance Δ [14].

One more thing to be noted is that the primal grid displacement variables m_i are contained in neither the adjoint gdPDEs eq. 3.28, nor in the final expression for the sensitivities eq. 3.38. Therefore, the solution of the primal gdPDEs is not required for the computation of the sensitivity derivatives (of course they must be solved to renew the internal mesh). Only the adjoint gdPDEs must be solved for the computation of the sensitivities. The adjoint gdPDEs depend on adjoint flow quantities, but do not affect the solution of the adjoint flow problem. This means, that the adjoint gdPDEs can be solved at a very low cost, at a post-processing stage, after the solution of the adjoint flow PDEs.

This concludes the theory on the continuous adjoint formulation used in the simulations presented in the following chapter.

Chapter 4

Shape Optimization Results

4.1 BMW Workflow : ShapeModule

ShapeModule is the BMW shape optimization workflow into which the PCOpt OpenFOAM-based primal and adjoint solvers were integrated. ShapeModule allows the user to connect to various tools or solvers which will compute the primal and adjoint solution and, then, communicate the necessary geometry (optimization patch i.e. part of the geometry being optimized) and sensitivity derivatives back to ShapeModule where the necessary geometry updates for optimization will be computed. ShapeModule is functionally divided into three different sections :

- Core : Database, Vertex morphing implementation
- Algorithmic : Optimization algorithms like Steepest descent.
- Interface : Responsible for sending the sensitivities to ShapeModule and returning the geometry updates to the software responsible for solving the primal and adjoint problems.

Before optimization can be performed using ShapeModule, a .json (JavaScript Object Notation) file has to be setup to configure the simulation and the individual solvers for primal and adjoint solution should also be configured.

The .json file contains optimization settings such as the optimization algorithm to be used, list of objectives and constraints, name and type of output files, maximum allowed displacement (step size), as well as function type and filtering radius used on the sensitivities and displacements.

4.1.1 Vertex Morphing

Vertex Morphing [22], [23], [24] is a geometry parameterization that allows an easy to setup, node-based shape optimization . In node-based optimization methods, the shape variation is described through the nodes of the discretized (i.e. meshed) geometry. In other words, the surface node positions are the design variables. An

immediate advantage of node -based methods is that all the available degrees of freedom are used as design variables, thus giving a larger design space. In a larger design space the objective is allowed to take on a wider range of values, which can possibly allow it to reach a lower value during optimization. A disadvantage is the possible shape irregularities (resulting surface can be "noisy"). The solution to this issue would be the application of a distance-dependent smoothing filter on the resulting sensitivities and displacements of each node, which weighs the sensitivities /displacement of the node with those of its neighbors.

4.2 Integration of the PCOpt Solvers into Shape-Module

In this present master thesis, the task of coupling the OpenFOAM-based Primal and Adjoint Solvers developed by PCOpt/NTUA with the BMW optimization software "ShapeModule" was performed. ShapeModule is responsible for receiving the computed sensitivities, smoothing them, performing steepest descent and updating the surface mesh, using the technique known as "Vertex Morphing" [22], [23], [24].

A simplified diagram of the whole procedure is as follows

- Solve the primal equations.
- Solve the adjoint equations.
- Compute sensitivity derivatives.
- Send sensitivities to ShapeModule.
- ShapeModule smoothes these sensitivities and computes surface-node displacements using steepest descent.
- The computed displacements are smoothed and sent back to OpenFOAM.
- Volume mesh is updated in OpenFOAM (Updated through mesh movement, not remeshing). More specifically, OpenFOAM uses the surface node displacements computed by ShapeModule as boundary conditions to solve the Laplacian gdPDEs (eqs. 3.7) and compute the new internal nodes positions.

So, the first step was the coupling between the PCOpt/NTUA software and ShapeModule, ensuring I/O compatibility, i.e. ensuring that the sensitivity derivatives are sent into Shape-Module in the format expected by the latter.

4.3 Cases - Results

4.3.1 3D S-Bend Tube

The coupling of the PCOpt flow and adjoint solvers with ShapeModule was first tested on the simple case of a 3D duct with an S-Bend geometry and a circular cross-section.

Minimization of Total Pressure Losses (Δp_t) in a Laminar Flow

The aim of this run was to minimize the total pressure losses Δp_t from the inlet to the outlet. A Reynolds number of 1000 was chosen (laminar flow). Regarding the boundary conditions, at the inlet a Dirichlet boundary condition of 1.2m/s and a Neumann boundary condition on the pressure was chosen. At the outlet, a Dirichlet B.C. of 0 Pa on the pressure (incompressible flow) and a Neumann zero gradient condition on the velocity were imposed. Along the solid walls, zero Dirichlet conditions on the velocity and zero-gradient conditions for the pressure were imposed.

The objective function is

$$J = -\int_{S_{I,O}} \left(p + \frac{1}{2}{v_i}^2\right) v_j n_j dS \tag{4.1}$$

Differentiation of the above objective function yields

$$\begin{aligned}\frac{\delta J}{\delta b_n} = &-\int_{S_{I,O}} \frac{\delta}{\delta b_n}\left(p + \frac{1}{2}{v_i}^2\right) v_j n_j dS - \int_{S_{I,O}} \left(p + \frac{1}{2}{v_i}^2\right) \frac{\delta v_j}{\delta b_n} n_j dS \\ &- \int_{S_{I,O}} \left(p + \frac{1}{2}{v_i}^2\right) v_j \frac{\delta (n_j dS)}{\delta b_n}\end{aligned}$$

Since the above integrals are defined over the duct inlet and outlet, which are fixed i.e. non-controlled patches, the third integral on the RHS of the above equation is zero, since $\dfrac{\delta (n_j dS)}{\delta b_n} = 0$ over the above boundaries.

Therefore, we have

$$\begin{aligned}\frac{\delta J}{\delta b_n} &= -\int_{S_{I,O}} \frac{\delta}{\delta b_n}\left(p + \frac{1}{2}{v_i}^2\right) v_j n_j dS - \int_{S_{I,O}} \left(p + \frac{1}{2}{v_i}^2\right) \frac{\delta v_j}{\delta b_n} n_j dS \\ &= -\int_{S_{I,O}} \frac{\delta p}{\delta b_n} v_j n_j dS - \int_{S_{I,O}} \frac{\delta}{\delta b_n}\left(\frac{1}{2}{v_i}^2\right) v_j n_j dS \\ &\quad - \int_{S_{I,O}} \left(p + \frac{1}{2}{v_i}^2\right) \frac{\delta v_j}{\delta b_n} n_j dS \Rightarrow\end{aligned}$$

$$\frac{\delta J}{\delta b_n} = \int_{S_{I,O}} (-v_j n_j) \frac{\delta p}{\delta b_n} dS + \int_{S_{I,O}} [-v_i v_j n_j - \left(p + \frac{1}{2} {v_j}^2\right) n_i] \frac{\delta v_i}{\delta b_n} dS \qquad (4.2)$$

The optimization process ran for 34 cycles and stopped due to worsening of the mesh quality. Mesh failure is expected to happen at some point, since the mesh is updated through adaptation and not remeshed after each cycle. The convergence can be seen in fig. 4.1.

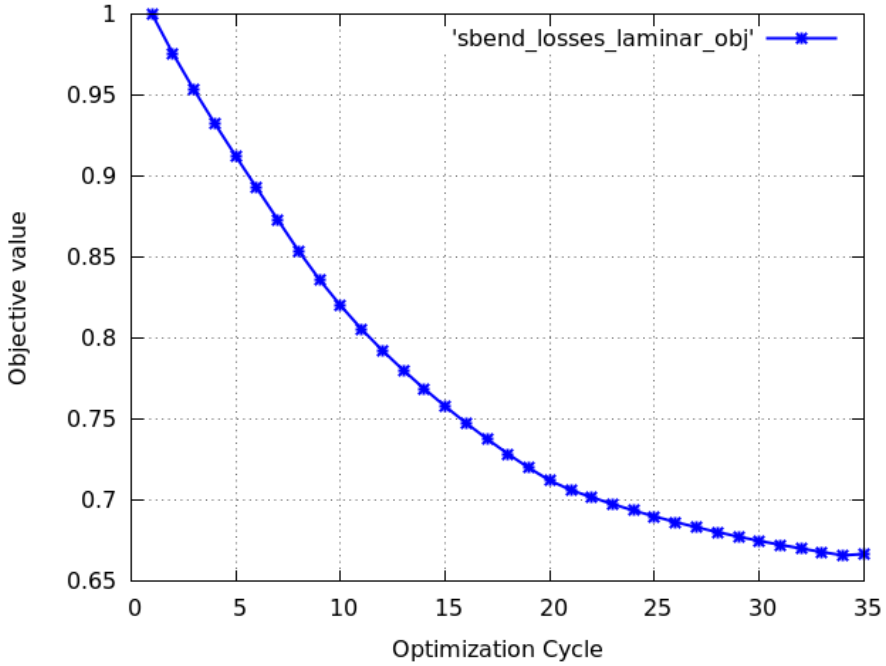

Figure 4.1: *Δp_t optimization of the S-bend duct, laminar flow. Objective function convergence. Over the course of 34 optimization cycles, there has been a reduction of 33.3% in the objective value.*

The final geometry of the duct in comparison with its initial form is presented in fig. 4.2

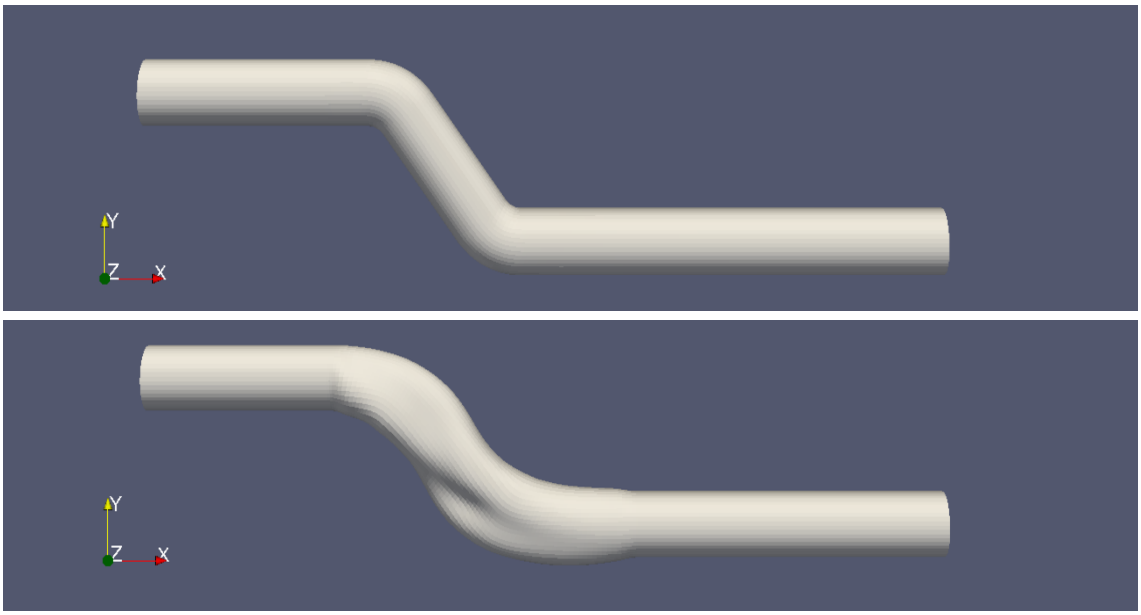

Figure 4.2: *Δp_t optimization of the S-bend duct, laminar flow. Duct initial (above) and final (below) geometry.*

The inward or outward displacement of the geometry nodes can be seen more clearly in fig. 4.3, where the cumulative normal displacement field (i.e. the total displacement vectors projected on the respective normal-to-the-surface vectors) is depicted.

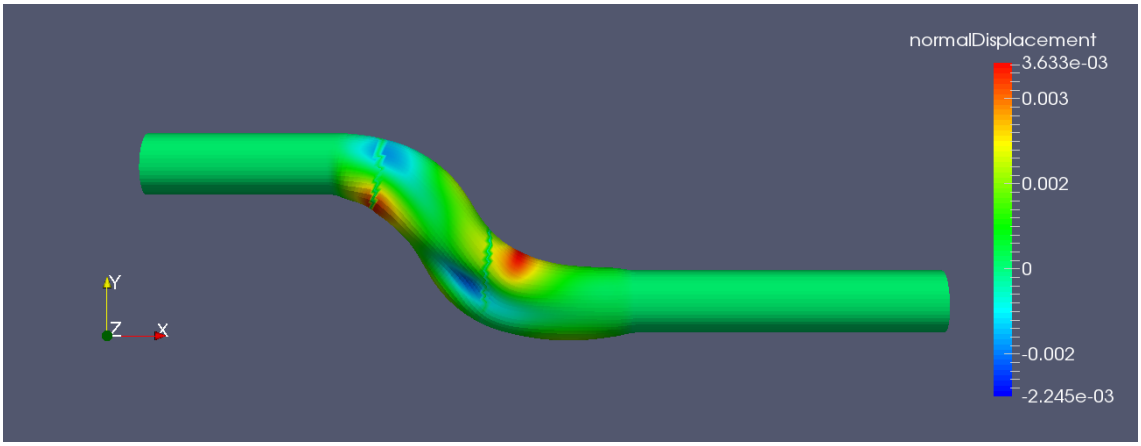

Figure 4.3: *Δp_t optimization of the S-bend duct, laminar flow. Cumulative normal displacement field on the final geometry. Blue coloring indicates inward displacement of the nodes w.r.t. their initial position, whereas green yellow and red indicate outward displacement.*

The velocity field inside the duct for the initial and final geometry can be seen in figs. 4.4 and 4.5. The section on which velocity isolines are plotted is the symmetry plane of the duct.

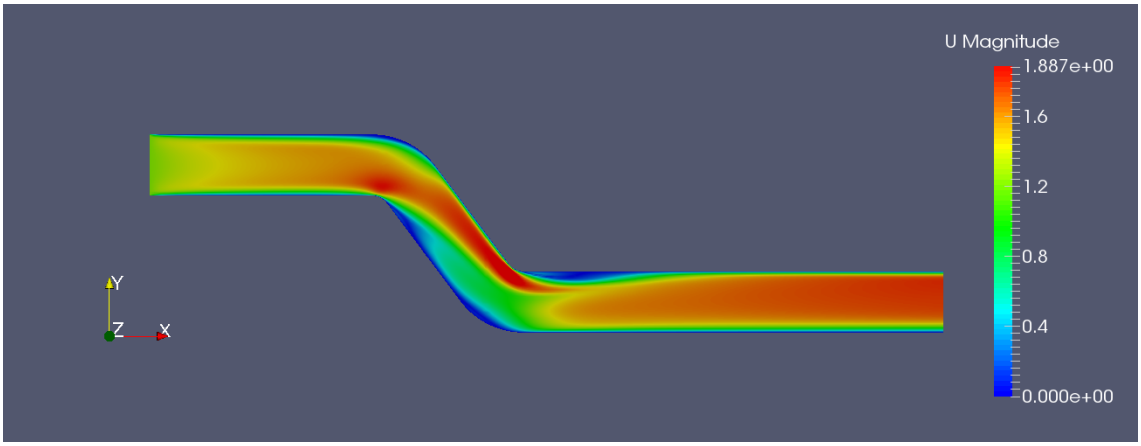

Figure 4.4: *Δp_t optimization of the S-bend duct, laminar flow. Velocity field inside the duct for the initial geometry. Section along the duct symmetry plane.*

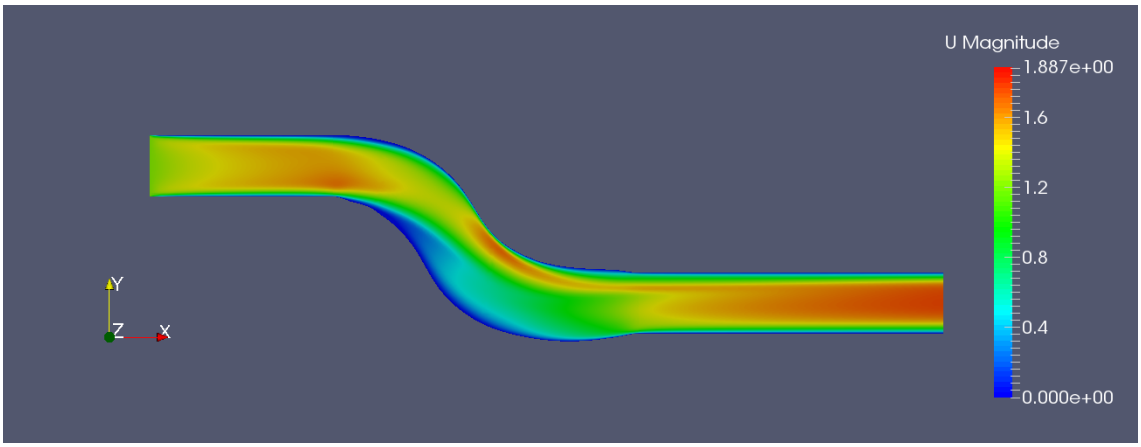

Figure 4.5: *Δp_t optimization of the S-bend duct, laminar flow. Velocity field inside the duct for the final geometry. Section along the duct symmetry plane.*

The total pressure inside the duct can be seen in figs. 4.6 and 4.7.

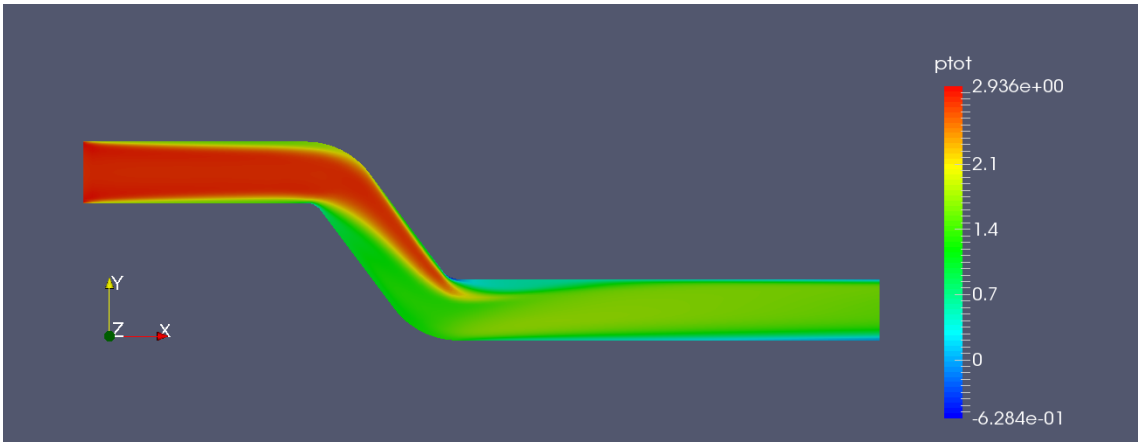

Figure 4.6: *Δp_t optimization of the S-bend duct, laminar flow. Total pressure inside the duct for the initial geometry. Section along the duct symmetry plane.*

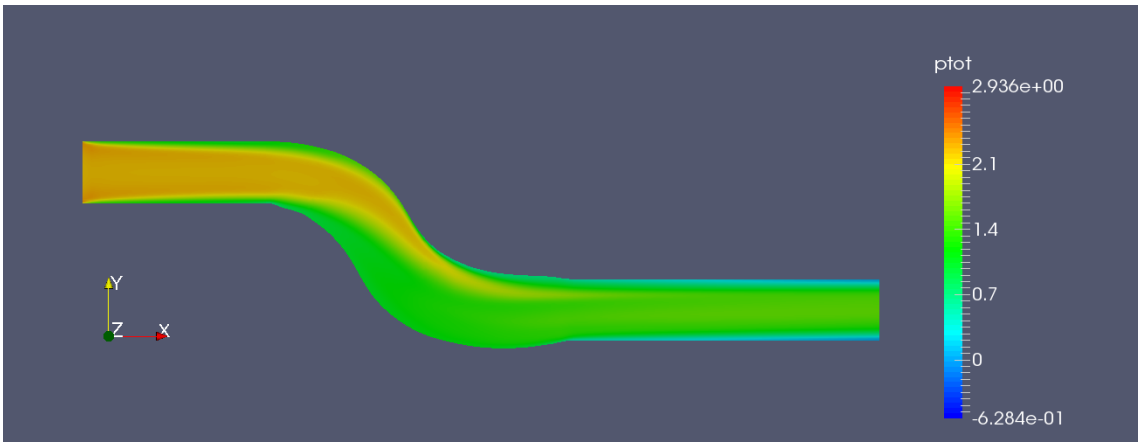

Figure 4.7: *Δp_t optimization of the S-bend duct, laminar flow. Total pressure field inside the duct for the final geometry. Section along the duct symmetry plane.*

"Minimization of Total Pressure Losses (Δp_t)" Objective Function in Turbulent Flow

Next, the S-Bend duct was optimized for a turbulent flow, using the total pressure losses objective.

The case was left to run for 25 cycles. The objective function decreased up until the 18th cycle, upon which the optimum was reached and the objective function value oscillated around the optimum value. Thus, the simulation was manually stopped. The objective function values during the optimization can be seen in fig. 4.8

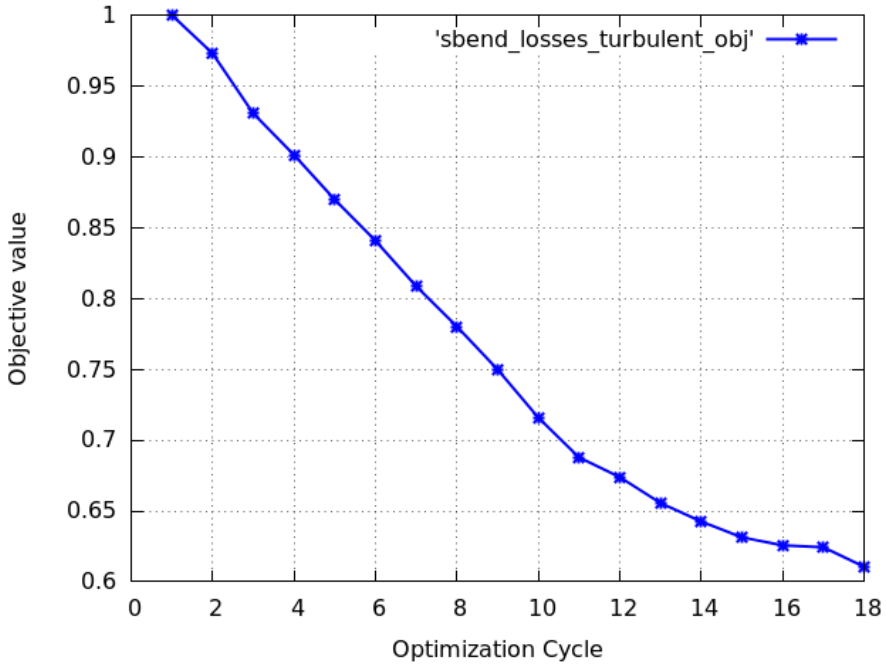

Figure 4.8: Δp_t *optimization of the S-bend duct, turbulent flow. Objective function value during the optimization. After 16 optimization cycles, there has been a reduction of 38.86% in the objective value. After the 18th cycle there is an oscillation of the objective around a value, since the optimum has been reached.*

The final geometry and the field of the cumulative normal displacement can be seen in fig. 4.9

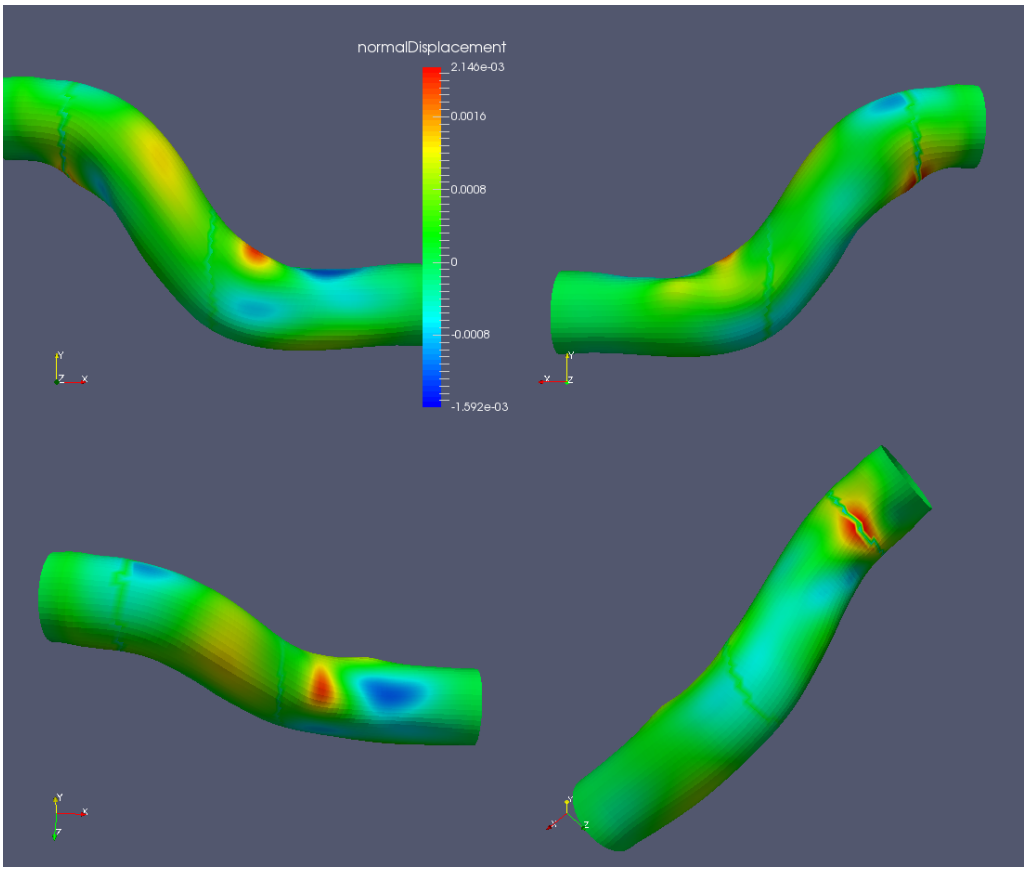

Figure 4.9: *Δp_t optimization of the S-bend duct, turbulent flow. Cumulative normal displacements field on the final geometry.*

The total pressure field inside the initial and final duct geometry can be seen in figs. 4.10, 4.11.

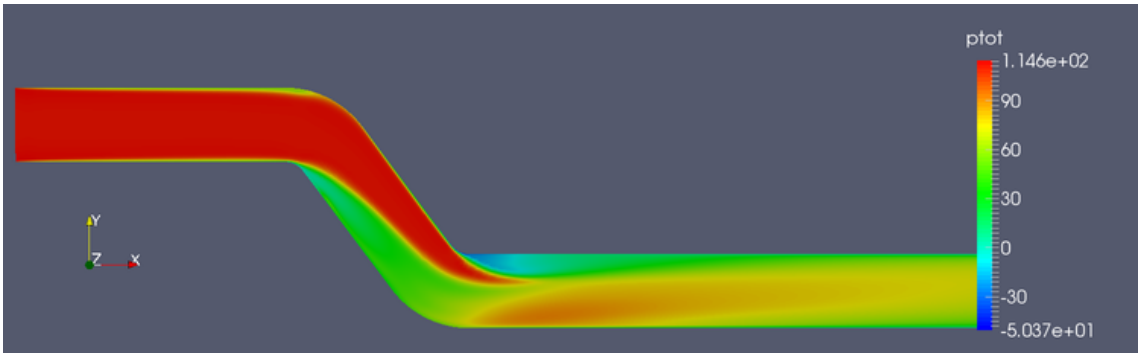

Figure 4.10: *Δp_t optimization of the S-bend duct, turbulent flow. Total pressure for the initial geometry. The section shown is along the duct symmetry plane.*

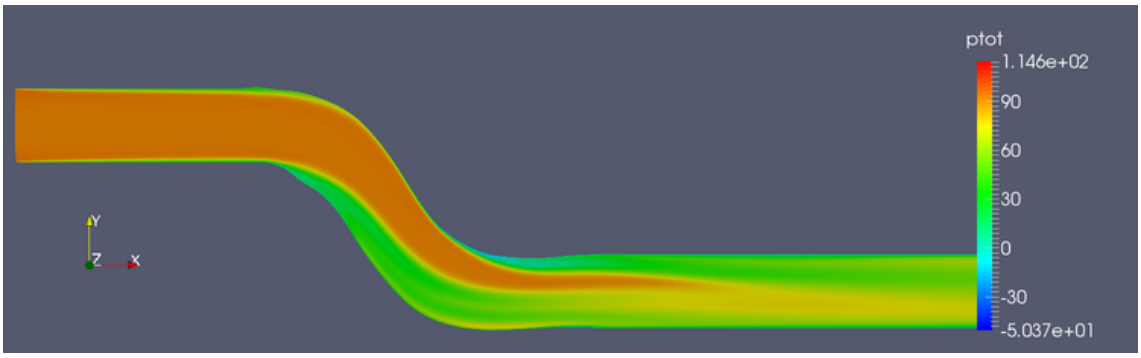

Figure 4.11: *Δp_t optimization of the S-bend duct, turbulent flow. Total pressure field inside the duct for the final geometry. The section presented is along the duct symmetry plane.*

The velocity field for the initial and final geometry can be seen in figs. 4.12, 4.13

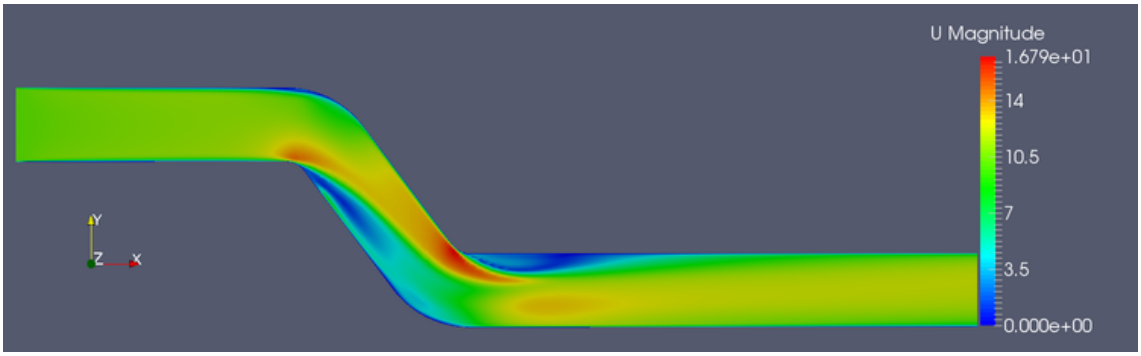

Figure 4.12: *Δp_t optimization of the S-bend duct, turbulent flow. Velocity field for the initial geometry. Section along the duct symmetry plane.*

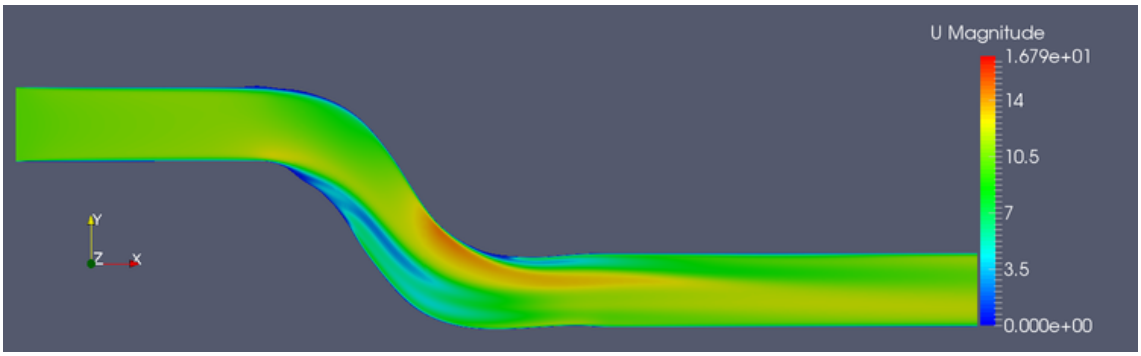

Figure 4.13: *Δp_t optimization of the S-bend duct, turbulent flow. Velocity field for the final geometry. Section along the duct symmetry plane.*

"Noise" Minimization

Next, the same geometry was optimized anew, using an objective function that is linked to noise generation (see [25]). This objective function is given by

$$J = \int_{\Omega'} {\nu_t}^2 d\Omega \tag{4.3}$$

where ν_t is the turbulent viscosity and Ω' is a volume area, where it is desired to minimize turbulence and, therefore, the associated noise. In the case of the S-Bend tube, Ω' is chosen to be a volume at the exit of the tube, as can be seen in fig. 4.14.

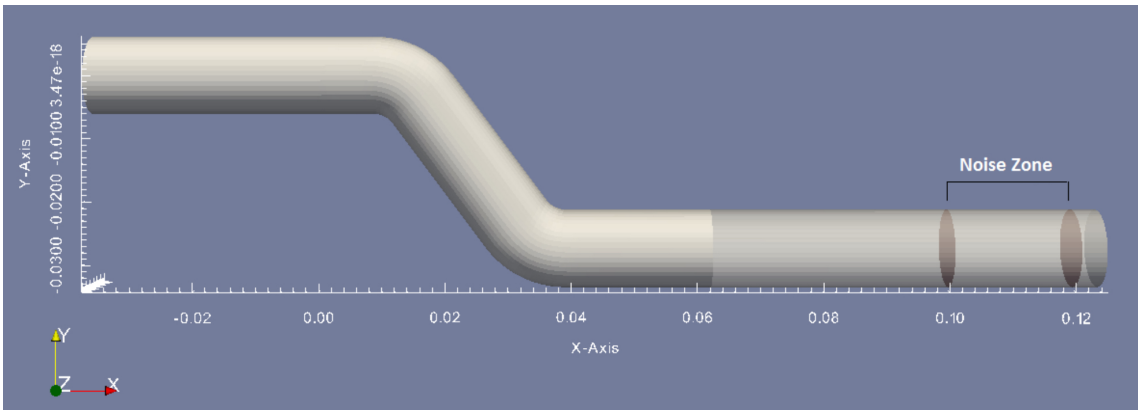

Figure 4.14: *"Noise" optimization of the S-bend duct. Noise zone defined at the exit of the tube. This is the volume area Ω' where the noise-related objective is defined.*

The differentiation of the above noise-related objective function yields

$$\frac{\delta J}{\delta b_n} = \frac{\delta}{\delta b_n} \int_{\Omega'} {\nu_t}^2 d\Omega = \int_{\Omega'} \frac{\partial {\nu_t}^2}{\partial b_n} d\Omega + \int_{S'} {\nu_t}^2 n_k \frac{\delta x_k}{\delta b_n} dS \Rightarrow$$

$$\frac{\delta J}{\delta b_n} = \int_{\Omega'} 2\nu_t \frac{\partial \nu_t}{\partial b_n} d\Omega + \int_{S'} {\nu_t}^2 n_k \frac{\delta x_k}{\delta b_n} dS \tag{4.4}$$

where the Leibniz theorem was used.

The first term on the RHS of eq. 4.4 contributes to the Field Adjoint Equations, whereas the second one to the Sensitivity Derivatives.

This case ran for 22 optimization cycles. During the first 3 cycles the objective decreased, whereas for the cycles 4 to 9 the objective oscillated, alternately increasing and decreasing. From the 9th cycle on, the objective dropped steadily. The results of the optimization can be seen in figs. 4.15 and 4.16

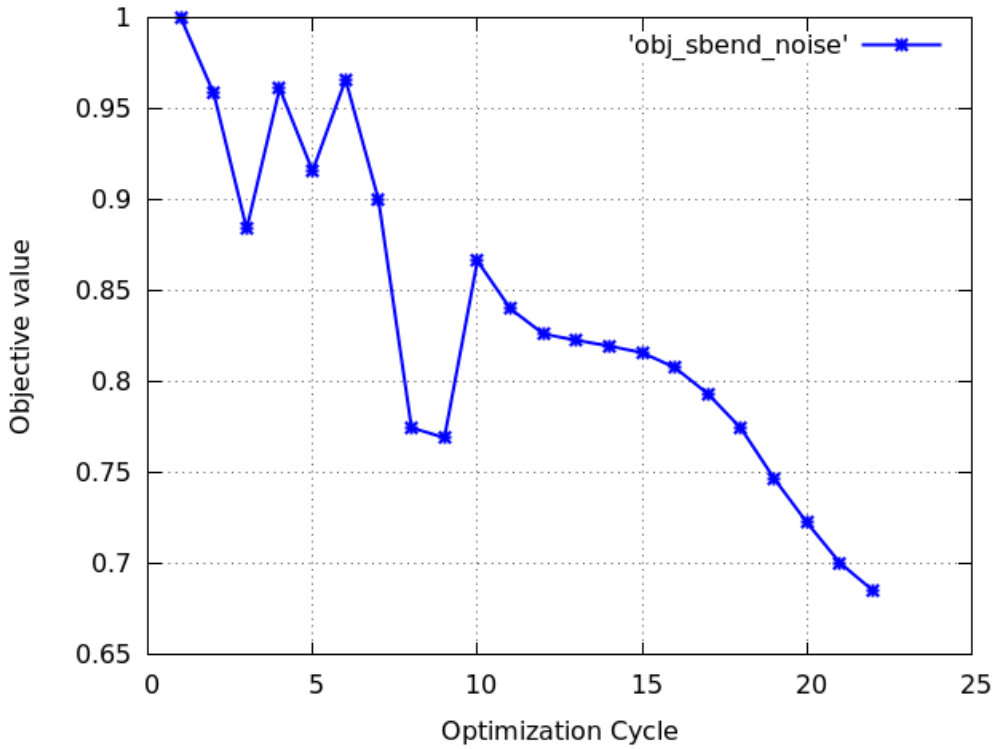

Figure 4.15: *"Noise" optimization of the S-bend duct. Objective function convergence. The total reduction in the objective corresponds to 31.46%.*

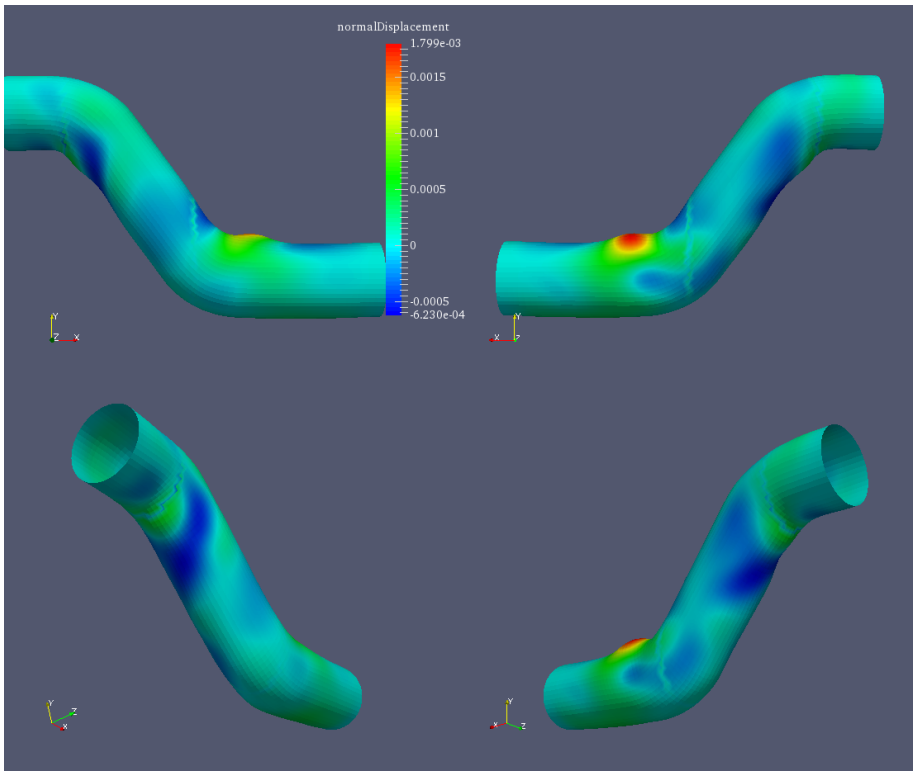

Figure 4.16: *"Noise" optimization of the S-bend duct. Cumulative normal displacement field on the final geometry. Blue coloring indicates inward displacement of the nodes w.r.t their initial position, whereas green, yellow and red indicate outward displacement of the nodes.*

4.3.2 The HVAC Duct

Minimization of "Noise" in the HVAC Duct

The second geometry that was optimized was that of an HVAC duct. The objective being minimized is the "Noise" objective function defined in eq.4.3. The geometry of the duct, the controlled patch and the volume where the objective function is defined can be seen in fig. 4.17 (in blue and green respectively).

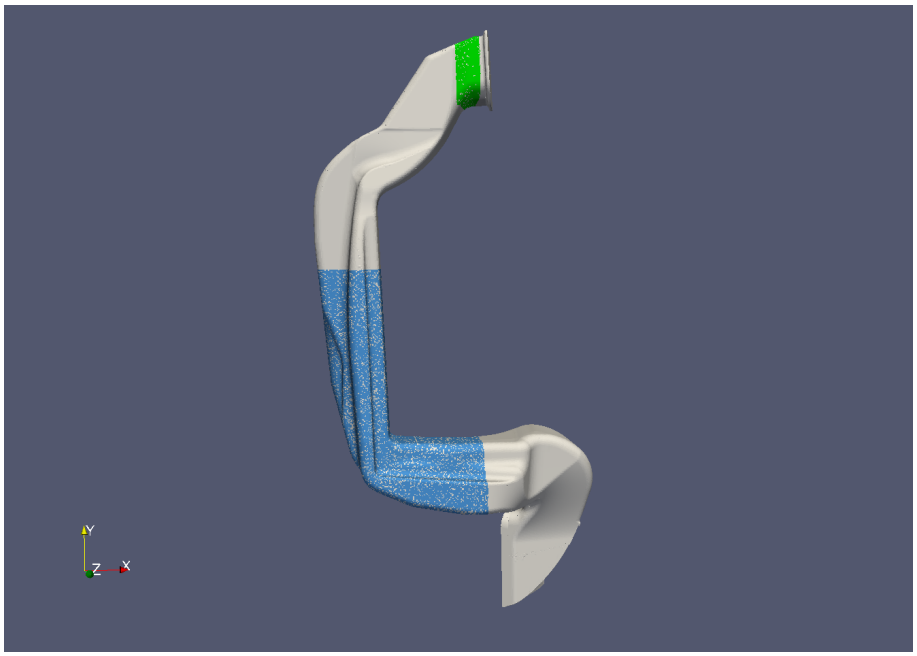

Figure 4.17: *"Noise" optimization of the HVAC duct. Controlled patch(blue) and objective integration volume(green).*

The optimization ran for 33 cycles, after which the objective values began oscillating and the process was manually stopped. The oscillation of the objective was caused by oscillatory behavior in the primal solution. The convergence of the objective function can be seen in fig. 4.18

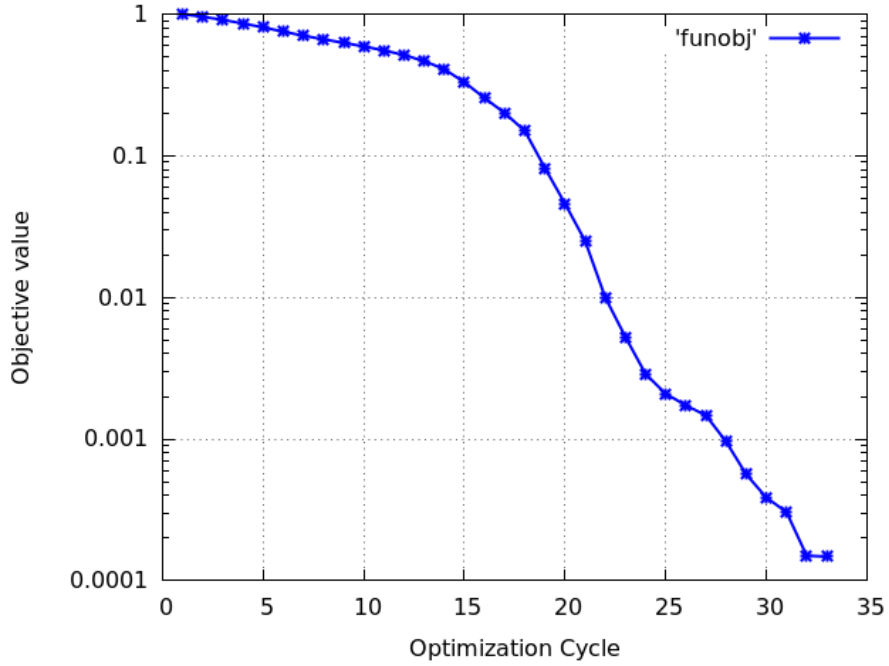

Figure 4.18: *"Noise" optimization of the HVAC duct. Objective function evolution during optimization. Over the 33 optimization cycles, there has been a reduction of 99.99% in the objective function value compared to its initial value.*

The initial and final geometry can be seen in figs. 4.19 and 4.20.

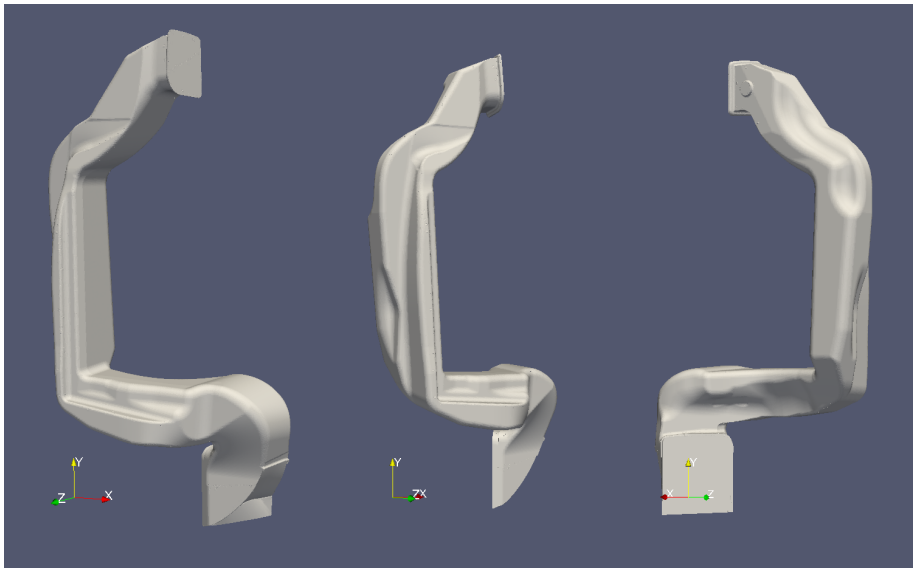

Figure 4.19: *"Noise" optimization of the HVAC duct. Initial HVAC duct geometry.*

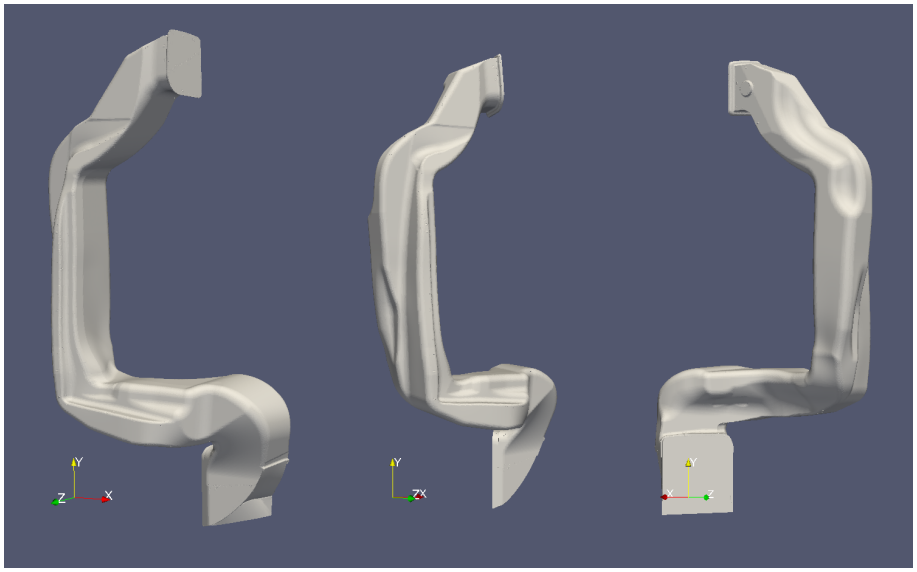

Figure 4.20: *"Noise" optimization of the HVAC duct. Final HVAC duct geometry. The inlet is the lower end of the duct, whereas the outlet the upper end.*

The inward or outward displacement of the geometry nodes can be seen in fig. 4.21, where the cumulative normal displacement field is depicted.

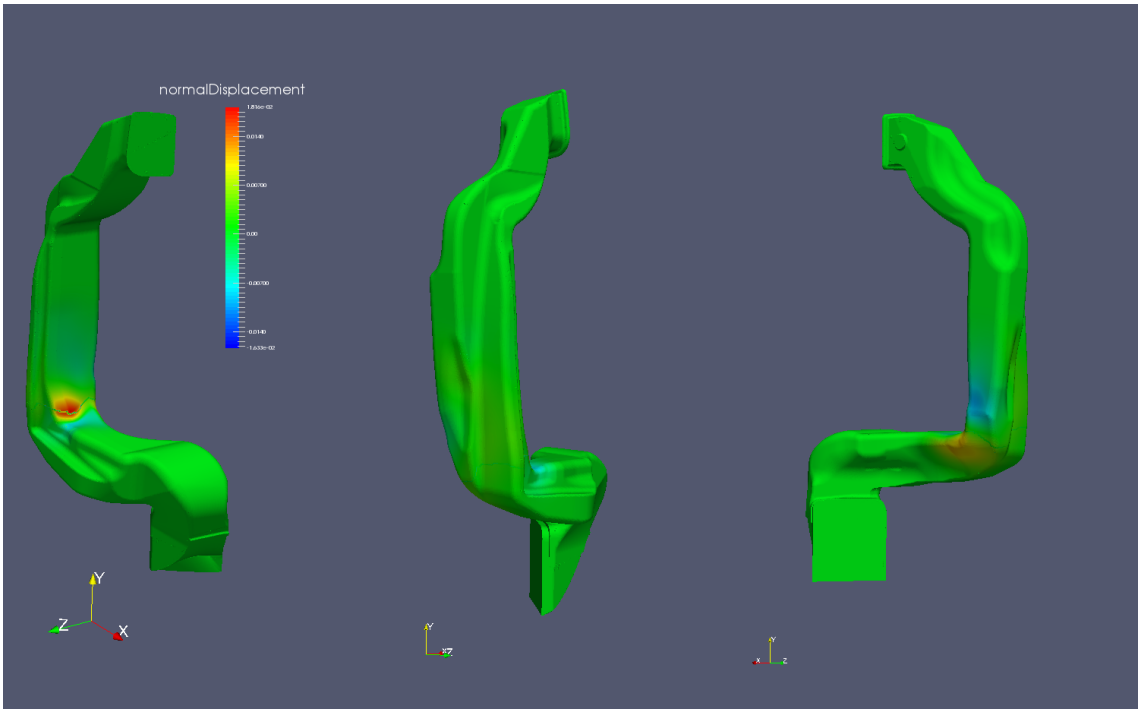

Figure 4.21: *"Noise" optimization of the HVAC duct. Cumulative normal displacement field on the final geometry. Blue coloring indicates inward displacement of the nodes w.r.t their initial position, whereas green, yellow and red indicate outward displacement of the nodes.*

Minimization of Total Pressure Losses Δp_t for Laminar Flow in the HVAC Duct

Next, the geometry of the HVAC Duct was optimized, with the aim of minimizing the total pressure losses from inlet to outlet. The case ran for 16 cycles, after which the mesh failed. The objective decreased for the first 14 cycles and then oscillated during the last two, until the run stopped at the 16th cycle. The convergence of the objective function can be seen in fig. 4.22

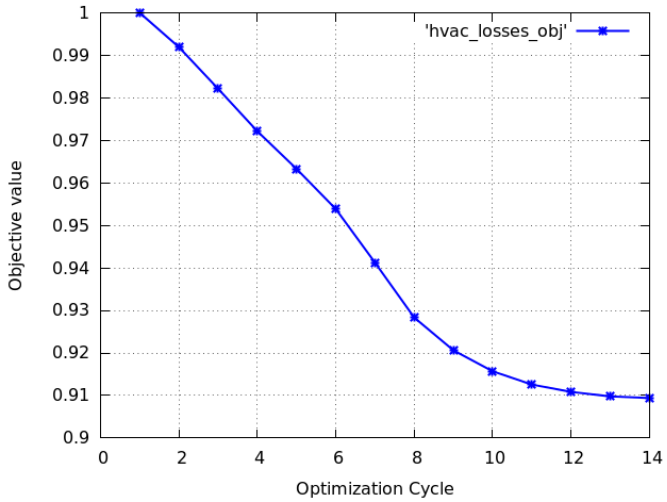

Figure 4.22: *"Δp_t" optimization of the HVAC duct. Objective function evolution during optimization. After 14 optimization cycles, the reduction in the objective has been 9%.*

The initial and final shape of the ducts is presented in figs. 4.23 and 4.24.

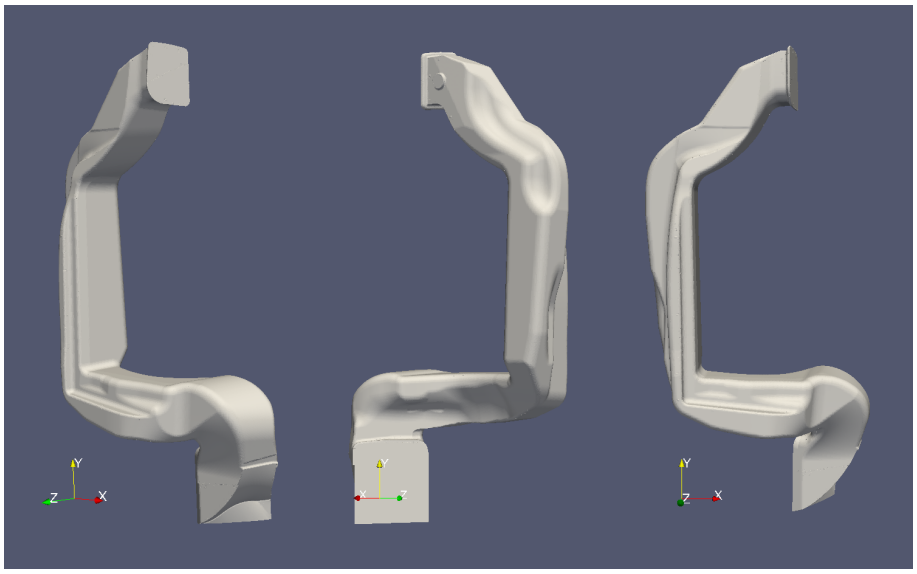

Figure 4.23: *"Δp_t" optimization of the HVAC duct. Initial HVAC duct shape.*

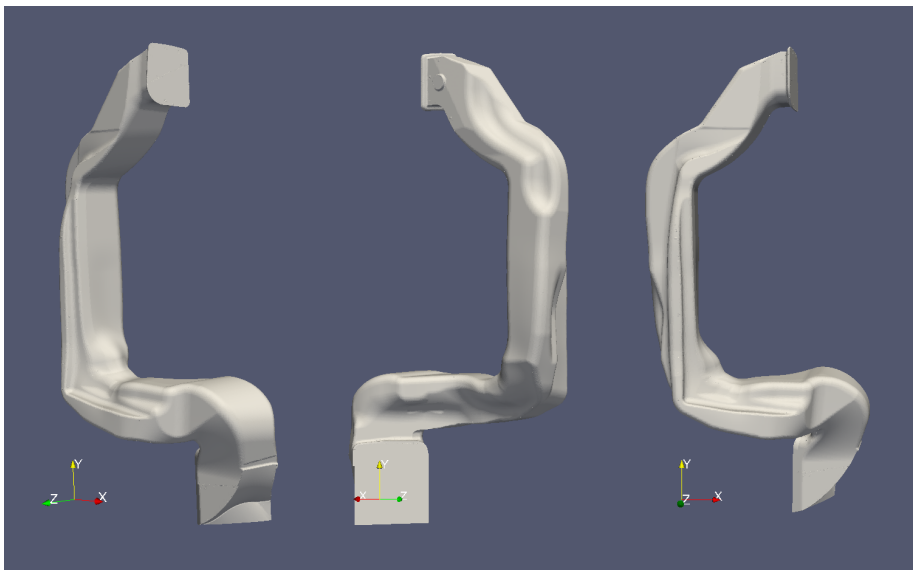

Figure 4.24: *"Δp_t" optimization of the HVAC duct. Final HVAC duct shape.*

The cumulative normal displacement of the geometry nodes can be seen in fig. 4.25.

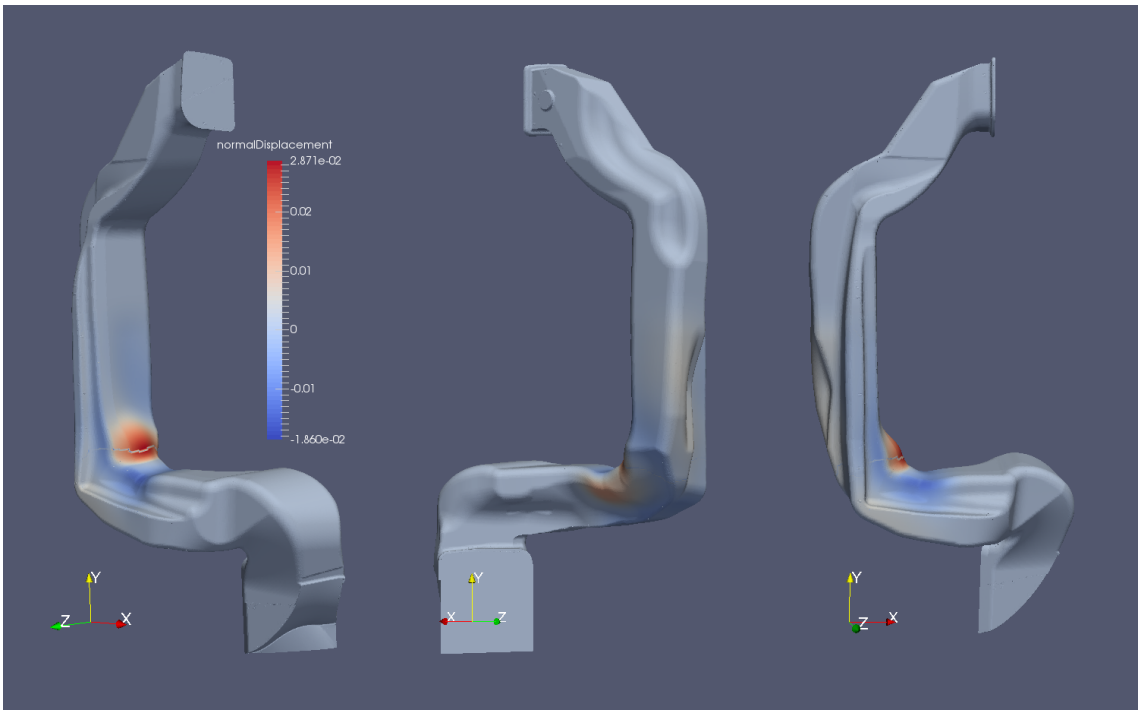

Figure 4.25: *"Δp_t" optimization of the HVAC duct. Cumulative normal displacement field on the final geometry. Blue coloring indicates inward displacement of the nodes w.r.t their initial position, whereas green, yellow and red indicate outward displacement of the nodes.*

The area of the duct with the most pronounced displacement is the 90^o bend after the inlet. The nodes of the bend have been displaced outwards, i.e. in the direction of the normal vector, to reduce the curvature of the bend and thus the pressure losses.

Chapter 5

Summary-Conclusions

The first part of this thesis deals with the use of the Kirchhoff Integral Method for noise computation. Aeroacoustic analogies, such as the KIM, are extremely useful when noise prediction must be performed at the far-field of a source, rendering the cost of CFD computations prohibitive. The method allows the pressure at a receiver to be predicted, by integrating the pressure and its derivatives on a surface enclosing the source. To test the correctness of the code implementing the Kirchhoff mathematical formula, mononpoles and dipoles were chosen as noise sources, for which analytical equations giving the induced pressure field exist. This allowed the comparison of the pressure calculated by the KIM to that given by the analytical formulas. During the comparison, coincidence of the results was observed.

Next optimization of the source (monopole or dipole) position was performed after defining an appropriate objective function, which was the integral of the squared difference of the pressure time-series at the receiver and a target pressure time-series. Having thus defined the objective function, the derivatives of the pressure w.r.t. the design variables (i.e. source coordinates) were required in order to compute the sensitivity derivatives and perform steepest descend. For that reason, the KI formula was analytically differentiated, yielding an analytical formula for the computation $\delta p'/\delta b_n$. The same derivatives were computed using finite differences, and the resulting sensitivities were compared. Again the two methods produced very similar results.

In the first part of the thesis, is was thus demonstrated that pressure computation can be performed without the need for analytical or CFD calculations over a domain extending from acoustic source to observer. Instead, the KIM can be used for noise prediction, using the CFD or analytically obtained data from a domain in the near-field of the source. It was also demonstrated that the KI Formula can be analytically differentiated and used for the computation of the sensitivity derivatives required to perform optimization of the source position in order to achieve a target pressure at the receiver. In the future, the implementation of the KIM could be coupled with CFD to perform shape optimization for aeroacoustic noise reduction. To use the adjoint method for that, the differentiation of the KIM performed in this thesis, would also have to be coupled with the adjoint problem to the flow.

In the second part of this master thesis, the continuous adjoint method developed

by PCOpt/NTUA was coupled with the BMW optimization workflow "ShapeModule". The adjoint formulation used was the Enhanced SI formulation, which avoids the calculation of the grid sensitivities in the inside of the domain, thus having the advantage of low cost while maintaining high accuracy in the computed sensitivites. The fully differentiated Spalart-Allmaras model was used to deal with the variation of the turbulent viscosity, thus avoiding the "frozen turbulence assumption", which has been shown to produce much less accurate and, sometimes, wrongly signed sensitivities. After the integration of the PCOpt software into ShapeModule, two geometries were optimized. One was an HVAC duct of a passenger vehicle. The aim there was to minimize noise perceived by the passengers. To that end, an appropriate noise-related objective function was chosen, which is defined as the volume integral of the squared turbulent viscosity. Minimization of this objective has been shown to minimize noise as well. The other geometry optimized was an S-bend duct with a circular cross-section. The ducts shape was optimized using two different objective functions. The first one is the "noise" objective function, which was also used for the HVAC duct and the other is the "total pressure losses" objective function, which, as denoted by its name, aims at the minimization of the total pressure losses between inlet and outlet. Optimization of the S-bend geometry using the "total pressure losses" objective was performed both for laminar and turbulent flows.

The coupling between the two softwares was successful and there was a very satisfactory reduction per cycle in the objective function for all cases (Even higher reductions could have been obtained if the geometry was being remeshed instead of updated). Especially in the case of the HVAC duct with the surrogate objective for noise, there was a dramatic decrease in the objective function.

Εθνικό Μετσόβιο Πολυτεχνείο
Σχολή Μηχανολόγων Μηχανικών
Τομέας Ρευστών
Εργαστήριο Θερμικών Στροβιλομηχανών
Μονάδα Παράλληλης Υπολογιστικής Ρευστοδυναμικής & Βελτιστοποίησης

Αεροακουστική Πρόβλεψη Θορύβου & Βελτιστοποίηση Μορφής με Χρήση της Συνεχούς Συζυγούς Μεθόδου.

Εκτενής Περίληψη Μεταπτυχιακής Εργασίας
Υπολογιστική Μηχανική
Διατμηματικό Πρόγραμμα Μεταπτυχιακών Σπουδών

Αικατερίνη Η. Καρώνη

Επιβλέπων
Κυριάκος Χ. Γιαννάκογλου , Καθηγητής ΕΜΠ

Αθήνα, Ιούλιος 2018

Αεροακουστική Πρόβλεψη Θορύβου με χρήση της μεθόδου ολοκληρώματος Kirchhoff

Το πρώτο μέρος της παρούσας εργασίας ασχολείται με τη χρήση της ΚΙΜ για τον υπολογισμό του θορύβου. Οι αεροακουστικές αναλογίες, όπως η ΚΙΜ, είναι εξαιρετικά χρήσιμες όταν η πρόβλεψη του θορύβου πρέπει να πραγματοποιηθεί μακριά από την πηγή του θορύβου, καθιστώντας το κόστος των υπολογισμών CFD σε ένα χωρίο εκτεινόμενο από την πηγή έως και τον δέκτη απαγορευτικό. Η μέθοδος επιτρέπει την πρόβλεψη της πίεσης σε έναν δέκτη, μέσω ολοκλήρωσης της πίεσης και των παραγώγων της σε μια επιφάνεια που περικλείει την πηγή. Για να δοκιμαστεί η ορθότητα του κώδικα που εφαρμόζει τον μαθηματικό τύπο Kirchhoff, επελέγησαν ένα μονόπολο και ένα διπόλο ως πηγές θορύβου. Για αυτές τις πηγές υπάρχουν αναλυτικές εξισώσεις που δίνουν το επαγόμενο πεδίο πίεσης. Αυτό επέτρεψε τη σύγκριση της πίεσης που υπολογίστηκε από το ΚΙΜ με αυτή που δίνεται από τους αναλυτικούς τύπους. Κατά τη σύγκριση, παρατηρήθηκε σύμπτωση των αποτελεσμάτων.

Στη συνέχεια, πραγματοποιήθηκε βελτιστοποίηση της θέσης πηγής, αφού ορίστηκε μια κατάλληλη συνάρτηση κόστους ως το ολοκλήρωμα του τετραγώνου της διαφοράς της χρονοσειράς της πίεσης σε έναν δέκτη και μιας χρονοσειράς πίεσης-στόχου. Έχοντας ορίσει έτσι τη συνάρτηση κόστους, οι παράγωγοι της πίεσης ως προς τις μεταβλητές σχεδιασμού (δηλαδή τις συντεταγμένες της πηγής) απαιταιτούνται για τον υπολογισμό των παραγώγων ευαισθησίας και την πραγματοποίηση απότομης καθόδου. Για το λόγο αυτό, ο τύπος του ΚΙ διαφορίστηκε αναλυτικά, δίνοντας έτσι έναν αναλυτικό τύπο για τον υπολογισμό των $\delta p'/\delta b_n$. Οι ίδιες παράγωγοι υπολογίστηκαν χρησιμοποιώντας πεπερασμένες διαφορές και οι προκύπτουσες ευαισθησίες συγκρίθηκαν. Και πάλι οι δύο μέθοδοι έδωσαν παραπλήσια αποτελέσματα.

Ο τύπος του ολοκληρώματος Kirchhoff εξάγεται μετά από επίλυση της κυματικής εξίσωσης (εξ. 1.33) μέσω της μεθόδου των συναρτήσεων Green [4]. Η κυματική εξίσωση είναι μια δεύτερης τάξης υπερβολικού τύπου γραμμική διαφορική εξίσωση για την περιγραφή κυμάτων (φωτός, ακουστικών κλπ.) και προκύπτει μετά από αναδιάταξη των εξισώσεων Navier-Stokes που διέπουν την ροή ενός συμπιεστού συνεκτικού ρευστού [1], [2], [3]. Η τελική μορφή της κυματικής εξίσωσης, γραμμένης για την ακουστική πίεση, είναι

$$\frac{1}{(a^2)^0}\frac{\partial^2 p'}{\partial t^2} - \Delta p' = Q_p \tag{5.1}$$

όπου Q_p ο όρος πηγής

Για ακίνητο μέσον, σταθερό δέκτη και ακίνητη επιφάνεια ολοκλήρωσης, ο τύπος του ολοκληρώματος Kirchhoff γράφεται

$$\underline{p'}(\mathbf{x},t) = \frac{1}{4\pi}\int\limits_{\partial V_B : f=0}\left(\frac{\mathbf{r}\cdot\mathbf{n}}{r^3}p' + \frac{\mathbf{r}\cdot\mathbf{n}}{cr^2}\frac{\partial p'}{\partial t} - \frac{1}{r}\frac{\partial p'}{\partial n}\right)dS \tag{5.2}$$

όπου $\mathbf{r}$ είναι η απόσταση ανάμεσα στο εκάστοτε στοιχείο της επιφάνειας ολοκλήρωσης Kirchhoff και τον δέκτη, $\mathbf{n}$ είναι το κάθετο στην επιφάνεια Kirchhoff διάνυσμα, με

κατεύθυνση από την επιφάνεια προς τον δέκτη και $r = |\mathbf{r}|$ είναι η απόσταση μεταξύ στοιχείου και δέκτη, όπως φαίνεται και στο σχ. 5.1

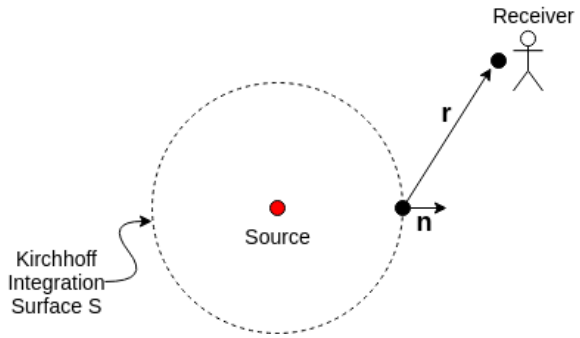

Σχήμα 5.1: *Πηγή, επιφάνεια ολοκλήρωσης και δέκτης*

Η εξ. 1.63 επιτρέπει τον υπολογισμό της πίεσης $\underline{p}'(\mathbf{x}, \mathbf{t})$ σε οποιαδήποτε θέση βρισκόμενη εκτός μιας επιφάνειας ολοκλήρωσης η οποία εσωκλείει όλα τα σώματα και τις πηγές, αν η διαταραχή της πίεσης p' και οι παράγωγοι $\frac{\partial p'}{\partial \tau}$ και $\frac{\partial p'}{\partial n}$ είναι γνωστές επί της επιφάνειας. Οι ποσότητες p', $\frac{\partial p'}{\partial \tau}$ και $\frac{\partial p'}{\partial n}$ πρέπει να υπολογιστούν σε χρόνο $\tau = t - r/c$. Ο χρόνος τ είναι ο ¨καθυστερημένος χρόνος¨. Ένα σήμα που φθάνει στον δέκτη σε χρόνο t εξεπέμφθη από την πηγή σε χρόνο $t - r/c$, όπου r είναι η απόσταση μεταξύ πηγής και παρατηρητή και c είναι η ταχύτητα του ήχου.

Οι πηγές ήχου που μελετήθηκαν στην εργασία αυτή είναι μονόπολα και δίπολα. Το μονόπολο είναι μια πηγή που εκπέμπει ήχο ομοιόμορφα προς όλες τις διευθύνσεις. Η εξίσωση που δίνει το δυναμικό της ταχύτητας που επάγεται από ένα μονόπολο είναι

$$\phi(\mathbf{x}, t) = \frac{A}{4\pi r} e^{i\omega(t - r/c)} \tag{5.3}$$

όπου A το πλάτος και ω η συχνότητα ταλάντωσης της πηγής.

Σε αντίθεση με το μονόπολο, ένα δίπολο δεν εκπέμπει ήχο ομοιόμορφα προς όλες τις διευθύνσεις. Η ακόλουθη έκφραση δίνει το δυναμικό της ταχύτητας που επάγεται από ένα δίπολο

$$\phi(\mathbf{x}, t) = \nabla \left[\frac{A}{4\pi r} e^{i\omega(t - r/c)} \right] \cdot \mathbf{d} \tag{5.4}$$

όπου $\mathbf{d}$ το διάνυσμα κατευθυντικότητας (δηλ. η διεύθυνση του άξονα ταλάντωσης του διπόλου).

Οι παραπάνω αναλυτικές εξισώσεις για μονόπολο και το δίπολο, χρησιμοποιούνται προς επαλήθευση των αποτελεσμάτων που δίνει η σχέση του Kirchhoff. Η χρήση απλών ακουστικών πηγών με γνωστή αναλυτική λύση είναι συνήθης πρακτική για τον έλεγχο της ορθότητας υπολογισμών αεροακουστικής (βλ. [6], [7], [8]).

Για την περίπτωση του μονοπόλου, η σύγκριση της χρονοσειράς της διαταραχής της πίεσης που προκύπτει μέσω ολοκληρώματος Kirchhoff, με αυτήν που προκύπτει μέσω των αναλυτικών σχέσεων, φαίνεται στο σχ. 5.2. (Η διάδοση του θορύβου εξετάζεται

σε ακίνητο ρευστό στον τριδιάστατο χώρο).

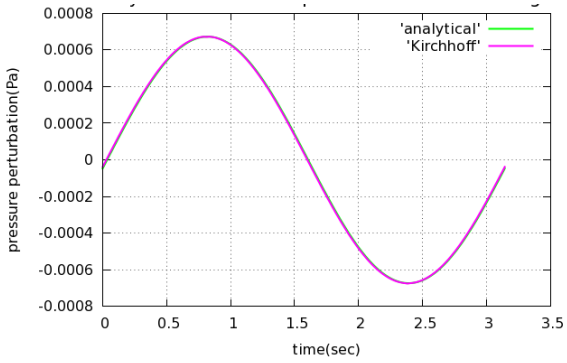

Σχήμα 5.2: *Μονόπολο. Χρονοσειρά της διαταραχής της πίεσης σε δέκτη στο (-10,2,-6). Πηγή τοποθετημένη στο (0,0,0). Η χρονοσειρά που προκύπτει από τις αναλυτικές σχέσεις του μονοπόλου (πράσινο) συμπίπτει πλήρως με αυτήν που προκύπτει από χρήση του ολοκληρώματος Kirchhoff.*

Αφού έγινε αναλυτική διαφόριση του τύπου του Kirchhoff, πραγραμτοποιήθηκε, όπως αναφέρθηκε, βελτιστοποίηση της θέσης της πηγής ώστε να επιτευχθεί συγκεκριμένη χρονοσειρά πίεσης στον δέκτη. Η σύγκριση των παραγώγων ευαισθησίας που προκύπτουν από διαφόριση του Kirchhoff με αυτές που προκύπτουν από πεπερασμένες διαφορές παρουσιάζεται στο σχ. 5.3. (Τα αποτελέσματα του πρώτου μέρους παρουσιάζονται αναλυτικά στο πλήρες (αγγλικό) κείμενο).

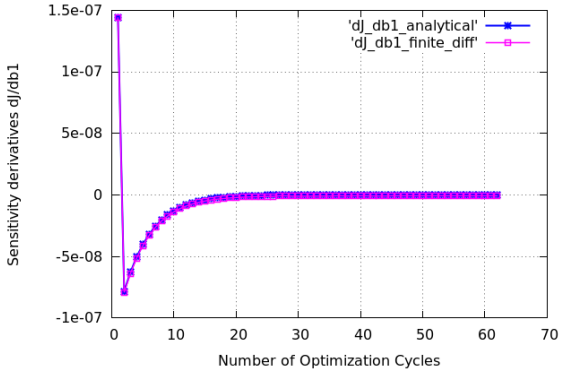

Σχήμα 5.3: *Μονόπολο. Σύγκριση παραγώγων ευαισθησίας $\delta J/\delta b_1 = \delta J/\delta x_s$ που προέκυψαν από παραγώγιση του ολοκληρώματος του Kirchhoff με αυτές που προέκυψαν από πεπερασμένες διαφορές. Παρατηρείται πλήρης τάυτιση των παραγώγων.*

Βελτιστοποίηση Μορφής με Χρήση της Συνεχούς Συζυγούς Μεθόδου

Το δεύτερο τμήμα της εργασίας, υλοποιήθηκε στην BMW Μονάχου και σχετίζεται εν μέρει με την παραγωγή θορύβου. Στην αυτοκινητοβιομηχανία, συνήθεις πηγές θορύβου και, συνεπώς, δυσφορίας είναι οι μονάδες HVAC (Heating, Ventilation and Air Conditioning) καθώς και τα συστήματα εξάτμισης. Μέρος του δευτέρου τμήματος ασχολείται με τη βελτιστοποίηση μορφής με στόχο τη μείωση θορύβου. Αυτό δεν γίνεται μέσω της χρήσης μεθόδων της αεροακουστικής αλλά μέσω επιλογής μιας κατάλληλης υποκατάστατης (surrogate) συναρτήσεως κόστους, η ελαχιστοποίηση της οποίας έχει δειχθεί ότι ελαχιστοποιεί και τα επίπεδα θορύβου. Για τη βελτιστοποίηση μορφής χρησιμοποιήθηκε το αναπτυχθέν στην ΜΠΥΡ&Β /ΕΜΠ και βασισμένο σε OpenFOAM-2.3.1 συζυγές λογισμικό, σε σύζευξη με το λογισμικό βελτιστοποίησης της BMW *ShapeModule*. Η συζυγής διατύπωση που χρησιμοποιήθηκε ήταν η enhanced SI, η οποία αποφεύγει τον υπολογισμό των παραγώγων ευαισθησίας του πλέγματος στον όγκο του υπολογιστικού χωρίου, έχοντας έτσι το πλεονέκτημα του χαμηλού κόστους και διατηρώντας παράλληλα υψηλή ακρίβεια στις υπολογιζόμενες ευαισθησίες. Το πλήρως διαφορισθέν μοντέλο Spalart-Allmaras χρησιμοποιήθηκε για να αποφευχθεί η «παραδοχή παγωμένης τύρβης», η οποία έχει αποδειχθεί ότι παράγει πολύ λιγότερο ακριβείς και ενίοτε εσφαλμένα προσημασμένες ευαισθησίες. Μετά την ενσωμάτωση του λογισμικού του PCOpt στο ShapeModule, βελτιστοποιήθηκαν δύο γεωμετρίες. Η μία είναι ένας αγωγός HVAC ενός επιβατικού οχήματος. Στόχος ήταν η ελαχιστοποίηση του θορύβου που αντιλαμβάνονται οι επιβάτες. Για το σκοπό αυτό επελέγη μια κατάλληλη υποκατάστατη συνάρτηση κόστους για τον θόρυβο, η οποία ορίζεται ως το χωρικό ολοκλήρωμα του τετραγώνου της τυρβώδους συνεκτικότητας σε έναν όγκο ολοκλήρωσης κοντά στην έξοδο του αγωγού. Η ελαχιστοποίηση αυτής της συνάρτησης κόστους έχει αποδειχθεί ότι ελαχιστοποιεί και τον σχετιζόμενο με την τύρβη θόρυβο. Ο ίδιος αγωγός βελτιστοποιήθηκε και ως προς τις απώλειες ολικής πίεσης από την είσοδο στην έξοδο.

Η άλλη βελτιστοποιηθείσα γεωμετρία ήταν ένας αγωγός S-Bend κυκλικής διατομής, ο οποίος βελτιστοποιήθηκε αρχικά ως προς τις απώλειες ολικής πίεσης (στρωτή και τυρβώδης ροή) και, στην συνέχεια, με χρήση της υποκατάστατης συνάρτησης κόστους για τον θόρυβο.

Η συνεχής συζυγής μεθοδολογία που χρησιμοποιήθηκε στην εργασία και η οποία αναπτύχθηκε από την ΜΠΥΡ&Β/ΕΜΠ έχει δύο ιδιαίτερα χαρακτηριστικά

1. Πλήρης διαφόριση μοντέλων τύρβης και
2. Το ότι χρησιμοποιείται η συζυγής μέθοδος για την αποφυγή υπολογισμού των παραγώγων ευαισθησίας του πλέγματος (grid sensitivities) (για πρώτη φορά στην συνεχή συζυγή μέθοδο).

Σε αντίθεση με όλα τα προηγούμενα έργα πάνω στη συνεχή συζυγή μέθοδο, το [10] εισήγαγε την χρήση της συνεχούς συζυγούς μεθόδου τόσο για τις εξισώσεις της μέσης ροής όσο και για τις εξισώσεις του μοντέλου τύρβης (Spalart-Allmaras) αποφεύγοντας τη συχνή παραδοχή του να αμελούνται οι παράγωγοι του τυρβώδους ιξώδους

ως προς τις μεταβλητές σχεδιασμού, κοινώς γνωστή ως «παραδοχή παγωμένης τύρβης». Αποδείχθηκε ότι η διαφόριση του μοντέλου τύρβης και η εφαρμογή της συζυγούς μεθόδου είναι απαραίτητη για τον ακριβή υπολογισμό των παραγώγων ευαισθησίας. Η μη επίλυση της (/των) συζυγούς(/ων) εξισώσεως(/ων) του μοντέλου τύρβης οδηγεί σε λανθασμένες και, ακόμη χειρότερα, εσφαλμένα προσημασμένες παραγώγους ευαισθησίας που μπορεί να παραπλανήσουν τον αλγόριθμο βελτιστοποίησης. Περισσότερες λεπτομέρειες σχετικά με την διαφόριση του μοντέλου τύρβης Spalart-Allmaras μπορούν να βρεθούν στα [10], [14] και [18].

Το δεύτερο χαρακτηριστικό γνώρισμα του λογισμικού είναι, όπως αναφέρθηκε, ο τρόπος με τον οποίο χειρίζεται τις παραγώγους ευαισθησίας του πλέγματος, δηλαδή τις παραγώγους των συντεταγμένων του πλέγματος ως προς τις μεταβλητές σχεδιασμού $\frac{\delta x_k}{\delta b_n}$. Η βασική ιδέα της συζυγούς μεθόδου, που είναι η αποφυγή του υπολογισμού των όρων, των οποίων ο υπολογισμός κοστίζει, όπως π.χ. του $\frac{\delta p}{\delta b_n}$, μπορεί να επεκταθεί στις παραγώγους ευαισθησίας του πλέγματος. Ο υπολογισμός του $\frac{\delta x_k}{\delta b_n}$ μπορεί έτσι να αποφευχθεί με τη διαφόριση του μοντέλου μετατόπισης του πλέγματος και δημιουργία μιας συζυγούς εξίσωσης μετατόπισης του πλέγματος [11].

Η συνεχής συζυγής προσέγγιση για τη βελτιστοποίηση μορφής σχήματος, σε ροές που διέπονται από τις εξισώσεις Navier-Stokes μπορεί να διατυπωθεί με τρεις διαφορετικούς τρόπους, καθένας από τους οποίους παράγει μια διαφορετική έκφραση για τις παραγώγους ευαισθησίας [11]. Οι προκύπτουσες συζυγείς εξισώσεις και οριακές συνθήκες είναι ίδιες και για τις τρεις διατυπώσεις.

Η πρώτη διατύπωση, οδηγεί σε μια έκφραση που περιλαμβάνει μόνο ολοκληρώματα στα όρια της γεωμετρίας, δηλαδή επιφανειακά ολοκληρώματα (προσέγγιση SI). Αυτό σημαίνει ότι έχει χαμηλό υπολογιστικό κόστος, αλλά μπορεί, ανά περίπτωση, να υστερεί σε ακρίβεια. Η δεύτερη διατύπωση οδηγεί σε ένα άθροισμα τόσο επιφανειακών όσο και χωρικών ολοκληρωμάτων και αναφέρεται ως FI. Η διατύπωση FI είναι μεν ακριβής, αλλά έχει, λόγω των χωρικών ολοκληρωμάτων, καθώς της ανάγκης υπολογισμού των $\frac{\delta x_k}{\delta b_n}$, υψηλό κόστος. Η προσέγγιση Enhanced SI ($E-SI$) εξαλείφει την ανάγκη υπολογισμού των $\frac{\delta x_k}{\delta b_n}$ στον όγκο του υπολογιστικού χωρίου, μειώνοντας έτσι το κόστος, υπολογίζοντας παράλληλα τις παραγώγους ευαισθησίας με ακρίβεια αντίστοιχη αυτής της FI διατύπωσης [11].

Παρακάτω παρουσιάζεται συνοπτικά η συνεχής συζυγής προσέγγιση, [14] [15], [16], [17] σε χρονικά μόνιμες, ασυμπίεστες ροές. Χρησιμοποιήθηκε το μοντέλο τύρβης Spalart-Allmaras [14]. Η ακόλουθη ανάλυση μπορεί να βρεθεί με περισσότερες λεπτομέρειες στα [14] και [18].

Χρησιμοποιώντας τον συμβολισμό Einstein, όπου οι επαναλαμβανόμενοι δείκτες δηλώνουν άθροιση, οι εξισώσεις Navier-Stokes για μια ασυμπίεστη, χρονικά μόνιμη

ροή και το μοντέλο τύρβης Spalart-Allmaras γράφονται ως [14], [19], [20]

$$R^p = -\frac{\partial v_j}{\partial x_j} = 0 \tag{5.5α′}$$

$$R_i^v = v_j\frac{\partial v_i}{\partial x_j} - \frac{\partial}{\partial x_j}\left[(\nu+\nu_t)\left(\frac{\partial v_i}{\partial x_j}+\frac{\partial v_j}{\partial x_i}\right)\right] + \frac{\partial p}{\partial x_i} = 0\ , \qquad i = 1, 2(, 3) \tag{5.5β′}$$

$$R^{\tilde{\nu}} = v_j\frac{\partial \tilde{\nu}}{\partial x_j} - \frac{\partial}{\partial x_j}\left[\left(\nu+\frac{\tilde{\nu}}{\sigma}\right)\frac{\partial \tilde{\nu}}{\partial x_j}\right] - \frac{c_{b2}}{\sigma}\left(\frac{\partial \tilde{\nu}}{\partial x_j}\right)^2 - \tilde{\nu}P(\tilde{\nu}) + \tilde{\nu}D(\tilde{\nu}) = 0 \tag{5.5γ′}$$

όπου v_i είναι οι συνιστώσες της ταχύτητας, ν είναι η συνεκτικότητα, ν_t η τυρβώδης συνεκτικότητα και p η στατική πίεση διαιρούμενη με τη σταθερή πυκνότητα. Η μεταβλητή κατάστασης του μοντέλου τύρβης είναι το $\tilde{\nu}$ και το τυρβώδες ιξώδες μπορεί να γραφεί ως $\nu_t = \tilde{\nu} f_{v1}$. $P(\tilde{\nu})$ και $D(\tilde{\nu})$ είναι οι όροι παραγωγής και καταστροφής [14]. Οι όροι παραγωγής και καταστροφής εξαρτώνται, μεταξύ άλλων ποσοτήτων, από την απόσταση Δ από τον τοίχο.

Επιπλέον, δεδομένου ότι χρησιμοποιείται η $E - SI$ διατύπωση, οι εξισώσεις 3.7 πρέπει να συμπεριληφθούν στις εξισώσεις κατάστασης. Οι εξ. 5.4 και οι εξισώσεις μετατόπισης του πλέγματος μαζί με τις οριακές συνθήκες είναι οι εξισώσεις που διέπουν το πρόβλημα βελτιστοποίησης. Οι συζυγείς εξισώσεις έχουν ως εξής

$$R^q = -\frac{\partial u_j}{\partial x_j} + \acute{F}_\Omega^p = 0 \tag{5.6}$$

$$\begin{aligned} R_i^u =& u_j\frac{\partial v_j}{\partial x_i} - \frac{\partial (v_j u_i)}{\partial x_j} - \frac{\partial}{\partial x_j}\left[(\nu+\nu_t)\left(\frac{\partial u_i}{\partial x_j}+\frac{\partial u_j}{\partial x_i}\right)\right] + \frac{\partial q}{\partial x_i} + \acute{F}_{\Omega,i}^v \\ &+\tilde{\nu}_a\frac{\partial \tilde{\nu}}{\partial x_i} - \frac{\partial}{\partial x_l}\left(\tilde{\nu}_a\tilde{\nu}\frac{C_Y}{Y}e_{mjk}\frac{\partial v_k}{\partial x_j}e_{mli}\right) = 0\ ,\ i = 1, 2(, 3) \end{aligned} \tag{5.7}$$

$$\begin{aligned} R^{\tilde{\nu}_a} =& -\frac{\partial (v_j\tilde{\nu}_a)}{\partial x_j} - \frac{\partial}{\partial x_j}\left[\left(\nu+\frac{\tilde{\nu}}{\sigma}\right)\frac{\partial \tilde{\nu}_a}{\partial x_j}\right] + \frac{1}{\sigma}\frac{\partial \tilde{\nu}_a}{\partial x_j}\frac{\partial \tilde{\nu}}{\partial x_j} + 2\frac{c_{b2}}{\sigma}\frac{\partial}{\partial x_j}\left(\tilde{\nu}_a\frac{\partial \tilde{\nu}}{\partial x_j}\right) \\ &+\tilde{\nu}_a\tilde{\nu}C_{\tilde{\nu}} + \frac{\partial \nu_t}{\partial \tilde{\nu}}\frac{\partial u_i}{\partial x_j}\left(\frac{\partial u_i}{\partial x_j}+\frac{\partial u_j}{\partial x_i}\right) + (-P+D)\tilde{\nu}_a + \acute{F}_\Omega^{\tilde{\nu}} = 0 \end{aligned} \tag{5.8}$$

$$R_k^{m^a} = \frac{\partial^2 m_k^a}{\partial x_j^2} + \frac{\partial}{\partial x_j}\left\{u_i v_j\frac{\partial v_i}{\partial x_k} + u_j\frac{\partial p}{\partial x_k} + \tau_{ij}^a\frac{\partial v_i}{\partial x_k} - u_i\frac{\partial \tau_{ij}}{\partial x_k} - q\frac{\partial v_j}{\partial x_k}\right\} = 0 \tag{5.9}$$

Οι συζυγείς οριακές συνθήκες παρουσιάζονται στο πλήρες κείμενο και παραλείπονται για λόγους συντομίας. Μετά την εξαγωγή των συζυγών εξισώσεων και των οριακών τους συνθηκών, η τελική έκφραση των παραγώγων ευαισθησίας είναι

$$
\begin{aligned}
\frac{\delta F_{aug}}{\delta b_n} =& T_{SD}^{WF} - \int_{S_{W_p}} SD_1 \frac{\partial \tau_{ij}}{\partial x_m} n_j t_i^I n_m n_k \frac{\delta x_k}{\delta b_n} dS - \int_{S_{W_p}} SD_1 \tau_{ij} \frac{\delta (n_j t_i^I)}{\delta b_n} \frac{\delta x_k}{\delta b_n} dS \\
&+ \int_{S_{W_p}} SD_{2,i} v_{\langle t \rangle}^I \frac{\delta t_i^I}{\delta b_n} dS - \int_{S_{W_p}} SD_{2,i} \frac{\partial v_i}{\partial x_m} n_m n_k \frac{\delta x_k}{\delta b_n} dS \\
&- \int_{S_{W_p}} \left[\left(\nu + \frac{\tilde{\nu}}{\sigma} \right) \frac{\partial \tilde{\nu}_a}{\partial x_j} n_j + \frac{\partial F_{S_z}}{\partial \tilde{\nu}} n_z + \acute{F}_S^{\tilde{\nu}} \right] \frac{\partial \tilde{\nu}}{\partial x_m} n_m n_k \frac{\delta x_k}{\delta b_n} dS \\
&- \int_{S_{W_p}} (-u_{\langle n \rangle} + \phi_{\langle n \rangle \langle n \rangle}) \left(\tau_{ij} \frac{\delta (n_i n_j)}{\delta b_n} + \frac{\partial \tau_{ij}}{\partial x_m} n_m \frac{\delta x_k}{\delta b_n} n_k n_i n_j \right) dS \\
&- \int_{S_{W_p}} \phi_{\langle t^I \rangle \langle t^I \rangle} \left(\tau_{ij} \frac{\delta (t_i^I t_j^I)}{\delta b_n} + \frac{\partial \tau_{ij}}{\partial x_m} n_m \frac{\delta x_k}{\delta b_n} n_k t_i^I t_j^I \right) dS \\
&- \int_{S_{W_p}} (\phi_{\langle t^{II} \rangle \langle t^I \rangle} + \phi_{\langle t^I \rangle \langle t^{II} \rangle}) \left(\tau_{ij} \frac{\delta (t_i^{II} t_j^I)}{\delta b_n} + \frac{\partial \tau_{ij}}{\partial x_m} n_m \frac{\delta x_k}{\delta b_n} n_k t_i^{II} t_j^I \right) dS \\
&- \int_{S_{W_p}} \phi_{\langle t^{II} \rangle \langle t^{II} \rangle} \left(\tau_{ij} \frac{\delta (t_i^{II} t_j^{II})}{\delta b_n} + \frac{\partial \tau_{ij}}{\partial x_m} n_m \frac{\delta x_k}{\delta b_n} n_k t_i^{II} t_j^{II} \right) dS \\
&- \int_{S_{W_p}} n_i \frac{\partial F_{S_{W_{p,i}}}}{\partial x_m} n_m \frac{\delta x_k}{\delta b_n} n_k dS + \int_{S_{W_p}} F_{S_{W_{p,i}}} \frac{\delta n_i}{\delta b_n} dS + \int_{S_{W_p}} F_{S_{W_{p,i}}} n_i \frac{\delta (dS)}{\delta b_n} \\
&+ \int_{S_{W_p}} A_\Delta^{WF} \frac{\partial \Delta^P}{\partial b_n} dS + \int_{S_W} A_\Delta^{WF} \frac{\partial \Delta^P}{\partial b_n} dS + \int_\Omega \tilde{\nu} \tilde{\nu}_a C_\Delta \frac{\partial \Delta}{\partial b_n} d\Omega - \int_{S_W} \frac{\partial m_i^a}{\partial x_j} n_j \frac{\delta x_i}{\delta b_n} dS
\end{aligned}
\tag{5.10}
$$

όπου

$$
SD_1 = -u_{\langle t \rangle}^I + \phi_{\langle t^I \rangle \langle n \rangle} + \phi_{\langle n \rangle \langle t^I \rangle} \tag{5.11}
$$

$$
SD_{2,i} = (\nu + \nu_t) \left(\frac{\partial u_i}{\partial x_j} + \frac{\partial u_j}{\partial x_i} \right) n_j - q n_i + \frac{\partial F_{S_{W_{p,k}}}}{\partial v_i} n_k + \acute{F}_{S_{W_{p,i}}}^v \tag{5.12}
$$

$$
\phi_{ij} = \frac{\partial F_{S_{W_{p,k}}}}{\partial \tau_{ij}} n_k \tag{5.13}
$$

Αυτή είναι μια γενική έκφραση που μπορεί να χρησιμοποιηθεί με οποιαδήποτε συνάρτηση κόστους περιλαμβάνουσα χωρικά και επιφανειακά ολοκληρώματα. Όπως φαίνεται, η εξ. 5.9 περιέχει μόνο ένα χωρικό ολοκλήρωμα, και επομένως όλοι πλην του τελευταίου όρου μπορούν να υπολογιστούν με ένα πρακτικά αμελητέο κόστος. Ο υπολογισμός του τελευταίου όρου στην εξ. 3.38 μπορεί να γίνει με τη χρήση πεπερασμένων διαφορών, πράγμα που όμως θα είχε ως αποτέλεσμα το κόστος να αυξάνει γραμμικά με τον αριθμό των μεταβλητών σχεδιασμού N. Ως εναλλακτικός τρόπος αντιμετώπισης της διαφόρισης της απόστασης Δ από τον τοίχο, η εξίσωση Hamilton-Jacobi ($R_\Delta = \frac{\partial (c_j \Delta)}{\partial x_j} \Delta \frac{\partial^2 \Delta}{\partial x_j^2} - 1 = 0$, όπου $c_j = \frac{\partial \Delta}{\partial x_j}$), η οποία δίνει μια πολύ καλή προσέγγιση

του ευκλείδειου πεδίου απόστασης [14], μπορεί να χρησιμοποιηθεί ως ΜΔΕ διέπουσα την απόσταση Δ [21].

Η ίδια συζυγής διαδικασία χρησιμοποιείται, στη συνέχεια, για την εξάλειψη του χωρικού ολοκληρώματος του $\frac{\partial \Delta}{\partial b_n}$, όπως χρησιμοποιήθηκε για την εξάλειψη όλων των άλλων ¨ανεπιθύμητων' χωρικών ολοκληρωμάτων μέχρι στιγμής. Έτσι το γινόμενο της συζυγούς απόστασης Δ^a με την εξίσωση Hamilton-Jacobi προστίθεται στην έκφραση της επαυξημένης συνάρτησης κόστους. Ο όρος που περιέχει $\frac{\partial \Delta}{\partial b_n}$ τότε εξαλείφεται θέτοντας τον πολλαπλασιαστή του ίσο μηδέν, εξάγοντας έτσι την συζυγή εξίσωση για την απόσταση Δ [14]. Αυτά ολοκληρώνουν την θεωρία σχετικά με τη διατύπωση της συνεχούς συζυγούς μεθόδου που χρησιμοποιείται στις προσομοιώσεις που θα παρουσιστούν παρακάτω.

Το λογισμικό βελτιστοποίησης μορφής της BMW, ShapeModule, στο οποίο ενσωματώθηκαν ο επιλύτης της ροής και ο συζυγής επιλύτης της ΜΠΥΡ&Β/ΕΜΠ επιτρέπει στο χρήστη να συνδεθεί με διάφορα εργαλεία ή επιλυτές που θα λύσουν το πρωτεύον και το συζυγές πρόβλημα και, στη συνέχεια, θα στείλουν στο ShapeModule τις παραγώγους ευαισθησίας και το προς βελτιστοποίηση τμήμα της γεωμετρίας όπου οι μετατοπίσεις των οριακών κόμβων θα υπολογιστούν με χρήση της τεχνικής Vertex Morphing [22], [23], [24]. Το Vertex Morphing είναι μια παραμετροποίηση της γεωμετρίας με βάση τους κόμβους, δηλαδή, οι θέσεις των επιφανειακών κόμβων είναι οι μεταβλητές σχεδιασμού. Άμεσο πλεονέκτημα των μεθόδων αυτών, είναι το μεγαλύτερο 'design space' (περισσότερες μεταβλητές σχεδιασμού). Ένα μειονέκτημα είναι πιθανές ανωμαλίες στο σχήμα, καθώς η προκύπτουσα επιφάνεια μπορεί να είναι ¨θορυβώδης¨. Η λύση σε αυτό το ζήτημα είναι η εφαρμογή ενός φίλτρου εξομάλυνσης πάνω στις προκύπτουσες παραγώγους ευαισθησίας και στις μετατοπίσεις του κάθε κόμβου.

Παρακάτω παρουσιάζονται ενδεικτικά δυο από τις πέντε περιπτώσεις που τρέχτηκαν. Τα αποτελέσματα παρουσιάζονται αναλυτικά στο πλήρες κείμενο.

Ελαχιστοποίηση των Ολικών Απωλειών Πίεσης (Δp_t) σε Τυρβώδη Ροή

Η βελτιστοποίηση του αγωγού σχήματος S με στόχο την ελαχιστοποίηση των απωλειών ολικής πίεσης (τυρβώδης ροή) αφέθηκε να τρέξει για 25 κύκλους. Η συνάρτηση κόστους μειωνόταν μέχρι και τον 18^o κύκλο όπου και συνέκλινε στη βέλτιστη λύση. Η σύγκλιση φαίνεται στο σχ. 5.4

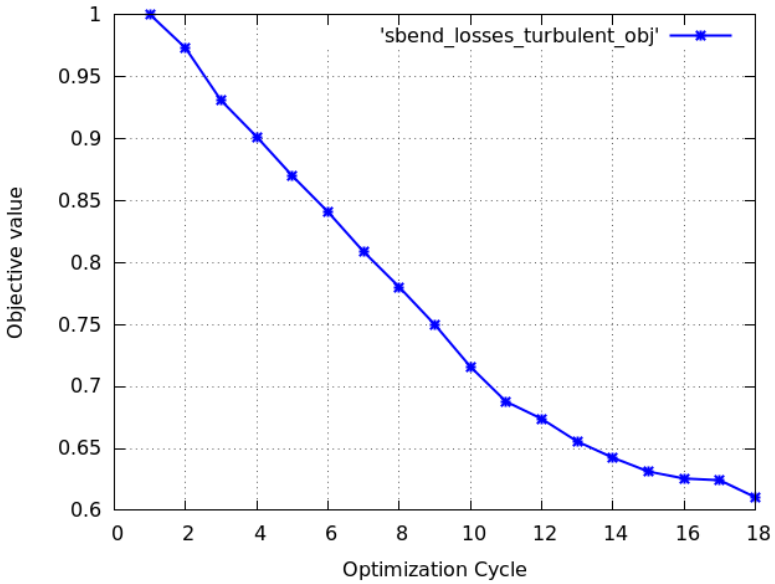

Σχήμα 5.4: *Ελαχιστοποίηση Δp_t στον αγωγό σχήματος S, τυρβώδης ροή. Ύστερα από 18 κύκλους παρατηρείται μείωση 38.86% στην τιμή της συνάρτησης κόστους.*

Το πεδίο των αθροιστικών καθέτων μετατοπίσεων στην τελική γεωμετρία φαίνεται στο σχ. 5.5

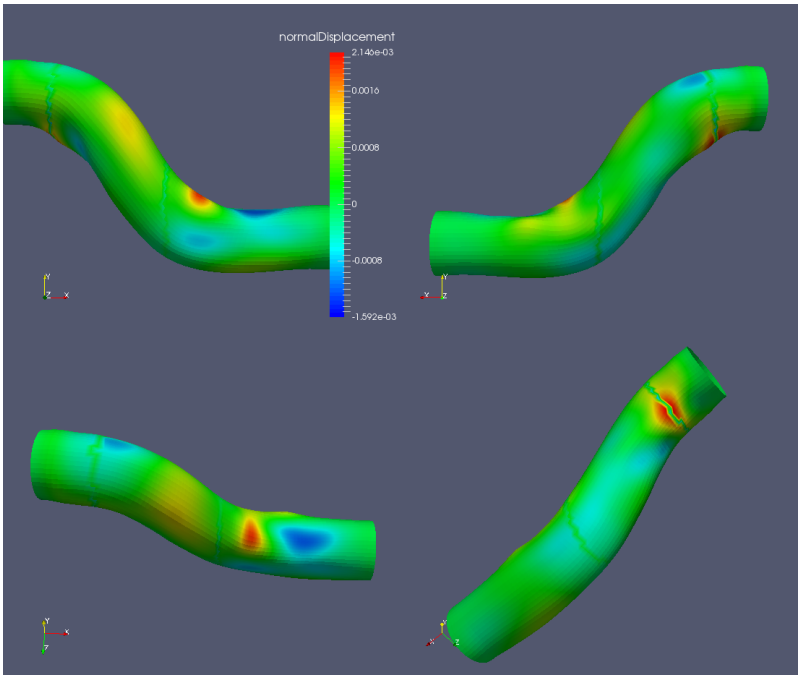

Σχήμα 5.5: *Ελαχιστοποίηση Δp_t στον αγωγό σχήματος S, τυρβώδης ροή. Πεδίο αθροιστικών καθέτων μετατοπίσεων στην τελική γεωμετρία.*

Το πεδίο της ολικής πίεσης εντός του αγωγού για την αρχική και τελική γεωμετρία φαίνεται στα σχ. 5.6, 5.7.

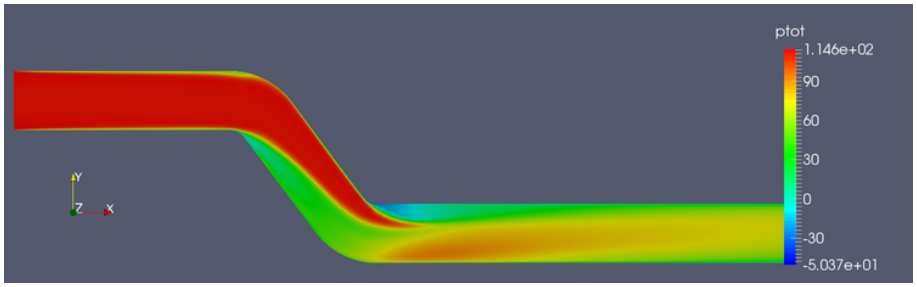

Σχήμα 5.6: *Ελαχιστοποίηση Δp_t στον αγωγό σχήματος S, τυρβώδης ροή. Ολική πίεση στην αρχική γεωμετρία. Τομή κατά μήκος του επιπέδου συμμετρίας του αγωγού.*

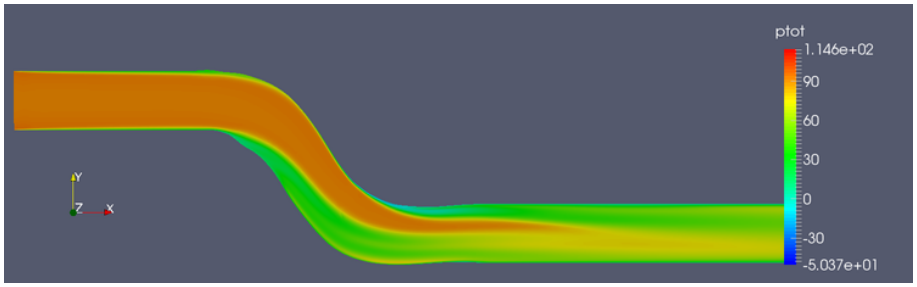

Σχήμα 5.7: *Ελαχιστοποίηση Δp_t στον αγωγό σχήματος S, τυρβώδης ροή. Ολική πίεση εντός της τελικής γεωμετρίας. Τομή κατά μήκος του επιπέδου συμμετρίας του αγωγού.*

Ελαχιστοποίηση Υποκατάστατης Συνάρτησης Κόστους για τον Θόρυβο στον HVAC Αγωγό

Η δεύτερη γεωμετρία που βελτιστοποιήθηκε ήταν αυτή ενός HVAC αγωγού. Η προς ελαχιστοποίηση συνάρτηση σε αυτήν την περίπτωση είναι η υποκατάστατη συνάρτηση κόστους για τον θόρυβο, οριζόμενη ως (βλ. [25])

$$J = \int_{\Omega'} {\nu_t}^2 d\Omega \tag{5.14}$$

όπου ν_t είναι η τυρβώδης συνεκτικότητα και Ω' ο όγκος όπου είναι επιθυμητή η ελαχιστοποίηση της τύρβης και του σχετιζομένου με αυτήν θορύβου. Στη συγκεκριμένη περίπτωση, επιλέγεται ως όγκος ολοκλήρωσης Ω', ένας όγκος λίγο πριν την έξοδο του αγωγού. Η γεωμετρία του αγωγού, το παραμετροποιημένο της τμήμα και ο όγκος ολοκλήρωσης της συνάρτησης κόστους φαίνονται στο σχ. 5.8 (χρωματισμένα με μπλε και πράσινο, αντίστοιχα).

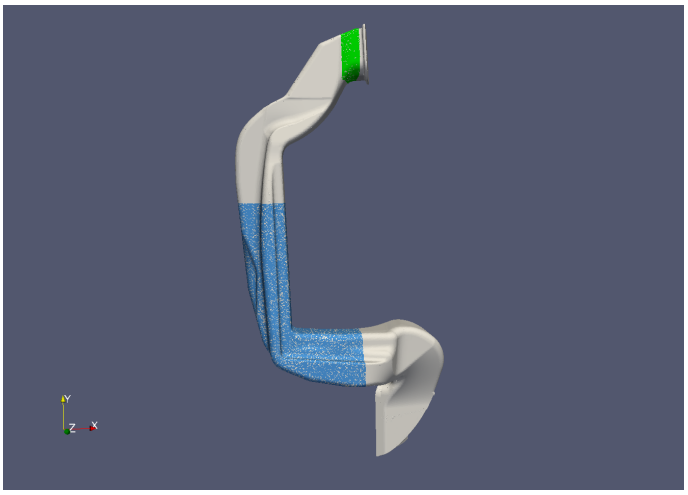

Σχήμα 5.8: *Ελαχιστοποίηση υποκατάστατης συνάρτησης κόστους για τον θόρυβο στον αγωγό HVAC. Παραμετροποιημένο τμήμα (μπλε) και όγκος ολοκλήρωσης της συνάρτησης κόστους (πράσινο).*

Η βελτιστοποίηση έτρεξε για 33 κύκλους, μετά τους οποίους παρουσίασε ταλαντωτική συμπεριφορά, οπότε και τερματίστηκε. Η ταλαντωτική συμπεριφορά στην συνάρτηση κόστους ήταν αποτέλεσμα της ταλαντωτικής συμπεριφοράς κατά την επίλυση του πρωτεύοντος προβλήματος. Η σύγκλισή της φαίνεται στο σχ. 5.9

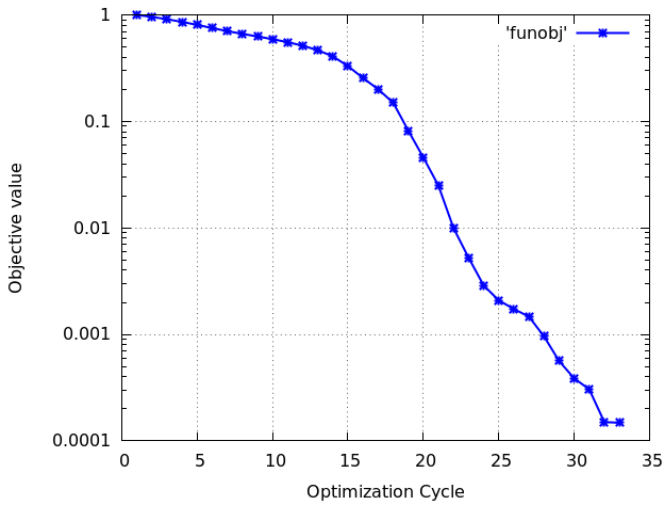

Σχήμα 5.9: *Ελαχιστοποίηση υποκατάστατης συνάρτησης κόστους για τον θόρυβο στον αγωγό HVAC. Μετά από 33 κύκλους βελτιστοποίησης, έχει υπάρξει μείωση κατά 99.99% στην τιμή της συνάρτησης κόστους, σε σύγκριση με την αρχική της τιμή.*

Το πεδίο των αθροιστικών μετατοπίσεων προβεβλημένων στο κάθετο διάνυσμα φαίνεται στο σχ. 5.10.

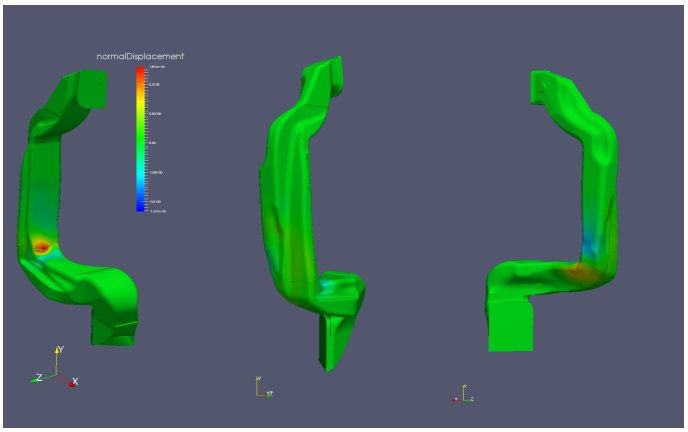

Σχήμα 5.10: *Ελαχιστοποίηση υποκατάστατης συνάρτησης κόστους για τον θόρυβο στον αγωγό HVAC. Πεδίο των αθροιστικών μετατοπίσεων προβεβλημένων στο κάθετο διάνυσμα. Μπλε χρωματισμός αντιστοιχεί σε μετατοπίσεις προς το εσωτερικό του αγωγού, ενώ κίτρινος και κόκκινος χρωματισμός σε μετατοπίσεις προς έξω.*

Περίληψη - Συμπεράσματα

Συνοψίζοντας, στο πρώτο μέρος της εργασίας απεδείχθη ότι ο υπολογισμός της πίεσης μπορεί να πραγματοποιηθεί χωρίς την ανάγκη αναλυτικών ή CFD υπολογισμών σε ένα πεδίο που εκτείνεται από ακουστική πηγή έως και τον παρατηρητή. Αντ΄ αυτού, η KIM μπορεί να χρησιμοποιηθεί για την πρόβλεψη του θορύβου, χρησιμοποιώντας τα CFD ή αναλυτικά δεδομένα από έναν χωρίο κοντά στην πηγή. Εδείχθη επίσης, ότι ο τύπος του KI μπορεί να διαφοριστεί αναλυτικά και το αποτέλεσμα, $\delta p'/\delta b_n$, να χρησιμοποιείται για τον υπολογισμό των παραγώγων ευαισθησίας που απαιτούνται για τη βελτιστοποίηση της θέσης της πηγής. Μελλοντικά θα μπορούσε να πραγματοποιηθεί σύζευξη του ολοκληρώματος Kirchhoff με CFD με στόχο την gradiend-based βελτιστοποίηση μορφής για την αεροακουστική. Για να γίνει βελτιστοποίηση με βάση τη συνεχή συζυγή μέθοδο πρέπει να γίνει σύζευξη την αναλυτικής διαφόρισης του τύπου του Kirchhoff που πραγματοποιήθηκε στην εργασία αυτή, με τη συζυγή μέθοδο για την ροή.

Στο δεύτερο τμήμα, πραγματοποιήθηκε επιτυχής σύζευξη του συνεχούς συζυγούς λογισμικού της ΜΠΥΡ/ΕΜΠ με το optimization workflow της BMW, "ShapeModule" και τρέχθηκαν επιτυχώς 5 περιπτώσεις βελτιστοποίησης. Η ανανέωση του πλέγματος γινόταν με προσαρμογή για όλες τις περιπτώσεις. Δυνατότητα ακόμα μεγαλύτερης μείωσης της συναρτήσεως κόστους θα είχαμε αν γινόταν επαναπλεγματοποίηση. Σε όλες τις περιπτώσεις, υπήρξε μια πολύ ικανοποιητική μείωση της συνάρτησης κόστους ανά κύκλο. Ειδικά η βελτιστοποίση του HVAC αγωγού με χρήση της υποκατάστατης συνάρτησης κόστους για τον θόρυβο παρουσίασε μια δραματική μείωση της συνάρτησεως κόστους.

Bibliography

[1] Lighthill, MJ: *On sound generated aerodynamically i. general theory.* Proc. R. Soc. Lond. A, 211(1107):564–587, 1952.

[2] Delfs, J: *Lecture notes Grundlagen der Aeroakustik (Basics of aeroacoustics).* WS 2016/2017.

[3] Rienstra, SW and Hirschberg, A: *An introduction to acoustics.* Eindhoven University of Technology, 18:19, 2003.

[4] Roach, GF: *Green's functions.* Cambridge Univ. Press, 1982.

[5] Crighton, DG, Dowling, AP, Ffowcs-Williams, JE, Heckl, M, Leppington, FG, and Bartram, JF: *Modern methods in analytical acoustics lecture notes*, 1992.

[6] Kapellos, C and Hartmann, M: *A continuous adjoint approach for vehicle interior noise reduction.* 2016.

[7] Casalino, D: *An advanced time approach for acoustic analogy predictions.* Journal of Sound and Vibration, 261(4):583–612, 2003.

[8] Najafi-Yazdi, A., Brès, GA, and Mongeau, L: *An acoustic analogy formulation for moving sources in uniformly moving media.* In *Proceedings of the Royal Society of London A: Mathematical, Physical and Engineering Sciences*, volume 467, pages 144–165. The Royal Society, 2011.

[9] Roger, M: *Applied Aero-acoustics: prediction methods.* The von Karman institute for fluid dynamics, 1996.

[10] Zymaris, AS, Papadimitriou, DI, Giannakoglou, KC, and Othmer, C: *Continuous adjoint approach to the spalart–allmaras turbulence model for incompressible flows.* Computers & Fluids, 38(8):1528–1538, 2009.

[11] Kavvadias, IS, Papoutsis-Kiachagias, EM, and Giannakoglou, KC: *On the proper treatment of grid sensitivities in continuous adjoint methods for shape optimization.* Journal of Computational Physics, 301:1–18, 2015.

[12] Nielsen, EJ and Park, MA: *Using an adjoint approach to eliminate mesh sensitivities in computational design.* AIAA journal, 44(5):948–953, 2006.

[13] Mavriplis, DJ: *Discrete adjoint-based approach for optimization problems on three-dimensional unstructured meshes*. AIAA journal, 45(4):741–750, 2007.

[14] Papoutsis-Kiachagias, EM: *Adjoint Methods for Turbulent Flows, Applied to Shape or Topology Optimization and Robust Design*. PhD thesis, Laboratory of Thermal Turbomachines, NTUA, Athens, 2012.

[15] Mohammadi, B and Pironneau, O: *Applied shape optimization for fluids*. Oxford university press, 2010.

[16] Giannakoglou, KC, Papadimitriou, DI, Papoutsis-Kiachagias, EM, and Othmer, C: *Adjoint methods in cfd-based optimization: Gradient computation & beyond*. In *European Congress on Computational Methods in Applied Sciences and Engineering-ECCOMAS*, pages 10–24, 2012.

[17] Papoutsis-Kiachagias, EM, Giannakoglou, KC, and Othmer, C: *Adjoint wall functions: Validation and application to vehicle aerodynamics*, 2014.

[18] Papoutsis-Kiachagias, EM and Giannakoglou, KC: *Continuous adjoint methods for turbulent flows, applied to shape and topology optimization: Industrial applications*. Archives of Computational Methods in Engineering, 23(2):255–299, 2016.

[19] Versteeg, HK and Malalasekera, W: *An introduction to computational fluid dynamics: the finite volume method*. Pearson Education, 2007.

[20] Moukalled, F, Mangani, L, Darwish, M, *et al.*: *The finite volume method in computational fluid dynamics*. 2016.

[21] Papoutsis-Kiachagias, EM, Koch, J, Gkaragounis, K, and Giannakoglou, KC: *A continuous adjoint framework for shape and topology optimization and their synergistic use*. In *2018 AIAA/ASCE/AHS/ASC Structures, Structural Dynamics, and Materials Conference*, page 1389, 2018.

[22] Hojjat, M, Stavropoulou, E, and Bletzinger, K: *The vertex morphing method for node-based shape optimization*. Computer Methods in Applied Mechanics and Engineering, 268:494–513, 2014.

[23] Hojjat, M: *Node-based parametrization for shape optimal design*. PhD thesis, Universitätsbibliothek der TU München, 2015.

[24] Bletzinger, K, Hojjat, M, and Stavropoulou, E: *Form finding by shape optimization with the vertex morphing method–about the equivalence of sensitivity filtering and standard spline models*.

[25] Papoutsis-Kiachagias, EM, Magoulas, N, Mueller, J, Othmer, C, and Giannakoglou, KC: *Noise reduction in car aerodynamics using a surrogate objective function and the continuous adjoint method with wall functions*. Computers & Fluids, 122:223–232, 2015.